UNIVERSITA' DI PISA
Scuola di Dottorato in Ingegneria "Leonardo da Vinci"

Corso di Dottorato di Ricerca in
SICUREZZA NUCLEARE E INDUSTRIALE
Tesi di Dottorato di Ricerca
XXIII Ciclo

DEVELOPMENT OF CLOSURE RELATIONSHIPS FOR ADVANCED TWO-PHASE FLOW ANALYSIS

Autore:
BARBARA CALGARO
Tutori:
Prof. Ing. Walter Ambrosini
Dr. Ing. Nicola Forgione
Prof. Ing. Paolo Andreussi
Dr. Ing. Marco Bonizzi

SSD ING-IND/19

Anno 2012

Abstract

During this doctoral activity, developed at TEA Sistemi SpA with the contribution of the University of Pisa in the context of an R&D project funded by ENI E&P, the formulation of a new set of liquid-wall and gas-liquid interfacial friction factor correlations was performed. The attention was focused on the improvement of existing correlations when applied to the design of long transportation pipelines.

In this aim, a new set of data related to nitrogen-water flow in a 80 mm pipe operating at pressures in the range 5-25 bar has been used along with data published in the open literature (mainly concerning air-water flows at atmospheric pressure). These data were used to develop new correlations for friction factors in horizontal stratified gas-liquid flow conditions.

Moreover a new multi-field model called MAST (Multiphase Analysis and Simulation of Transition), recently developed at TEA Sistemi SpA with the support of ENI E&P and addressing the Oil&Gas field, was presented in detail during this activity and validated against experimental measurements for the investigation of the long slug flow sub-regime.

The content of this doctoral work is summarized below:

- Chapter 1 and Chapter 2 present the context of the investigation and the literature review of the horizontal two-phase flow models with a particular attention to the slug flow regime numerical prediction; a quick introduction to the problem of ill-posedness of the two-fluid model and to the most important numerical resolution approaches is also included;

- Chapter 3 presents the "four-field" model implemented in the MAST code; an overview on its validation against the Mandhane flow map (Mandhane et al., 1974) and against experimental measurements is performed;

- Chapter 4 contains the application of the "four-field" model implemented in MAST to the prediction of the long slug flow regime, together with its validation against experimental measurements;

- Chapter 5 contains a review of the state-of-art of the "Stratified Flow Model" with the modelization of a two-phase stratified gas-liquid flow in the case in which the flow experiences waves at the gas-liquid interface. Moreover, a literature review on existing friction factor correlations completes this chapter.

- Chapter 6 describes the experimental campaign performed by TEA Sistemi in the framework of the SESAME project, the databases from literature and the numerical tools developed during this doctoral work;
- In Chapter 7, the original contribution for developing new liquid-wall and interfacial friction factor correlations is presented.

Acknowledgements

The author wish to acknowledge the contributions made to this project by TEA Sistemi S.p.A. and ENI E&P, expressing gratitude for their support.

Special thanks must go to Prof. Ambrosini, Prof. Andreussi, Dott. Forgione and Dott. Bonizzi for being my tutors and having driven me during this doctoral activity.

Many thanks go to the TEA Sistemi lab guys and to Vittorio that with their work contribute to the success of my research.

I would like to thank all my former colleagues from TEA Sistemi and in particular Federica, Alice, Silvia, Sonia, Margherita, Elisabetta.

In addition, I thank for their contribution Eleonora and Leslie and my friends all over the world for their encouragement.

I dedicate this thesis to my family, in particular to my parents and my little brother, and to Luca for his precious support.

Table of contents

Index of Figures

Index of Tables

Chapter 1 Introduction

There are a lot of real life situations where multiphase flow is encountered. This important topic is at the basis of the present research, addressed at the same time in Oil&Gas, Nuclear and Chemical industries, but the detailed analysis has been extended here to the former field.

The most widespread multiphase flow example is the flow of a gas and a liquid phase; but the case with a secondary liquid phase or a solid phase better represents the peculiarity of several processes: liquid-liquid, gas-liquid-liquid, gas-liquid-solid flows need to be predicted and controlled.

Multiphase flow is frequently encountered, for example, when tasting some carbonated soft drinks, a beer, some sprinkling champagne, or in an air conditioned public area; or simply when a boiler is switched on to prepare a cup of tea.

But multiphase flows are encountered also when nanoparticles are transported by nanofluids in micro-channels to enhance heat transport in microchips and electronic devices. Again, multiphase mixtures of natural gas, crude oil and water are met at the exit of their reservoir and need to be transported to offshore or onshore processing facilities, before being used to drive a car or to take an airplane.

In several existing nuclear power plants, a mixture of water and bubbles nucleating, growing and coalescing represents the coolant fluid that enables the heat removal and the thermal energy transfer from the reactor core to the turbine and then to the electric energy generator.

When a multiphase flow occurs, the solution of the set of equations of such a complex system is a big challenge, far from keeping any single-phase flow model generally applicable. The development of mathematical and numerical methods for solving multiphase flows is something not yet completely achieved. This is particularly true for a gas-liquid two-phase flow that results in great difficulties for predicting the behavior of each phase; in fact, the shape of the interfaces between the phases is part of the solution itself.

In gas-liquid flows in horizontal pipes, for example, different flow patterns can be observed depending on phase velocities and on all the parameters of engineering significance (e.g., pipe geometry or physical properties of the mixtures). But at the same time, the transfer rate of momentum and mass between gas and liquid depends on the distribution of gas and liquid in the pipe cross section itself. This will be described in detail in Chapter 2.

1.1 Field of application

The European Union EU-27 baseline scenario to 2030, as published in the "European Energy and Transport – Trend to 2030 – Update 2007" report (Transport, 2008) foresees that the energy requirements will continue to increase up to 2030, see Figure 1. The primary energy consumption, in fact, will increase of some 200 Mtoe between 2005 and 2030.This amount will be overwhelmingly met by both renewable and natural gas, which are the only energy sources that increase their market shares. In particular, the natural gas demand is expected to expand considerably by 71 Mtoe up to 2030. But oil remains the most important fuel.

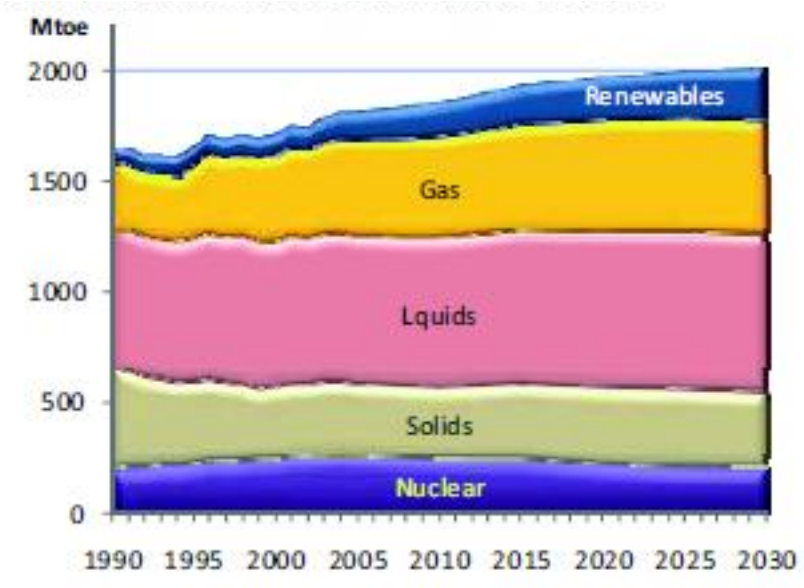

Figure 1: Primary energy requirements by fuel NEA OECD trends, (2007)

To complete the scenario solid fuels are projected to exceed their current level by 5% in 2030, following high oil and gas prices, and, although nuclear generation has been rising in recent years, nuclear energy production is predicted to be reduced of 20% in 2030 than it was in 2005.

Summarizing, the hydrocarbons import demand continues growing during next twenty years and import needs for oil and gas will grow too.

The same analysis could be extended worldwide, with 93% of incremental oil needs due to the growth of emerging economies. Total oil production is projected to reach 110 Mb/d (million barrels per day), up from 72.6 Mb/d in 2001.

The total volume of natural gas produced annually is projected to double from 2001 to 2030. The increase is more than 2000 Mtoe and is mainly due to emerging economies (60%) and secondarily to Europe-OECD (25%). The

latter, lacking additional gas resources, will import in 2030 about 40% of their gas needs, up from 18% in 2001.

The gas resources needed to cover incremental demand are concentrated in a small number of countries, namely in Middle East and in CIS, and secondarily in Africa. Therefore, access of developing and emerging economies to gas resources is projected to take place mainly through pipeline routes, new and existing ones.

In this context, the present work will focus on hydrocarbon transportation that is still a big issue, due to the need of longer pipelines, characterized by frequent changes in inclination, diameter and flow pattern conditions, bringing several concerns about operability, mechanical integrity of pipes and devices.

This is the reason why this research aims at contributing to increase transport efficiency and at avoiding technical constraints to improve the predictability of flow patterns and design tools accuracy.

1.2 Industrial context

Major problems in long hydrocarbon transportation pipelines are correlated to the slug flow regime, a pulsed sequence of intermittent plugs of gas and liquid traveling at a velocity very close to the one of the gas phase.

The impacts against bend, narrow curves or obstacles, and the resonance effects with the pipe system frequency, can cause the pipeline loss of integrity and the loss of the transported hydrocarbon into the environment.

Separators and slug catchers (Figure 2 and Figure 3), devices where the liquid slug is captured, separated from its plug of gas and purged from the bottom of the separator itself, could be installed along the line in order to reduce the probability of failure.

Their design should be optimized on the longest expected slug lengths in order to avoid that the two phases are not properly separated before the gas enters into the gas stream.

Incorrect predictions of slug flow occurrences, slug frequencies and slug lengths may be responsible for over sized separators and slug catchers affecting the construction costs.

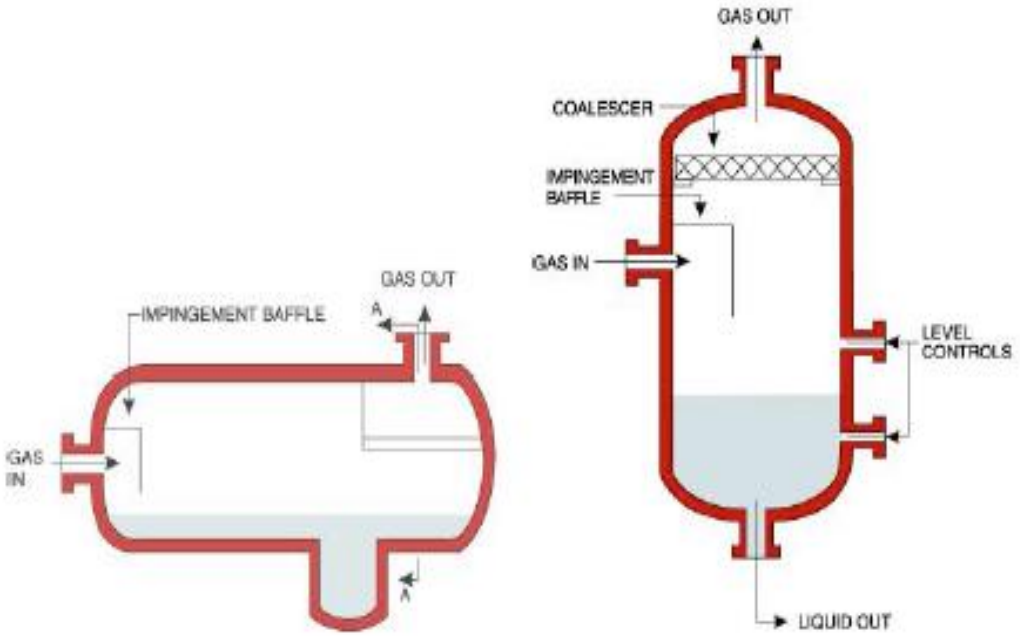

Figure 2: Schematic view of a separator
(from http://www.tfes.com/slugCatcher02.htm)

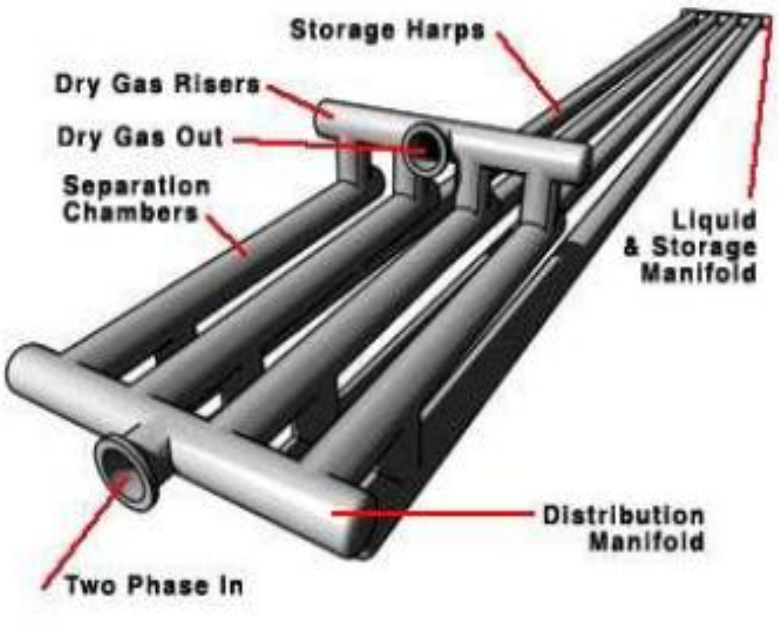

Figure 3: Schematic view of a slug catcher
(from http://www.tfes.com/slugCatcher02.htm)

Moreover, slug flow generates important pressure losses, often not predicted before operating the transportation line.

1.3 Existing approaches

In the last thirty years, major efforts have been devoted to the development of reliable calculation tools for the prediction of the slug flow occurrence as a function of the operating conditions (gas and liquid velocity, pipe diameter and inclination, etc.) .

Nowadays, the new proposed approaches are more and more similar to CFD simulations, with different investigation scales, down to the smaller detail of flow components (continuous gas, gas droplets, continuous liquid, liquid droplets). Due to the large scale of the simulated systems, 2D and 3D fluid dynamics calculations are too time and CPU consuming to be feasible.

In Oil&Gas field, the 1D calculation has been the privileged approach and several different models have been proposed and commercialized since the 70's, when the petrol industry started financing research programs in the effort of better predicting flow patterns in long and inclined pipelines.

The common characteristic of all 1D models is the incapability of exactly calculating the 2D and 3D phenomena. Actually, these are often not requested details, because they involve scales smaller then a diameter and the same phenomena are included in properly defined closure laws, i.e., in equations that enable to adapt the same mathematical model to all flow patterns.

In particular, different flow models have been developed in order to simulate slug flow pattern and its transient behavior.

The first complete set of numerical resolution equations for horizontal two phase flow was proposed by Dukler and Hubbard and was called the "unit-cell model" presented in Figure 4 (Dukler and Hubbard, 1975). Here, the slug body and the slug tail have been presented as the same computational unit. In that case, only average holdup and pressure gradients were investigated.

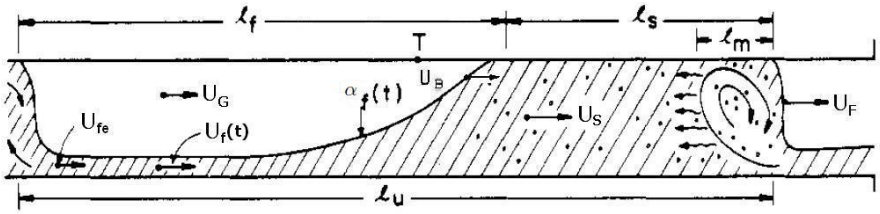

Figure 4: Slug unit-cell model (Dukler and Hubbard, 1975)

The total unit length is the sum of the contributions of the liquid slug length and of the film region length . This first approach to the problem assumes no slip conditions inside the liquid slug between the gas bubbles and the liquid. The flow is assumed horizontal, with a stable slug.

The input requirements are the most limiting aspect of the model: the user has to know in advance the slug frequency and the liquid phase fraction in the slug.

Later on, Barnea and Taitel, (1993) revised the model proposed by Dukler and Hubbard by extending the applicability of the unit-cell model also to upward and downward inclined pipes.

They defined a more comprehensive "equivalent cell" model (Barnea and Taitel, 1993), but the purpose was again the calculation of average pressure gradient and the required input information are slug velocity, slug void, slug body length, etc..

But the major constraints with these "steady-state" models come from their impossibility of predicting the transient behavior of this flow pattern, e.g., changes in slug frequencies due to pipe inclination.

Since the late '80s a great effort has been done to develop more accurate transient methods that could improve the design of transportation pipelines in the case of fast changing flow rates, terrain induced slugging and severe slugging.

The most important contributions were collected in commercial codes as OLGA (Bendiksen et al., 1991), TACITE (Pauchon et al., 1994) and PLAC (Black et al., 1990).

All of these codes implement a transient one-dimensional system of governing equations solved on a fixed grid. The OLGA and the PLAC codes are based on the two-fluid model (Ishii, 1975), the TACITE code adopted the drift-flux model approach (Zuber and Findlay, 1965). They all need closure laws to solve the flow regime problem: the OLGA and the TACITE codes for instance select between separated and distributed flow through a minimum slip concept (minimum gas velocity).

From a computational point of view the most commonly encountered transient methods for slug flow prediction could be summarized in the following categories: "empirical slug specification", "slug tracking" and "slug capturing".

Examples of the first group are "unit-cell"-like approaches, where the two-fluid model is in fact coupled with a slug flow sub-model where all the most important information on slug flow are given by closure laws.

To the second group belongs, among the others, the OLGA code. The peculiarity of a slug-tracking model lies in its capability of simulating abrupt changes in the system geometry, such as an inclined pipeline that undergoes rapid changes in its inclination. From the slug flow point of view, this technique enables the simulation of the growth or the collapse of a slug body

through the simulation of the pick-up process at the slug front or through the shedding rate at the slug tail.

Usually a slug tracking code has been written in a Lagrangian type of discretized equations, where the computational nodes translate together with the slug body and the liquid film when the slug moves into the pipe. Their limitation is that a steady state hypothesis on the slug distribution in the pipeline is needed in order to start the transient simulation. Reasonable results are obtained as a function of the starting distribution.

An advanced slug tracking method has been developed by Nydal and Banerjee, (1996) defined as a Lagrangian dynamic slug tracking simulator. They created an object-oriented approach in C++ language where gas bubbles and liquid slugs are treated as computational objects.

The third group is the one of "slug capturing" models and this approach is the basis of transient codes such as TRIOMPH, whose origins come from the work of Prof. Issa and collaborators (Issa and Woodburn, 1998; Issa and Kempf, 2003), and MAST (Bonizzi et al., 2009) which is investigated in detail in the present work.

This technique solves the two-fluid model equations with conservation of mass and momentum separately for each phase and the same set of equations is solved independently from the flow pattern developed in the pipe.

The "slug capturing" is a technique in which the slug flow regime is predicted as a mechanistic and an automatic outcome of the growth of hydrodynamic instabilities (Issa and Kempf, 2003).

This is feasible and gives reasonable results in particular for the prediction of slug flow if an Eulerian resolution method is adopted with a sufficiently refined mesh size in order to catch numerically the onset of instability naturally occurring between a liquid and a gas flowing with different density and velocity.

The first comprehensive resolution method applying the "slug capturing" model was the research code TRIOMPH that has been developed by Prof. Issa and collaborators to predict slug flow appearance in various pipe inclinations (Issa and Abrishami, 1986) .

In that context, when the validation of the code took place, the influence on the solution for this kind of numerical tools of the chosen stratified-wavy friction factor correlations was stated clearly (Issa et al., 2006).

As it will be explained in detail during next sections, this is key information to understand the importance and the role of the present research in the international scientific context.

The present research, in fact, deals with the analysis and the improvement of the "slug capturing" model called MAST (Bonizzi et al., 2009) that applies a "four-field" model approach, based on a system of ten equations (four continuity equations, four momentum equations and two energy equations), and that was born to improve the prediction of the transition between stratified and slug flow pattern, experienced frequently by two-phase gas-liquid flows along an hydrocarbon transportation pipeline, as it will be explained in detail in the next chapters.

1.4 Present contribution

This research has been performed at TEA Sistemi S.p.A., in collaboration with DIMNP and the University of Pisa, in occasion of the development of a new 1D multiphase flow transient code MAST for the design of long oil and gas transportation pipelines.

The present work is focusing, in particular, on the definition of the best available friction factor correlations (phase-wall and interfacial) and on the proposal of new ones. These are implemented in a simpler, steady-state, 0D, C++ code.

Despite the highly random behavior of the flow and the large number of flow regimes experienced by gas and liquid, modern transient multiphase flow simulators need to postulate a limited number of idealized flow patterns, or possibly a flow pattern independent mathematical model.

This is the approach of "Multiphase Analysis and Simulation of Transitions – MAST" code, a multiphase 1D transient flow simulator, developed at TEA Sistemi, that enables the solution of a flow map independent model, called the "four-fields" model and that is presented as the improvement of the "two fluid model".

In fact, with MAST the modelization and the simulation of transient multiphase flows could be enhanced by the postulation of a limited number of idealized flow patterns in which a temporal and spatial variation of the volume fractions of all the participating phases (gas continuous, liquid continuous, gas dispersed, liquid dispersed) could be foreseen by a complete set of balance equations.

The contribution of the present work is the investigation of available friction factor correlations for the prediction of the phase-wall and the interfacial gas-liquid shear stresses, considering the best existing models and proposing a new set of correlations.

During the present activity, the applicability of the MAST code has been extended to a peculiar slug flow pattern sub-regime, called the long slug

regime, theorized for the first time by Woods and Hanratty, (1999). In particular, the experimental measurements obtained during the research of Kristiansen, (2004) and Kadri et al., (2009a) have been successfully reproduced by the code.

1.5 Chapters outline

The thesis is organized in eight chapters and their topics are summarized below.

- Chapter 1 presents the technological and industrial context in which the present work was born, with a brief overview of existing approaches and of the goals of this research.

- Chapter 2 presents the literature review and the state-of-the-art of the horizontal two-phase flow models with a particular attention to the slug flow regime numerical prediction: the typical two-phase flow patterns and the origin of their definition are described. The most frequently used two-phase flow models are briefly introduced (two-fluid model, drift-flux and HEM models); a quick introduction to the problem of ill-posedness of the two-fluid model and to the most important numerical resolution approaches is also included.

- In Chapter 3, the" slug capturing" technique is introduced and the "four-field" model implemented in MAST is presented with the description of the peculiarities of this new code; an overview on its validation against the Mandhane flow map (Mandhane et al., 1974) and against experimental measurements is also performed.

- Chapter 4 contains the presentation of the long slug flow regime as a variant of the most commonly encountered slug flow in hydrocarbon transportation pipelines. Here an original activity is proposed based on the application of the "four-field" model implemented in MAST to the prediction of this slug flow sub-regime, together with its validation against experimental measurements. The long slug flow is not observed during high pressure operational conditions but in older offshore fields, with lower pressure and phase velocities; the long slug may form and originate considerably long plugs of liquid. In the first part of this chapter, conclusions and experiences from other authors are presented and commented.

- Chapter 5 contains a review of the state-of-art of the "Stratified Flow Model". It describes the interactions between the phases in both steady and transient two-phase stratified flows. The modelization of a two-phase stratified gas-liquid flow is presented in the case in which the

flow experiences waves at the gas-liquid interface. Moreover, a literature review and the description of the most valuable existing friction factor correlations constitute the major part of this chapter.

- At the beginning of Chapter 6 the experimental campaign performed by TEA Sistemi in the framework of the SESAME project, under sponsorship of ENI E&P, is presented. These data, together with databases available from literature, were used to develop new sets of closure equations for friction factors.

- In Chapter 7, the original contribution for developing new liquid-wall and interfacial friction factor correlations is proposed and all the steps necessary to their definition are described; the presentation span from the selection of the form of the correlations, on the basis of the theory presented in this thesis, to the comparison with already existing models;

- In Chapter 8, conclusions and possible future developments to improve the results of this research will be presented.

Chapter 2 Review of the literature

2.1 Introduction

Multi-phase flow has been analyzed in depth for decades in order to find a suitable way to predict in time and space the behavior of phases flowing together in a pipe. This is still an open field for researchers.

A phase is an entity that describes a specific thermodynamic state of the matter which, in general, could be solid, liquid and gas.

In multiphase flow different phases may coexist together as in boiling water, gas-oil flows. Multiphase flow systems can be found in several industrial activities and the prediction of their behavior is of dominant importance in particular for safety issues.

Examples of critical operation of a multiphase system are the occurrence of instabilities or of abrupt changes in flow pattern regime.

These two dynamic phenomena are important in a strategic energy field as Oli&Gas and in the nuclear industry, where the risk of any deviation from normal operating conditions has to be minimized; but they are just examples of the wide range of phenomena that a multiphase flow could undergoes.

In offshore production systems, where a mixture of crude oil and gas is transported from offshore drilling platforms to the shore or to floating distribution points, the connection is performed through very long pipelines, with steep variations in temperature profile and pipe inclination (Figure 5).

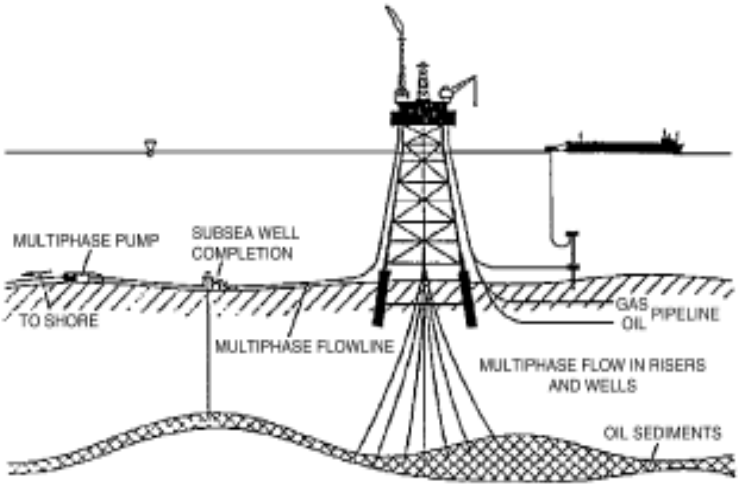

Figure 5: Multi-phase flow in oil production (Hewitt, 2005)

In the nuclear field, usually, the heat extracted from the nuclear reactor core is used to generate water vapor to drive a turbine-generator conventional system able to produce electric power.

Here the presence of a vapor-liquid two-phase flow has to be analyzed in depth and the knowledge of its behavior has high priority during the assessment of normal operating conditions or accidental transients in order to guarantee the safe and efficient operation of all power plants (Figure 6).

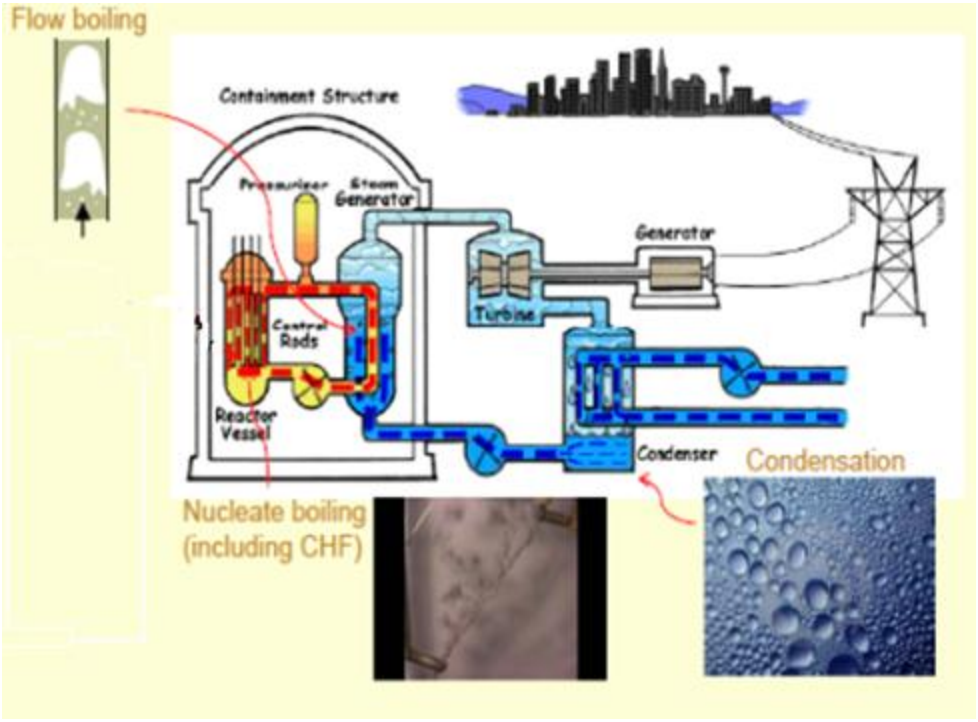

Figure 6: Two-phase flows in nuclear power plants

When two or more phases flow inside a duct, the problem of the determination of the location of their interfaces is faced; in fact, as already said, they cannot be a priori determined because they are part of the solution itself.

In the analysis of a single phase flow the knowledge of geometrical parameters that describe its flowing in the pipe, i.e. its interaction with the pipe wall, enables the calculation of the velocity distributions, the shear stresses, the pressure drops and the other relevant parameters.

Instead, in presence of two or more phases flowing together, all the flow properties (shear stresses, pressure drop, velocity profiles, etc.) are necessary to find the distribution of each phase in the pipe. Obviously, the phases distribution in the pipe cross section influences, at the same time, all the other flow properties.

A special role is played by the velocities with which, for instance, the two phases flow. The gas phase usually flows faster in the axial direction and this

fact determines an axially varying holdup because of waves, i.e., varying gas phase volume fraction, often evaluated quantitatively by void fraction.

The different distribution of the gas phase in the control volume, as described in experimental observations, determines the distinction among different flow patterns.

The difficulties in the prediction of phase distribution in the pipe is, then, transposed to the problem of local flow patterns prediction for each multiphase flow condition.

2.2 Typical Two-Phase Flow Patterns

A two-phase gas-liquid flow consists of two phases interacting while distributed in complex geometries that change in space and in time. These configurations are called flow patterns or flow regimes, they represent the most commonly encountered gas-liquid distribution and their description could be simplified focusing on few cases with similar configurations.

In experimental gas-liquid flow observations, by varying the gas or the liquid velocity, a large number of flow patterns can be defined. Pipe inclinations, downward or upward, may change the flow patterns occurrence.

The most widely accepted flow pattern definitions adopted for horizontal pipes are presented below and in Figure 7.

- Stratified flow: at low liquid and gas flow rates, gravitational effects cause the total separation of the two phases. The liquid flows along the bottom of the tube and the gas flows on the top with a smooth interface. If the gas velocity is increased, the interfacial shear forces increase, rippling the liquid surface and producing a wavy interface.

- Intermittent-slug flow: at slightly higher gas and liquid flow rates, the stratified liquid level grows and becomes progressively stratified-wavy, a transition regime between stratified and slug flow, until the liquid blocks the whole cross-section of the pipe. The “slug” or “plug” of liquid is then accelerated by the gas flow. An elongated gas bubble moving over a thin liquid film exists intermittently together with the slug of liquid.

- Dispersed-bubble flow: at high liquid flow rates and for a wide range of flow rates, small gas bubbles are dispersed throughout a continuous liquid phase. The buoyancy makes the bubbles to accumulate in the upper part of the tube.

- Annular flow: at a high gas flow rates, the gas creates a ring or annulus of liquid around the inside of the tube which, due to gravity, is thicker

at the bottom. Some liquid may also be entrained in the gas core as small-dispersed droplets.

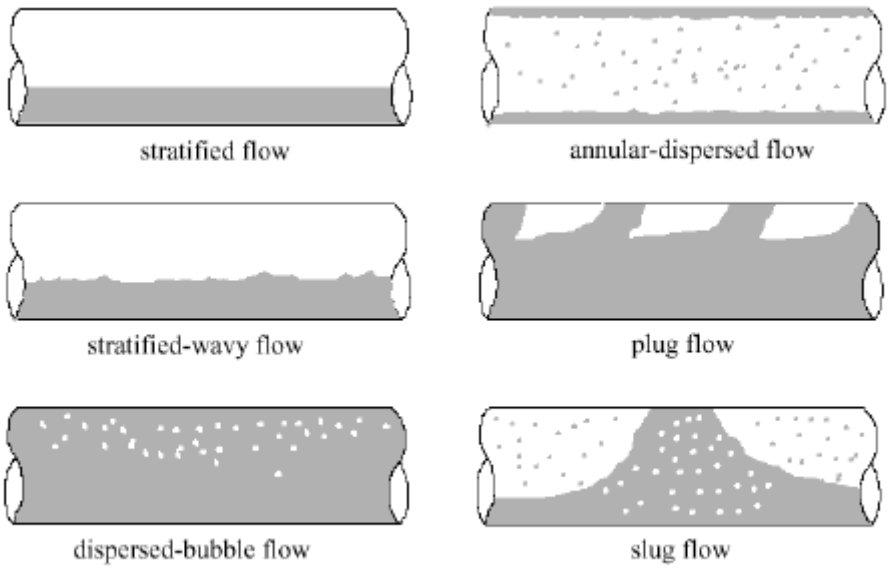

Figure 7: Flow pattern regimes in horizontal two-phase flow (Saha, 1999)

Each one of the flow patterns presented has a great number of possible sub-regimes before the transition to the neighboring flow regime; but it is often necessary a simplification in order to obtain an analytical representation.

In literature, several flow regime maps have been presented by Mandhane et al., (1974), Figure 8 and Table 1, Taitel and Dukler, (1976), Barnea, (1987), Petalas and Aziz, (1998), in order to define flow regime transition rules.

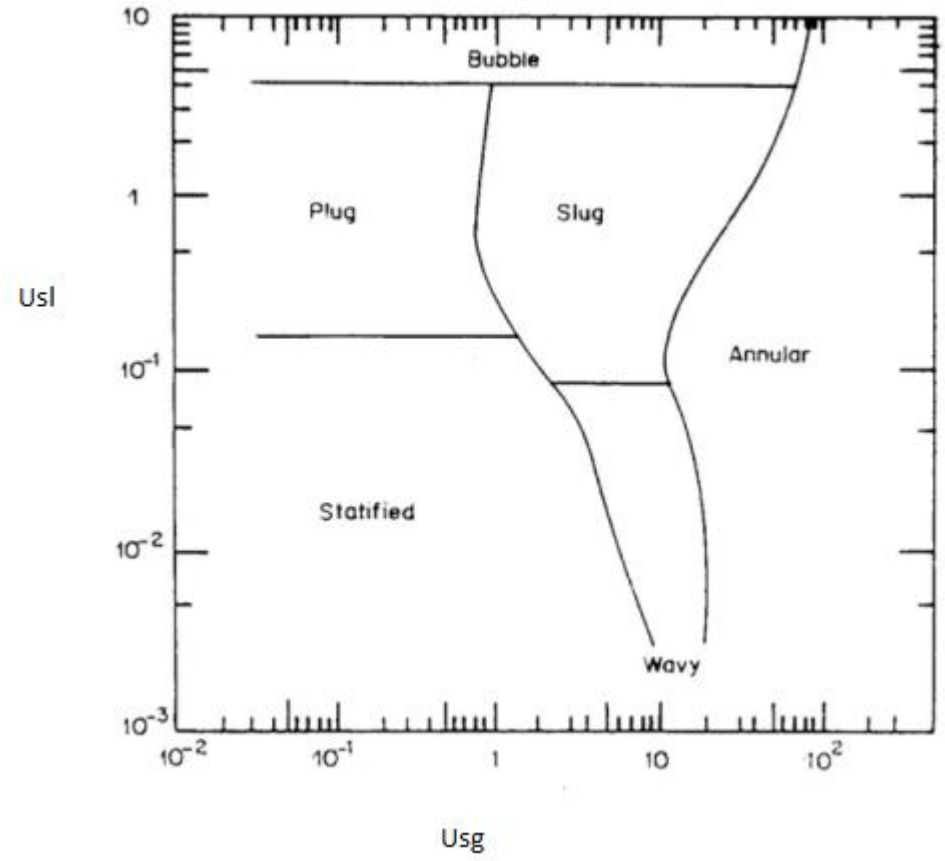

Figure 8: Mandhane, 1974 flow map

Parameters	Variation boundaries
Pipe diameter	12.7 – 165.1 [mm]
Liquid density	705 – 1009 [kg/m3]
Gas density	0.8 – 50.5 [kg/m3]
Liquid viscosity	$3*10^{-4}$-$9*10^{-2}$ [Pa s]
Gas viscosity	10^{-5}-$2.2*10^{-5}$ [Pa s]
Surface tension	24-103 [mN/m]
Liquid superficial velocity	0.09-731 [cm/s]
Gas superficial velocity	0.04-171 [m/s]

Table 1: Mandhane, 1974 flow map validity domain

But it is since the work of Taitel and Dukler, (1976) that **a systematic approach to the physical modeling of flow pattern transitions** was firstly attempted for horizontal flow. The same did few years later Taitel et al., (1980) in the case of vertical flow.

They remarked that physical models of various flow patterns developed to predict pressure losses and liquid holdup should also be able to define the boundaries of each flow pattern. So, Taitel and Dukler, (1976) proposed a complete flow map, in Figure 9, for horizontal flow, where the transition

criteria between flow patterns are ruled by different expressions, numbered from 1 to 4 and described below.

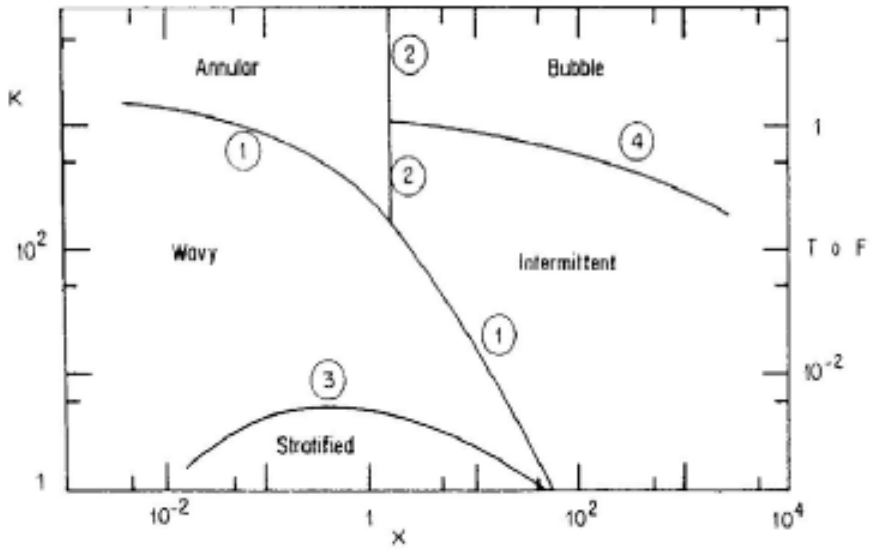

Figure 9: Theoretical flow map (Taitel and Dukler, 1976)

Taitel and Dukler, (1976) elaborated, in fact, the equilibrium stratified flow regime momentum balance equations of both gas and liquid in a dimensionless form by dividing all the terms by $(dP/dx)_{GS}$ which represents the pressure losses in the gas phase:

$$X^2 f_1(h_L/D) - f_2(h_L/D) - 4Y = 0 \qquad (1)$$

where $f_1(h_L/D)$ and $f_2(h_L/D)$ are functions of the dimensionless liquid height h_L/D.

The variables X^2 and Y are equal to $X^2 = \frac{(dP/dx)_{SL}}{(dP/dx)_{SG}}$ and $Y = \frac{(\rho_L - \rho_G)g \sin\beta}{(dP/dx)_{SG}}$ and they will be used in further definitions.

With reference to Figure 9, the curve 1) describes the relation between X and a Froude number described below:

$$Fr = \sqrt{\frac{\rho_G}{\rho_L - \rho_G}} \frac{U_{SG}}{\sqrt{Dg \cos\theta}} \qquad (2)$$

the curve 2) is defined by a constant value of X; the curve 3) describes the value of K as a function of X:

$$K = \left[\frac{\rho_G U_{SG}^2 U_{SL}}{(\rho_L - \rho_G) g \nu_L \cos \vartheta} \right]^{1/2} \tag{3}$$

in curve 4) T is equal to:

$$T = \left[\frac{(dP/dx)_{SL}}{(\rho_L - \rho_G) g \cos \vartheta} \right]^{1/2} \tag{4}$$

and D, ϑ, P, x, ρ_G, ρ_L, g, ν_L are respectively the pipe diameter, the pipe inclination, the pressure, the Cartesian coordinate parallel to the flow direction, the gas density, the liquid density, the acceleration gravity, the kinematic liquid viscosity. U_{SG} and U_{SL} are the superficial gas and liquid velocities respectively. The authors plotted for the first time, for each value of (h_L/D), the pair $X-Y$ that satisfy the equation (1), see Figure 10.

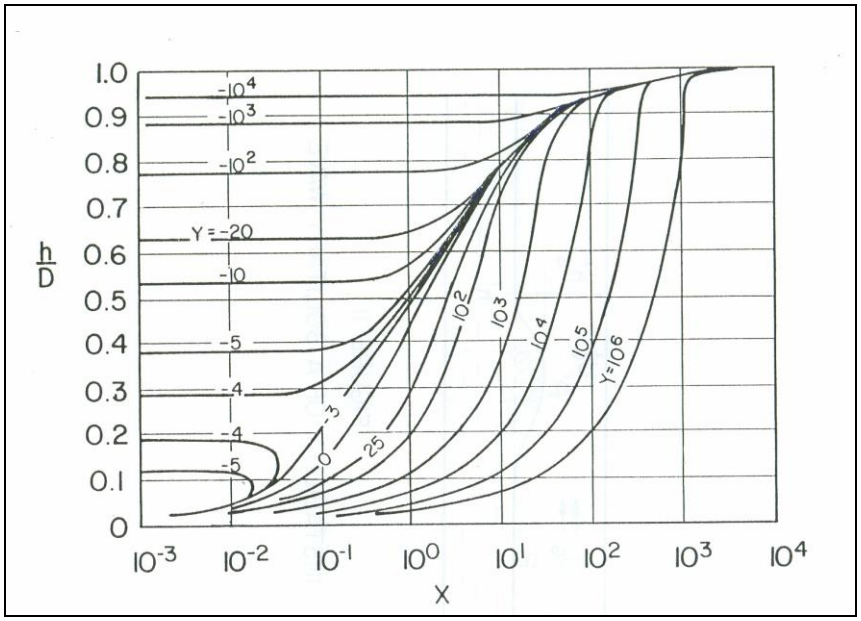

Figure 10: Liquid Height in Stratified Flow by Taitel and Dukler, (1976)

In Figure 11 the map proposed by Taitel and Dukler, (1976) is presented enriched by some pictures from experimental observations (http://www.Termopedia.com).

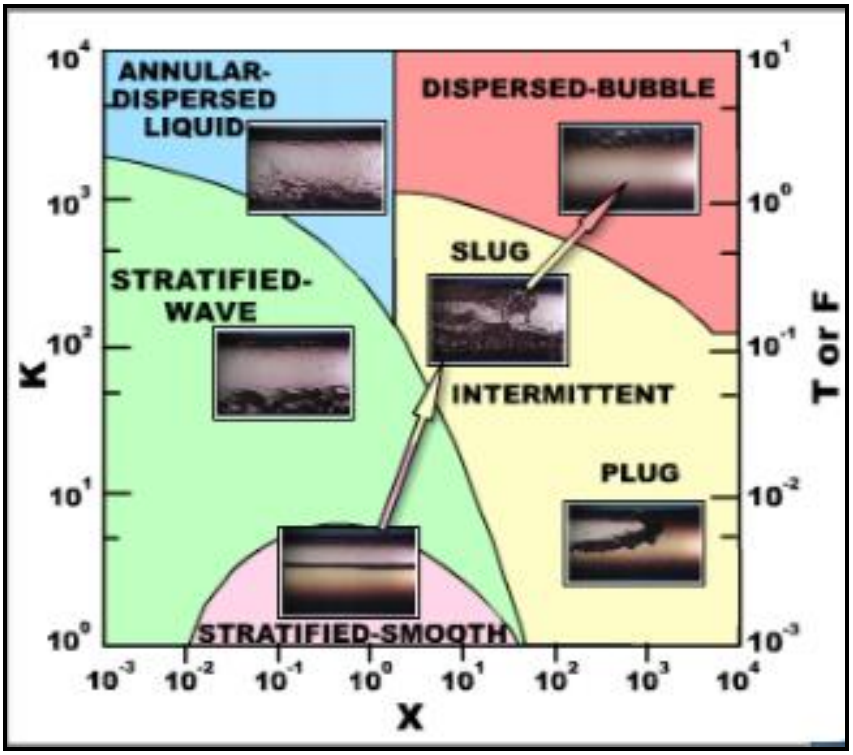

Figure 11: Taitel and Dukler flow map
(from http://www.Termopedia.com)

Taitel and Dukler associated the transition from the stratified flow pattern with the growth of a finite disturbance at the gas-liquid interface and they stated that, if the liquid level is sufficiently higher than a range of values between 0.35 and 0.5), slug flow will be the stable flow pattern; otherwise, only large disturbance waves will be formed and the two phases arrange themselves in an annular-like flow pattern.

More details on the stratified, stratified-wavy flow pattern and the departure mechanisms from it to other flow patterns will be presented in next sections.

2.3 Review of two-phase flow models

A brief review of the most important two-phase flow models is here referred to one-dimensional two-phase flow in pipes, for which multiple examples in real life industrial applications have been already given in previous section (flow of oil and gas in a pipeline, flow of water and steam in nuclear reactor, etc.).

In this section the review will focus on the existing approaches to two phase flow analysis in order to create the basis for further discussions on the "four-field" model of the MAST code, described in detail in Chapter 3.

The major difficulties in the description of, at least, two phases flowing together in a pipe are linked to the presence of their interfaces. An interface

defines the boundaries with which the phases can communicate each other mass, momentum and energy.

The behavior of the entire flow can vary considerably across an interface. Despite the apparent regular organization of phases into flow regimes or flow patterns, where a sort of simplification of the average interface could be done to make easier their analytical description, the interfaces themselves can fluctuate widely in space and time and they appear to have unbounded degrees of freedom.

A good set of mathematical governing equations enables the description of the two-phase flow systems, if accurately solved by numerical techniques, and the investigation and prediction of mean flow features, with as limited as possible uncertainties in their specifications.

An important role is played by the chosen physical model that is the basis for the definition of the system of equations. Often experience and validation only could provide the needed verification because the real interactions between phases, e.g., in a crude oil transportation pipeline, are of great complexity to be analytically predicted.

In particular, this is true for time-dependent phenomena inside long transportation pipeline where stratified flow may abruptly alternate to slug or annular flow.

A mathematical model should have a generic formulation in order to predict different complex behavior and to be collected into a fully comprehensive numerical resolution method.

During the last decades it was found that, to be able to fulfill these requirements, the mathematical model must be written for the two phases as they are two independent "fields"; if for each field a separate set of balance equations is written, it takes the name of "two-fluid model". Simpler representation, from an analytical point of view, is offered by the so called "mixture models" (Homogeneous Equilibrium Model (HEM), Drift-Flux Model (DFM)) with which only highly coupled gas-liquid flow conditions can be represented.

The "two-fluid model" approach, with separate continuity and momentum equations for each phase and two independent velocity fields in its formulation, has been developed to properly take into account the dynamic interactions between phases. It has been demonstrated that a two-fluid model can be more useful to the analyses of wave propagation (Liao et al., 2008) and flow regimes identification (Kawaji and Banerjee, 1987).

In fact, if the two phases are weakly coupled so that the waves can propagate in each phase with different velocities, the two-fluid model should be used to

study these phenomena. The analysis of the flow regimes, can be explained by the fact that changes between flow patterns occur mainly due to the instabilities at interfaces and to interfacial momentum transfer because they govern the dynamics between the phases (Omgba-Essama, 2004).

More detailed information and a review of the major differences among two-phase flow modes will be presented below, starting from the most detailed one.

2.3.1. General presentation of two-fluid model governing equations

In the two-fluid model, the separate phase conservation equations are based on an averaging procedure that allows both phases to co-exist, according to a sort of probability of being in the control volume, and that leads to the definition of the local instantaneous void fraction.

The phases are then seen from an Eulerian point of view and for each of them local average are defined quantities at each point of the computed space. The phases interact with each other through their interfaces. For instance, if the gas has a higher velocity then the liquid, a shear force (drag force) acting on the liquid will appear at the interface. An opposite drag force exerted by the liquid on the gas is then produced.

The phases exchange in this way mass, momentum and energy through their interfaces but, even if the presence of interfaces has been taken into account formally in the equations, after the averaging procedure information about interface properties is lost.

In this way, the description of detailed phenomena of each phase could not be obtained except by correlations, often called closure laws added to the system of equations.

Several authors (Ishii, 1975; Drew, 1983; Daniels et al., 2003, Zuber, 1964, Yadigaroglou and Lahey, 1976) proposed different versions of this "six-equation" model that has all balance equations defined independently for each of the two phases.

Here the volume averaged derivation of balance equations for a two-phase flow in a duct (Banerjee and Chan, 1980) are presented, associating the variables to the flow situation in Figure 12.

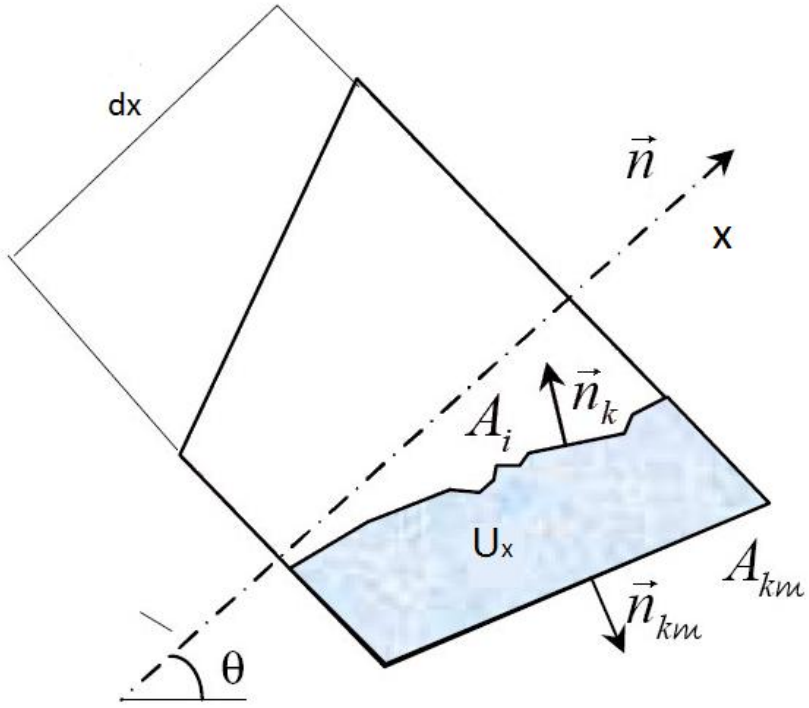

Figure 12: General representation of two fluids flowing in a pipe

The generic balance equation for the general property φ_k of phase k has the form:

$$\frac{\partial}{\partial t}(\rho_k \varphi_k) + \nabla \cdot (\rho_k \varphi_k \vec{U}_k) + \nabla \cdot \vec{J}_{\varphi,k} = \rho_k S_{\varphi,k} \tag{5}$$

where $\vec{J}_{\varphi,k}$ and $S_{\varphi,k}$ represent the superficial diffusive flux and the source term.

In order to obtain a volume averaged set of balance equations, they need to be integrated over the volume $V_k(z,t)$. The equations should be manipulated making use of the Gauss' theorem and the Liebnitz's rule in order to interchange derivative and volume integral operations.

In case of **a flow in a pipe in isothermal conditions**, where the axial component x is the only important one, the following equations can be obtained for the phase k:

Mass Conservation equation

$$\frac{\partial}{\partial t}(\varepsilon_k \rho_k) + \frac{\partial}{\partial x}(\varepsilon_k \rho_k U_k) = 0 \tag{6}$$

Momentum Conservation Equation

$$\frac{\partial}{\partial t}(\varepsilon_k \rho_k U_k) + \frac{\partial}{\partial x}(\varepsilon_k \rho_k U_k^2) = -\varepsilon_k \frac{\partial P_k}{\partial x} - \Delta P_{ki} \frac{\partial \varepsilon_k}{\partial x} + \frac{\partial}{\partial x}(\varepsilon_k \tau_k) + (\frac{S_{kw}\tau_{kw}}{A}) + (\frac{S_{ki}\tau_{ki}}{A}) - \varepsilon_k \rho_k g \sin\theta \quad (7)$$

where ε_k, ρ_k, U_k, P_k are respectively the volumetric fraction, the density, the velocity and the pressure of phase k.

ΔP_{ki} is known as the interfacial pressure difference. τ_k is the viscous stress. S_{kw} and τ_{kw} are the phase k-wall contact perimeter and stress. S_{ki} and τ_{ki} are the interfacial perimeter and the interfacial stress.

Globally the two terms on the left hand side (l.h.s.) of Eq. (7) are respectively the rate of change and the axial advection; on the right hand side (r.h.s.) there are respectively the phase k pressure gradient, the interfacial pressure term, the wall pressure term, the wall friction, the interfacial friction, the body force.

Additional contributions should be included in the (r.h.s) of Eq. (7) in case of highly non-homogeneous gas-liquid flow in order to better describe phenomena at the interface due to interfacial forces F_{ki}.

In particular, in the most accurate presentations of two-fluid model approaches, the interfacial viscous term, or drag, F_{Di} is only one of the postulated contribution to interfacial momentum together with the virtual mass term F_{vmi} the Basset F_{Bi}, the lift F_{Li} and the collision forces F_{ci}.

Each of the mentioned forces should be provided to the system of equations by a closure law. These closure laws will be presented in the following section.

2.3.1.1. Constitutive equations

The closure laws are needed to substitute the unknown terms in the balance equations with known correlations, enabling the prediction of the missing values; but they have limited validity in term of phase pressures, velocities, void fractions, etc..

Several authors, depending on the operating conditions they are working with, propose their own set of closure laws.

In particular, in the case of the two fluid model, for instance in its formulation with the mass, momentum and energy balance equations, called the six-equation model, there are 14 unknowns, 8 variables (ε_k, ρ_k, U_k, P_k) and several closure laws concerning the interfacial pressure difference P_{ki}, the shear stresses at the wall and at the interface (F_{kw}, F_i), the mass transfer rates, the heat transfer coefficients and the thermodynamic state relationships

Closure laws for phase pressure terms

The pressure terms have been defined in literature in different ways. In particular, three formulations are available:

$$\varepsilon_k \frac{\partial}{\partial x} P_k + \Delta P_{ki} \frac{\partial \varepsilon_k}{\partial x} = \frac{\partial (\varepsilon_k P_k)}{\partial x} - P_{ki} \frac{\partial \varepsilon_k}{\partial x} = \frac{\partial (\varepsilon_k \Delta P_{ki})}{\partial x} + \varepsilon_k \frac{\partial P_{ki}}{\partial x} \qquad (8)$$

where $\Delta P_{ki} = P_k - P_{ki}$ is often called as the interfacial pressure difference.

So, the unknown variables to be defined through closure relation are P_k and P_{ki} with k = G, L.

Speaking about the **phase pressure** P_k, the first and easier approach, among the existing models, is the single pressure model. It assumes that the same pressure is shared between the two phases $P_G = P_L = P_k(\rho_k)$.

In case of highly uncoupled phases, a different formulation could be necessary and a two-pressure model is then introduced: examples of closure relations are proposed by several authors (Ransom and Hicks, 1984; Glimm et al., 1999; Saurel and Abgrall, 1999; Cheng et al., 2002). Even if the most widely used approach is still the single pressure one.

Large investigation efforts have been devoted to the model of the **interfacial pressure** P_{ki} and authors as Barnea and Taitel, (1993) suggested an expression for the stratified flow regime while Drew and Passman, (1999) gave an alternative expression for bubbly flow. Both relations are given as:

$$\begin{cases} P_{Gi} - P_{Li} = \sigma \dfrac{\partial h_L^2}{\partial x^2} & \text{Stratified flow} \\ P_{Gi} - P_{Li} = 2\dfrac{\sigma}{r_B} & \text{Bubbly flow} \end{cases} \tag{9}$$

where σ is the surface tension, h_L is the liquid height and r_B is the bubbles radius.

As it will be explained later on, often the interfacial pressure is assumed to be the same in the liquid and the gas phases; therefore $P_{Gi} = P_{Li} = P_I$.

The **interfacial pressure difference** term, or interfacial pressure difference, represented mostly as $\Delta P_{ki} = P_k - P_{ki}$ is not present in earlier version of two-fluid models, such as TRAC (TRAC-PD2, 1981) and OLGA (Bendiksen et al., 1991).

Nevertheless, its contribution could play an important role in the solution of systems of balance equations wherever the loss of hyperbolicity of the model may relevant in some operating conditions.

So, taking into account this term could enable the accurate analysis of gravity waves and interfacial instability in case of stratified flow. This is the reason why most recent two-fluid codes add the pressure correction term in their formulations.

In literature there are several examples of the representation of this term, but its validity is often flow regime dependent.

The case of the stratified flow is then taken into account and one of the first contributions was proposed by Barnea and Taitel, (1996), who obtained for the gas and the liquid the following formulations for the hydrostatic heads in the liquid and in the gas phase:

$$\begin{cases} \dfrac{\partial \varepsilon_L P_L}{\partial x} = \varepsilon_L \rho_L g \cos\theta \dfrac{\partial h_L}{\partial x} \\ \dfrac{\partial \varepsilon_G P_G}{\partial x} = \varepsilon_G \rho_G g \cos\theta \dfrac{\partial h_G}{\partial x} \end{cases} \tag{10}$$

Similar expressions are proposed also by other authors (Taitel and Dukler, 1976; Barnea and Taitel, 1993; Barnea and Taitel, 1996) and used in two-fluid models; but different versions can be found, too (Lahey and Drew, 1988).

Closure laws at the interface

The **interfacial friction term** F_{ki} has been formulated in order to take into account the stresses acting at the interface between phases. In particular, there are several contributions that merge into this variable, as already said.

In the following a short revision of their meanings and of some closure formulations that exist in literature is presented.

The interfacial shear stress is often presented as the contribution of the **viscous drag at the interface** F_{Di} only and the other terms are neglected.

Several authors define it as the contribution of two independent terms in order to provide reliable values for both separated and dispersed flow patterns.

Often its formulation is highly flow regime dependent. As the example given by Ishii and Mishima, (1984) that suggested the following combination:

$$F_{ki}^{D} = \left\langle -\tau_{ki} \nabla \varepsilon_k \right\rangle_k + \overline{F_{ki}} \tag{11}$$

In this way the authors consider both cases of separated flow, with the first term weighted on the volumetric fraction, and of dispersed flow, with the second term that is the area-averaged particle drag.

For stratified flows the interfacial drag takes the well-known form (Taitel and Dukler, 1976) presented below, where the most important contribution is given by the interfacial shear stress of the gas phase:

$$F_{ki}^{D} = \left\langle -\tau_{ki} \nabla \varepsilon_k \right\rangle_k = -\tau_{Gi} \frac{S_i}{A} \tag{12}$$

Where S_i is the interfacial perimeter and τ_{Gi} is the interfacial shear stress for the gas phase, called in the later on simply τ_i, and authors agree on its representation as follows:

$$\tau_i = \frac{1}{2} f_i \rho_G (U_G - U_L) \left| U_G - U_L \right| \tag{13}$$

The term formally represented through the introduction of ad hoc closure laws is the interfacial friction factor, f_i; there is a great number of correlations for its evaluation, depending on the flow pattern that has to be represented and of the operational conditions.

A brief review of the most important friction factor correlations will be presented in the Chapter 5.

In case of dispersed bubble flow the drag force assumes the meaning classically adopted in fluid mechanics and takes the shape presented below:

$$\overline{F_{Gi}} = \frac{3}{4} \frac{\rho_L \varepsilon_L C_D}{D_B} (\overline{U}_r) \left| \overline{U_r} \right| \tag{14}$$

where C_D is the drag coefficient, D_B the bubble diameter, U_r the relative velocity. The term C_D is represented through multiple possible closure laws is the drag coefficients. A reference paper is by Ishii and Zuber, (1979).

An additional contribution, a term that is part of the interfacial momentum transfer and is called **the virtual mass force,** F_i^v, should be included in the r.h.s of Eq. (7) in case the pressure differences due to relative acceleration between phases with different velocities reaches important values. This term represents the non-viscous behavior of the interfacial forces and is useful to avoid complex eigenvalues in the six-equation two-fluid model when it describes highly non-homogeneous two phase flow conditions.

The virtual mass has been defined in order to complete the interfacial forces when an exclusively algebraic formulation for viscous stress is not sufficient.

The virtual mass term in the phasic momentum equations account for the effect of local mass displacement in the case of a relative acceleration between the two phases.

The existence of such a force was first deduced by Lamb, (1932) for frictionless (irrotational) flows around spheres and it might be generalized with

$$F_i^{\upsilon} \approx f(\varepsilon_G)\rho_m \left\{ \frac{\partial U_G}{\partial t} + U_L \frac{\partial U_G}{\partial x} - \frac{\partial U_L}{\partial t} - U_G \frac{\partial U_G}{\partial x} \right\} \tag{15}$$

ρ_m is the mixture density.

Even if the discussion on the formulation of this term is open, the expression by Drew et al., (1979) which offers the most general form containing first order space and time derivatives is often taken as reference:

$$F_i^{\upsilon} = c_{vm}\rho_L \varepsilon_L \left\{ \frac{\partial U_r}{\partial t} + U_L \frac{\partial U_G}{\partial x} - U_G \frac{\partial U_L}{\partial x} - (d-1)U_r \frac{\partial U_r}{\partial x} \right\} \tag{16}$$

where U_r is the relative velocity.

This expression still includes two open parameters: d, introduced by Drew, accounts for the gas volume fraction and varies from 2, if ε_G tends to zero, and 0, if ε_G tends to 1, and it makes the expression changing the sign if there is pure gas or pure liquid; the factor c accounts for the actual spatial phases distributions.

For instance in RELAP5, (1984) d is set to 1. Several authors personalize to their field of application the formulation for virtual mass term because, even if there is a common agreement about the need for derivative terms in the interfacial momentum coupling expression taking into account non viscous effects. Nevertheless, there is at present no way to deduce these terms completely from basic principles and therefore it may not be free from some uncertainties.

The introduction of virtual mass forces only, or pressure correction terms only, does not result in a fully hyperbolic system of equations for all two-phase flow conditions. They should be applied together to extend the validity of the set of equations proposed.

Closure laws at the pipe wall

Concerning **the wall shear stresses** F_{kw}, the stresses acting on the phase at the wall, there are several authors that proposed different methodologies to model

them. The most widely applied formulation, defined for fully developed two-phase flow, is proposed below:

$$F_{kw} = T_{kw} = -\tau_k \frac{S_k}{A} \tag{17}$$

where the S_k is the wetted perimeter of the phase k and τ_k is the shear stress of the same phase.

The closure law requested in this equation is the wall shear stress given as a function of the phase-wall friction factor:

$$\tau_k = \frac{1}{2} f_k \rho_k U_k |U_k| \tag{18}$$

A wide number of different correlations exist in literature to predict the gas- and liquid-wall friction factors; it is a common practice to model the two-phase wall friction factors as a corresponding single-phase one.

Further details will be given about friction factor correlations in Chapter 5.

2.3.1.2. Analysis of the single pressure model peculiarities

To enable the prediction of gas and liquid properties in some two-phase flow patterns, i.e. the investigation of the phenomena characterizing the slug movements in a pipeline with the gas phase undergoing volume changes due to compressibility effects, a general system of four equations based on the two-fluid model approach should be applied.

The easiest formulation of the two-fluid model has equal pressures in the gas and in the liquid phase. Then, after additional simplifying assumptions (immaterial interfaces, and neglecting axial diffusion terms) and several definitions to describe the distribution of the two phases in the control volume, Figure 13, the system of equations is presented below:

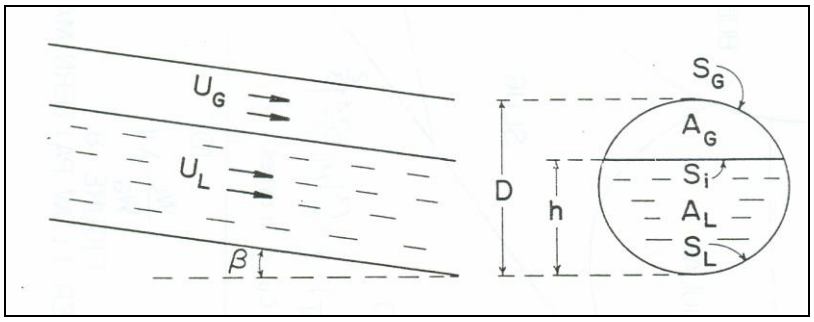

Figure 13: Stratified gas-liquid flow in inclined pipe

Gas and Liquid Mass Conservation Equations:

$$\begin{cases} \dfrac{\partial(\varepsilon_G \rho_G)}{\partial t} + \dfrac{\partial(\varepsilon_G \rho_G U_G)}{\partial x} = \psi_G \\ \dfrac{\partial(\varepsilon_L \rho_L)}{\partial t} + \dfrac{\partial(\varepsilon_L \rho_L U_L)}{\partial x} = -\psi_G \end{cases} \tag{19}$$

Gas and Liquid Momentum Conservation Equations:

$$\begin{cases} \dfrac{\partial}{\partial t}\left(\varepsilon_G \rho_G U_G\right) + \dfrac{\partial}{\partial x}\left(\varepsilon_G \rho_G U_G^2\right) = -\varepsilon_G \dfrac{\partial P}{\partial x} - \dfrac{\tau_G s_G}{A} - \dfrac{\tau_i s_i}{A} + g\varepsilon_G \rho_G \sin\beta + \psi_G U_A \\ \dfrac{\partial}{\partial t}\left(\varepsilon_L \rho_L U_L\right) + \dfrac{\partial}{\partial x}\left(\varepsilon_L \rho_L U_L^2\right) = -\varepsilon_L \dfrac{\partial P}{\partial x} - \dfrac{\tau_L s_L}{A} + \dfrac{\tau_i s_i}{A} + g\varepsilon_L \rho_L \sin\beta - \psi_G U_A \end{cases} \tag{20}$$

where ε_G, ε_L are the gas and liquid volumetric fraction; τ_G, τ_L and τ_i are respectively the wall-gas, wall-liquid and gas-liquid shear stresses; ψ_G is the mass transfer rate from the liquid to the gas. P is the common gas and liquid pressure.

In more complete versions of the liquid phase balance momentum equation the interfacial pressure difference has been taken into account in order to manage hyperbolicity of equations at the margin of the well-posedness of the two-phase

set of balance equations in several operational conditions. Bonizzi, (2003) suggested for the TRIOMPH code the following formulation:

$$P_c \frac{\partial \varepsilon_L}{\partial x} = \rho_L \varepsilon_L g \cos\theta \frac{\partial h_L}{\partial x} \tag{21}$$

Alternative formulations could be found in scientific literature, among the others a possible approach is (Omgba-Essama, 2004):

$$P_c = \rho_L \varepsilon_L g \cos\theta \frac{\partial h_L}{\partial \varepsilon_L} \tag{22}$$

2.3.2. Peculiarities of mixture models: HEM and DRIFT FLUX

The complete two-fluid model discussed above is not needed for many practical applications. In a mixture models, the two-phase conservation equations are combined in single equations for each phase.

In order to obtain the information that is then lost, some empirical correlations relating the phase velocities to each other, or the cross-sectional distribution of velocities and the local void fractions, are needed.

The **Homogeneous Equilibrium Model (HEM)** is a simplified two-phase flow representation to be used in case of highly coupled gas and liquid phases, i.e., during such flow patterns as the bubbly flow. This is a pseudo single-phase formulation that ignores all interfacial transfer processes.

The gas and liquid are not represented as two separate entities with different behavior, and, on the contrary, they are strictly interconnected and phenomena such as wave propagation are not predicted.

However, despite its partial description of two-phase flow phenomena, this modelization enables the simulation of a wide range of situations in many thermal-hydraulic fields.

In particular, several industrial codes applied in the nuclear and oil&gas fields are still based on a HEM model because of its simplicity and applicability to a wide range of operational conditions, without the important constraints imposed by the need of optimized numerical methods: ill-posedness and non-conservative flux terms do not occur in the HEM model. For these reasons it is a good choice for the development of numerical methods used to handle compressible flow equations and shock waves.

Here, the two phases are in equilibrium of momentum and they move at the same mixture velocity, U_m. In practice they are combined in the same momentum balance equation.

The two equation model for one-dimensional isothermal flow is presented below:

Gas and Liquid Mass Conservation Equations

$$\begin{cases} \dfrac{\partial(\varepsilon_G \rho_G)}{\partial t} + \dfrac{\partial(\varepsilon_G \rho_G U_M)}{\partial x} = 0 \\ \dfrac{\partial(\varepsilon_L \rho_L)}{\partial t} + \dfrac{\partial(\varepsilon_L \rho_L U_M)}{\partial x} = 0 \end{cases} \tag{23}$$

$$\frac{\partial \rho_m}{\partial t} + \frac{\partial(\rho_m G_m)}{\partial x} = 0 \tag{24}$$

Gas and Liquid Momentum Conservation Equations

$$\frac{\partial \rho_m U_m}{\partial t} + \frac{\partial(\rho_m U_m^2 + P)}{\partial x} = F_W - \rho_m g \sin\theta \tag{25}$$

where ρ_m is the mixture density, G_m the mass flow rate and the F_w mixture wall shear stress:

$$\rho_m = \{\rho_G \varepsilon_G\} + \{\rho_L \varepsilon_L\} \tag{26}$$

$$G_m = \{\rho_G \varepsilon_G U_G\} + \{\rho_L \varepsilon_L U_L\} \tag{27}$$

$$F_w = -\frac{1}{2D} f_w \rho_M U_M |U_M| \tag{28}$$

The **Drift Flux Model (DFM)** is a mixture model but capable of higher detail than the HEM model. In fact it takes into account partially mechanical non-equilibrium between the phases and a DRIFT FLUX algebraic relation is then added.

The gas is hypothesized to have a slightly different velocity than the mixture one, called “drift velocity” and added to the volumetric centre of the mixture.

In particular, the drift velocity is geometry and flow regime dependent. It is easier to use a semi-empirical relationship for the relative motion between phases rather than use the full two-fluid model.

The relative velocity is expressed in terms of the mixture center of mass velocity and the vapor drift velocity.

There are several possible formulations for the DRIFT FLUX model, depending on the specified form of the drift velocity used.

For example, in one of the most important formulation of Ishii (1977), the drift velocity has been defined in term of a mean value:

$$V_j = \frac{\langle U_{SG} \rangle}{\langle \varepsilon \rangle} - \langle j \rangle \tag{29}$$

where U_{SG} is the volumetric flux of the gas, U_{SL} is the volumetric flux of the liquid and $j = U_{SG} + U_{SL}$.

The mean drift velocity has been then related to the local drift velocity with the following relation:

$$V_{gj} = \frac{U_G}{\varepsilon} - j \tag{30}$$

$$\overline{V_{gj}} = \left\langle \frac{\varepsilon (j + V_{gj})}{\langle \varepsilon \rangle} - j \right\rangle = \langle\langle V_{gj} \rangle\rangle + (C_0 - 1)\langle j \rangle \tag{31}$$

where the double parenthesis $\langle\langle \ \rangle\rangle$ represents the void fraction weighted mean value, i.e. $\langle\langle F_k \rangle\rangle = \frac{\langle \varepsilon_k F_k \rangle}{\varepsilon_k}$ and $C_0 = \frac{\langle \varepsilon_j j \rangle}{\langle \varepsilon \rangle \langle j \rangle}$.

Finally, the resulting cross sectional averaged void fraction is then obtained $\langle \alpha \rangle = \frac{\langle U_{SG} \rangle}{C_0 \langle j \rangle + \langle\langle V_{gj} \rangle\rangle}$ (32)

Other earlier drift flux models were proposed by Zuber and Findlay, (1965) and Wallis, (1968). They differ from each other in particular for of the averaging functions and for the distribution effects accounting.

A further approach is the void-quality relationship of Lockhart-Martinelli (Wallis, 1968). It links the void and the quality through an algebraic correlation called the Martinelli parameter obtained with an empirical approach:

$$\langle \alpha \rangle = \left(X_{tt}^{0.8} \right)^{-0.378} \tag{33}$$

where the Martinelli parameter is presented below:

$$X_{tt} = \left[\frac{(\partial P / \partial x)_L}{(\partial P / \partial x)_G} \right]^{1/2} = (\frac{\rho_G}{\rho_L})^{1/2} (\frac{\mu_L}{\mu_G})^{n/2} \left(\frac{1 - \langle x \rangle}{\langle x \rangle} \right)^{\frac{2-n}{2}} \tag{34}$$

where $n = 0.2$.

2.3.3. Ill-posedness and hyperbolicity analysis of presented models

Before trying to reach the solution through linearization and numerical integration of the previously presented two-phase flow model equations, the attention should be focused on their mathematical classification and on the existence and validity of their solution.

In fact, the systems of equations presented before for the Single Pressure Two-Fluid and Homogeneous Equilibrium Model-HEM models are examples of hyperbolic problems, at least under some operation conditions. The HEM, in particular, is always hyperbolic and with real eigenvalues under all operating conditions. This is not the case for the Two-Fluid model, as described hereafter.

The purpose of determining the parameter ranges in which the governing equations of a physically plausible scenario are hyperbolic, coincides with the answer to the question if the model satisfy the Cauchy initial-value problem formulation and it possesses a unique and stable solution in space and time (well-posed problem).

Mathematically, the Cauchy problem of a model is presented by:

$$\begin{cases} U_t + J^i U_i = S(U) \quad for\ t \geq 0 \\ U(t=0,x) = f(x) \end{cases} \tag{35}$$

where $J^i U_i$ is the Jacobian matrix (m x m).

It is said to be well-posed if for every $f \in C^\infty(x)$ there exists a solution $U(t,x) \in C^\infty(t,x)$ that is unique and stable (i.e. depending continuously on the values of initial data given) and such that

$$\|U(t,x)\| \leq Ke^{\alpha t} \|f(x)\| \tag{36}$$

where K, α are independent of f, (Dinh et al., 2003).

This condition reflects the well-posedness in Hadamard's sense: the solutions are bounded and velocities of information propagation are finite.

The "standard" single pressure separated (i.e. non homogeneous) two-fluid model suffers from ill-posedness problem (Jones and Prosperetti, 1985), (Ramshaw and Trapp, 1978).

In fact, when the relative velocity between the liquid and gas exceeds a critical value, the governing equations do not possess real characteristics as it will be seen below.

To start this analysis, the system of equation should be described in matrix form, such as

$$M_A \frac{\partial \varphi}{\partial t} + M_B \frac{\partial \varphi}{\partial x} = S \tag{37}$$

where M_A and M_B are the matrices of coefficients functions of the flow properties and the vector φ represents all the dependent flow variables and S is the source term for the interfacial and wall mass and momentum contributions.

An always affordable tool to analyze the stability, or ill-posedness, of a system of equations is the characteristic analysis that is the calculation of eigenvalues in order to state the dependence of the solution on the prescribed initial data.

The problem is then reduced to the investigation of the equation:

$$\det(M_B - \lambda M_A) = 0 \tag{38}$$

with λ real eigenvalue.

2.3.3.1. Characteristic analysis of the two-fluid model

The characteristic analysis of the separated two-fluid model for incompressible gas phase can be performed. In this case the result will be more complex with a flow conditions dependent hyperbolicity.

The characteristic vector considered is $\varphi^T = (P, \varepsilon_G, U_L, U_G)$

$$M_A = \begin{bmatrix} 0 & \rho_L & 0 & 0 \\ 0 & \rho_G & 0 & 0 \\ 0 & 0 & \varepsilon_L \rho_L & 0 \\ 0 & 0 & 0 & \varepsilon_G \rho_G \end{bmatrix} \tag{39}$$

$$M_B = \begin{bmatrix} 0 & \rho_L U_L & \varepsilon_L \rho_L & 0 \\ 0 & U_G \rho_G & 0 & \varepsilon_G \rho_G \\ \varepsilon_L & \varepsilon_L \rho_L g \cos\theta \dfrac{dh}{d\varepsilon_G} & \varepsilon_L \rho_L U_L & 0 \\ \varepsilon_G & \varepsilon_G \rho_G g \cos\theta \dfrac{dh}{d\varepsilon_G} & 0 & \varepsilon_G \rho_G U_G \end{bmatrix} \tag{40}$$

The characteristic polynomial is obtain again with the condition $\det(M_B - \lambda M_A) = 0$ and has the form:

$$\begin{aligned} &\det(M_B - \lambda M_A) = \varepsilon_L(-\varepsilon_L \rho_L)\left[\varepsilon_G \rho_G^2 (U_G - \lambda)^2 - \varepsilon_G^2 \rho_G^2 g \cos\theta \frac{dh}{d\varepsilon_G}\right] - \\ &\varepsilon_G(-\varepsilon_G \rho_G)\left[-\varepsilon_L \rho_L^2 (U_L - \lambda)^2 - \varepsilon_L^2 \rho_L^2 g \cos\theta \frac{dh}{d\varepsilon_G}\right] = -\varepsilon_L^2 \varepsilon_G \rho_L \rho_G^2 (U_G - \lambda)^2 + \\ &\varepsilon_L^2 \varepsilon_G^2 \rho_L \rho_G^2 g \cos\theta \frac{dh}{d\varepsilon_G} - \varepsilon_L \rho_L^2 \varepsilon_G^2 \rho_G (U_L - \lambda)^2 - \varepsilon_L^2 \varepsilon_G^2 \rho_L^2 \rho_G g \cos\theta \frac{dh}{d\varepsilon_G} = \\ &-\varepsilon_L^2 \varepsilon_G \rho_L \rho_G^2 (U_G^2 - 2\lambda U_G + \lambda^2) - \varepsilon_L \rho_L^2 \varepsilon_G^2 \rho_G (U_L^2 - 2\lambda U_L + \lambda^2) \\ &+ \varepsilon_L^2 \varepsilon_G^2 \rho_L \rho_G (\rho_G - \rho_L) g \cos\theta \frac{dh}{d\varepsilon_G} \end{aligned} \tag{41}$$

With the following substitutions:

$a = -(\varepsilon_L \rho_L^2 \varepsilon_G^2 \rho_G + \varepsilon_L^2 \varepsilon_G \rho_L \rho_G^2)$; $b = +2(\varepsilon_L \rho_L^2 \varepsilon_G^2 \rho_G U_L + \varepsilon_L^2 \varepsilon_G \rho_L \rho_G^2 U_G)$ and

$$c = -\varepsilon_L \rho_L^2 \varepsilon_G^2 \rho_G U_L^2 - \varepsilon_L^2 \varepsilon_G \rho_L \rho_G^2 U_G^2 + \varepsilon_L^2 \varepsilon_G^2 \rho_L \rho_G (\rho_G - \rho_L) g \cos\theta \frac{dh}{d\varepsilon_G}$$

and so, the hyperbolicity of the system of equations is obtained as long as the following equation has real roots

$a\lambda^2 + b\lambda - c = 0$ and so if $\Delta = b^2 - 4ac > 0$, that brings to

$$\Delta = -4\varepsilon_L^3\varepsilon_G^3\rho_L^3\rho_G^3(U_G - U_L)^2 + 4(\varepsilon_L\rho_L^2\varepsilon_G^2\rho_G + \varepsilon_L^2\varepsilon_G\rho_L\rho_G^2)\varepsilon_L^2\varepsilon_G^2\rho_L\rho_G \cdot (\rho_G - \rho_L)g\cos\theta\frac{dh}{d\varepsilon_G} > 0 \quad (42)$$

requiring:

$$-\varepsilon_L^3\varepsilon_G^3\rho_L^3\rho_G^3(U_G - U_L)^2 + (\varepsilon_G\rho_L + \varepsilon_L\rho_G)\varepsilon_L^3\varepsilon_G^3\rho_L^2\rho_G^2 \cdot (\rho_G - \rho_L)g\cos\theta\frac{dh}{d\varepsilon_G} > 0 \quad (43)$$

that is clearly coincident with the well known expression that states the condition for the stability against **Kelvin-Helmoltz instabilities** growing and the limit for hyperbolicity:

$$(\rho_G\rho_L)(U_G - U_L)^2 < (\varepsilon_G\rho_L + \varepsilon_L\rho_G)(\rho_G - \rho_L)g\cos\theta\frac{dh}{d\varepsilon_G} \quad (44)$$

that is

$$(U_G - U_L)^2 < (\frac{\varepsilon_G}{\rho_G} + \frac{\varepsilon_L}{\rho_L})(\rho_G - \rho_L)g\cos\theta\frac{dh}{d\varepsilon_G} \quad (45)$$

This expression helps to understand why several authors (Liao et al., 2008; Gidaspow, 1974; Ramshaw and Trapp, 1978; Jones and Prosperetti, 1985; Song and Ishii, 2000) stated that the two-fluid model, consisting of two sets of conservation equations for mass and momentum for the gas and the liquid phase (as proposed by Wallis, 1969 and Ishii, 1975) could be an ill-posed one when the relative velocity between the liquid and the gas is greater than a critical value.

The hyperbolicity analysis should then be performed before implementing any two-fluid model in a computer program and, then, before converting it into a numerical form because its limitations in representing the real flow physics in the pipe should be clearly understood.

This critical value of the relative velocity depends on the pipe diameter, gravity, liquid level, etc. and could coincide with the Inviscid Kelvin-Helmoltz (IKH) stability condition in the case of stratified flow (Issa and Kempf, 2003).

Several authors observed that the occurrence of instability could trigger, as it is in real physics (Barnea and Taitel, 1994), the flow regime transition from stratified to slug and annular flow (Brauner and Maron, 1992).

This fact influenced the history of the computational methods proposed since the early beginning and the investigations of many researchers. In fact, different results can be obtained in term of velocities and of magnitude of

instabilities when the same set of equations is discretized with different schemes.

If a numerical scheme, employed to solve the two-fluid model becomes unstable, it may experience instabilities in different conditions than the ones that could be observed in real physical situations. In fact, the growth of numerical instabilities may occur earlier than the ill-posedness conditions, originating a numerical transition between two flow conditions that depends from the discretization method chosen (Liao et al., 2008).

2.3.4. Introduction to the most important numerical methods for flow equations

Once the mathematical model has been defined and analyzed, the approach to the fluid dynamic problem continues with the computation of the discretized equation and the research of the solution.

All conservation equations have a similar structure and may be assessed as a generic transport equation with one transient, one convection, one diffusion and one source term, that has the form:

$$\frac{\partial(\rho\varphi)}{\partial t}+\frac{\partial(\rho U_j\varphi)}{\partial x_j}=\frac{\partial}{\partial x_j}(\Gamma\frac{\partial\varphi}{\partial x_j})+q_\varphi \tag{46}$$

where $\rho, U_j,$ Γ and q_φ are supposed to be known. After the choice of the mathematical model, a suitable discretization method has to be chosen. This is a non linear problem because the velocity fields and the fluid properties are dependent, for instance, on the temperature profile or the turbulence field. However, often iterative methods that are used to solve the obtained discretized equation treat φ as the only unknown and the properties are considered fixed at the previous iteration.

A series of widely accepted methods exist through which the differential equations can be approximated by a system of algebraic equations as a function of the independent variables and of some discrete locations in space and time.

There are several possible approaches for discretization but the most important among them are the finite difference, the finite volume and the finite element ones.

The *finite difference* is the oldest method for the numerical solution of partial differential equations (PDEs) and it is also the simplest one to be used.

The starting point, after the set of conservation equations in differential form, is the definition of the solution domain covered by the discretization grid.

This grid is needed to obtain a discrete representation of the geometric domain on which the problem is to be solved, defining through the creation of nodes and boundaries the calculation location.

When more equations have to be solved on a same domain, it is possible that different discretization grids are used for the different equations. This facilitates the availability of flows or velocities (vector quantities) and density and pressure (scalar quantities) exactly where they are needed in a control volume formulation. Such a grid is often called "*staggered*" grid.

The staggered arrangement, introduced for the first time by Harlow and Welsh, (1965), has the great advantage of strongly coupling the velocity with the pressure field. The pressure is, in a staggered grid, calculated at the node located in the control volume center; while the velocity derivatives, as diffusive terms, are calculated on the cell boundaries. This organization helps to avoid some types of convergence problems and oscillations in pressure and velocity fields.

An alternative grid arrangement of variables, older than the staggered grid one, is the choice of storing all the variables at the same grid points, at the center of control volume, CV. Such a grid is called "*collocated*" and it has the great advantage of simplicity, comparing with staggered grid arrangement, in case of complicated solution domains, including discontinuity at boundaries and non-orthogonal grids.

The staggered grid arrangement has been widely adopted since 60's to 80's to solve the difficulties encountered with the pressure-velocity coupling and the occurrence of oscillations in the pressure field that was typical of collocated grids, such as the checkboard pattern in the solution with high decoupling (odd-even) between pressure and velocity.

But since 80's, when more complex geometries were introduced, the simplicity of collocated grids gained popularity. Its renaissance was confirmed during the same period when improved pressure-velocity coupling techniques were developed to overcome odd-even coupling errors.

For instance, Rhie and Chow, (1983) proposed a new momentum interpolation scheme to evaluate the cell face velocities, adopting the SIMPLE procedure for collocated variables.

Recent evolutions of this first method by Rhie and Chow, especially optimized for compressible two-fluid models, are the so-called Advection Upwind Splitting Methods (AUSM). Among them the AUSM+ was optimized and validated for the application to all scale of Mach number flows (Paillère et al., 2003; Nerinckx et al., 2004) through the implementation of special preconditioning strategies in case of low Mach numbers.

To solve the *incompressible standard two-fluid model* equations, the finite difference linearization methods together with a Newton iteration are commonly used (Liles and Reed, 1978; Mahaffy, 1982). But in industrial applications the complexity associated with the Jacobian calculation often reduces the efficiency of this approach.

The numerical solution is not always stable and theories have been introduced to fully understand the origin and the occurrence of this phenomenon.

In particular, for a given spatial mesh size, if an explicit calculation is performed, the time step that can be applied is limited because the time step must not be so large that the pressure wave propagates beyond the spatial domain of influence.

This fact produces some restrictions and the Courant-Friedrichs-Levy, (1928) (CFL) numerical stability condition:

$$\frac{U\Delta t}{\Delta x} \leq 1, \tag{47}$$

where the left hand side is known as the Courant number and U does not contain the sound speed in case of incompressible flow, plays an important role in any system in which information propagates through the calculation nodes to avoid the growing of unphysical instabilities.

As it is clearly explained by Figure 14 referring to an advection equation with forward or backward flow, the values at a certain point depend on the information within some area of the computational domain (shaded zone) as defined by the solution of the partial differential equation (such as advection speed, wave velocity, …). To have a stable numerical method the physical domain of dependency must be inside the computationally used grid points.

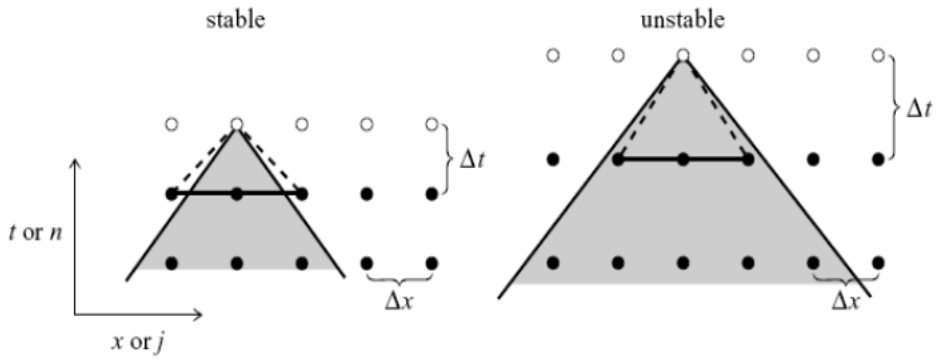

Figure 14: CFL condition representation
(from http://www.math.ucf.edu/~xli/Stability2010.pdf)

The *finite volume* method uses the integral form of the conservation equations, that for the generic flow properties, for steady state conditions, have the form:

$$\int_S \rho\varphi U \cdot n\, dS = \int_S \Gamma grad\varphi \cdot n\, dS + \int_\Omega q_\varphi d\Omega \tag{48}$$

It is of major importance for this model to know the values of the variable in all boundary locations of the CV. Then, values needed in the calculation nodes are obtained by interpolation.

In particular to obtain algebraic equations from surface and volume integrals, quadrature formulae should be used. At the end of the discretization process, in some cases, they coincide with the finite difference ones.

In particular, in order to identify the calculation node, the CV faces close to it and the adjacent calculation nodes, a special notation is adopted where the calculation node is called P and the adjacent calculation nodes are called as the cardinal points in capital letters; the boundary faces with the adjacent CVs are denoted with lower-case letters of the same cardinal point respectively (see Figure 15).

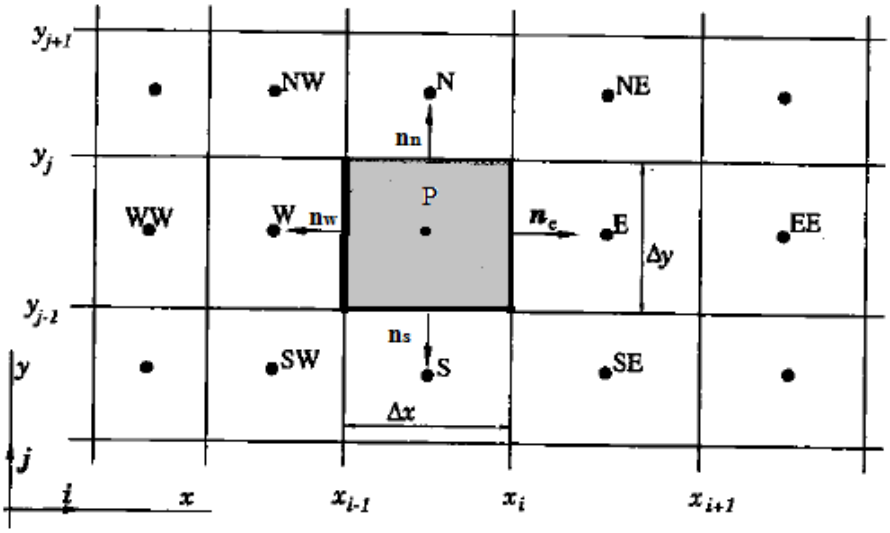

Figure 15: A typical control volume in a Cartesian 2D domain and the notation used to characterize the discretization grid

The upwind interpolation scheme approximates the variable on the basis of the node upstream, solution that is equivalent to the backward difference approximation:

$$\varphi_e = \begin{cases} \varphi_P \ if \ (U \cdot n)_e > 0; \\ \varphi_E \ if \ (U \cdot n)_e < 0 \end{cases} \tag{49}$$

This approach never gives oscillatory solution but it is numerically diffusive.

Another method is the linear interpolation method to approximate the variable between the face-center locations as a linear variation between two adjacent nodes:

$$\varphi_e = \varphi_E \lambda_e + \varphi_P (1 - \lambda_e) \tag{50}$$

where

$$\lambda_e = \frac{x_e - x_P}{x_E - x_P} \tag{51}$$

So, with the same linear approach adopted for the diffusive fluxes the approximation is:

$$(\frac{\partial \varphi}{\partial x})_e \approx \frac{\varphi_E - \varphi_P}{x_E - x_P} \tag{52}$$

For the finite volume technique higher order approximations are also possible, approximating for instance the variable profile between the nodes P and E by a quadratic law.

2.3.4.1. Solution of the discretized algebraic equations methods

As it could be for the example considered in the previous section, the results of discretization is a system of algebraic equations, which are linear or nonlinear depending on the nature of the partial differential equations to be solved.

In nonlinear cases, the discretized equations must be solved with an iterative technique that starts guessing the possible solution, linearizing the equation on the basis of the guessed value and adjusting the solution itself.

If the problem that should be solved is:

$$A\varphi = Q \tag{53}$$

with linear equations, the solution can be obtained with some direct or iterative methods, depending on the computational costs that direct methods require.

The basic method for *linear equations* is the **Gauss elimination method**. It aims at the reduction of a great matrix to a smaller one, substituting at each computational step the matrix elements with zero values. The Gauss elimination algorithm is composed of two parts: the forward elimination, that reduces the full matrix to an upper triangular one, and the back substitution, that computes the unknown.

This method is not usually used for sparse matrix deriving from the discretization of partial differential equations of fluid dynamic problems because its computational costs are quite high and are proportional to $n^3/3$.

A higher efficiency variant of the Gauss elimination method is the **LU decomposition method**. This method is based on the fact that any matrix could be factored into the product of a lower (L) and an upper (U) triangular matrix. In this way, the existence of this factorization allows the solution of the system of equations in two stages, both based on the back substitution phase.

The advantage of using the LU decomposition is in the possibility of avoiding the Gauss elimination stage.

The most important method, in case of ordinary differential equations for one-dimensional systems discretized by finite differences or finite volumes, is the **Thomas Algorithm** or the Tridiagonal Matrix Algorithm (TDMA).

To adopt this method, the equations must have a simple structure, with each equation containing only the variables at its own node and at its immediate left and right neighbors:

$$A_W^i \varphi_{i-1} + A_P^i \varphi_i + A_E^i \varphi_{i+1} = Q_i \tag{54}$$

The matrix A has non-zero values only in its main diagonal (represented by A_P^i) and on the diagonals immediately above and below it (represented by respectively A_E^i and A_W^i). This matrix is called a tridiagonal one.

This numerical solution method based on the existence of a tridiagonal matrix has a computational cost proportional to n and this fact suggests using this method, when possible, preferably to any other. This is the case for the MAST code.

It easily computed and it uses the Gauss elimination in a valuable way because for each row during the forward elimination only one element needs to be eliminated:

$$A_p^i \varphi_{i-1} = A_P^i - \frac{A_W^i A_E^{i-1}}{A_P^{i-1}} \tag{55}$$

The back substitution is easy as well and it bring to:

$$\varphi_i = \frac{Q_i^* - A_E^i \varphi_{i+1}}{A_P^i} \tag{56}$$

Sometime the choice of an iterative method for the solution of sets of linear equations is also valuable if it converges rapidly and, then, if in the matrix problem $A\varphi = Q$ solved through an iterative scheme such as $M\varphi^{n+1} = N\varphi^n + Q$ $A = M - N$ is a sparse matrix and M is diagonal, tridiagonal, triangular or block tridiagonal, block triangular.

The simplest procedure is the **Jacobi method**, where M is a diagonal matrix whose elements are the diagonal elements of A. This method requires for convergence a number of iteration proportional to the square of the number of grid points in one direction. So, it is more expensive than a direct method.

A derived version, that improved its efficiency is the **Gauss-Seidel method**. It converges twice as fast as the Jacobi method but further improvements were proposed, too.

An accelerated version of the Gauss-Seidel method is called the Successive-over-Relaxation or SOR method.

In the case of the example of the five-point discretization of the matrix equation, the method appears as:

$$\varphi_P^{n+1} = \omega \frac{Q_P - A_S\varphi_S^{n+1} - A_W\varphi_W^{n+1} - A_N\varphi_N^n - A_E\varphi_E^n}{A_P} + (1-\omega)\varphi_P^n \qquad (57)$$

where ω is the over-relaxation factor which must be greater than 1 for acceleration. For $\omega = 1$, the SOR methods coincides with the Gauss-Seidel method.

Other important iterative methods are the **Incomplete LU Decomposition ones**, proposed by Stone, (1968) for Navier-Stokes equations and for convection-diffusion problems, which have not discretization in symmetric matrices.

Another method, developed for elliptic problems but that is the basis of many others iterative methods, is the **Alternating Direction Implicit (ADI),** see Hageman and Young, (1981).

Another method is the **Steepest Descent method**. Here, for a special type of matrices that are *positive definite*, the problem of solving the system of equation coincides with the problem of finding the minimum of the function:

$$F = \frac{1}{2}\varphi^T A\varphi - \varphi^T Q = \frac{1}{2}\sum_{j=1}^{n}\sum_{i=1}^{n} A_{ij}\varphi_i\varphi_j - \sum_{i=1}^{n}\varphi_i Q_i \tag{58}$$

With respect to φ_i, the steepest downward path is then searched that is in the opposite direction of the gradient of the function. The lowest point on that line is then found and so the new guessed value is closer to the solution.

This method can be well improved and one of its simplest evolutions is the **Conjugate Gradient method.** About it, in fact, was stated that it is possible to minimize a function with respect to several directions simultaneously.

For instance, in the case of two directions both values of α_1 and α_2 could be found in order to minimize the function F in the plane $p^1 - p^2$ through

$$\varphi = \varphi^0 + \alpha_1 p^1 + \alpha_2 p^2 \tag{59}$$

where $p^1 \cdot Ap^2 = 0$ and the two vectors are in fact called *conjugate*. This method guarantees that the error is reduced on each iteration, but the size of the reduction depends on the search direction.

In any case, the conjugate gradient method is applicable only to symmetric systems and to generalize its application to system of equations not symmetric (any convection-diffusion equation) the asymmetric matrices should be converted in a symmetric one.

So after the pre-conditioning of the conjugate gradient method is applied to this system, the **Biconjugate Gradients method** is the resulting one (Fletcher, 1976). Other variants of the biconjugate gradient method, that are more stable and robust, have been developed: the **Conjugate Gradient Squared**, **CGS** (Sonneveld, 1989); the **CGS stabilized**, **CGSTAB** (Vorst and Sonneveld, 1990), the **GMRES** (Saad and Schultz, 1986)**,** the **3D CGSTAB**.

For the solution of *non-linear algebraic equations*, one of the most important methods is the Newton's method. In this case a good estimate of the solution has to be known. If the root of an equation $f(x) = 0$ is need, Newton's method linearizes the function around an estimated value of x using the first two terms of the Taylor series as:

$f(x) \approx f(x_0) + f'(x_0)(x - x_0)$.

Then, if the linearized function is set to zero a new estimation of the root is provided:

$x_1 = x_0 - \frac{f(x_0)}{f'(x_0)}$ or, in general, $x_k = x_{k-1} - \frac{f(x_{k-1})}{f'(x_{k-1})}$ and it continue until the change in the root $x_k - x_{k-1}$ is as small as possible.

When the estimate is close enough to the root it converges quadratically and the error at iteration k+1 is proportional to the square of the error at iteration k.

The Newton method is easily applied to any system of equations but is not often used to solve the two- fluid model equations because its overall cost is greater than the other iterative techniques (Banerjee and Mulpuru, 1979).

2.3.4.2. Solution of unsteady problems

The numerical methods applied in the discretization of time-variable PDE systems are basically the same that are applied for Ordinary Differential Equations (ODE).

$$\frac{d\varphi(t)}{dt} = f(t, \varphi(t)); \quad \varphi(t_0) = \varphi^0 \tag{60}$$

These methods defined for initial value problems, or Cauchy problems, are applicable to the solution of a first order ordinary differential equation set with an initial condition, such as:

So the solution φ^1 will be computed in time $t_1 = t_0 + \Delta t$ and could be considered as a new initial condition for the time step t_2.

The procedure can be summarized through the following equation

$$\int_{t_n}^{t_{n+1}} \frac{d\varphi}{dt} dt = \varphi^{n+1} - \varphi^n = \int_{t_n}^{t_{n+1}} f(t, \varphi(t)) dt$$

where the integral here is exact but to evaluate it the value of the solution, even if with some approximations, should be known.

So the integral could be approximated via four different methods, with the notation $\varphi^{n+1} = \varphi(t_{n+1})$:

- The explicit or forward Euler method: $\varphi^{n+1} = \varphi^n + f(t_n, \varphi^n)\Delta t$;
- The implicit or backward Euler method: $\varphi^{n+1} = \varphi^n + f(t_{n+1}, \varphi^{n+1})\Delta t$;

- The trapezoid rule: $\varphi^{n+1} = \varphi^n + \frac{1}{2}\left[f(t_n, \varphi^n) + f(t_{n+1}, \varphi^{n+1})\right]\Delta t$ (at the basis of the Crank-Nicolson method);
- The midpoint rule: $\varphi^{n+1} = \varphi^n + f(t_{n+\frac{1}{2}}, \varphi^{n+\frac{1}{2}})\Delta t$.

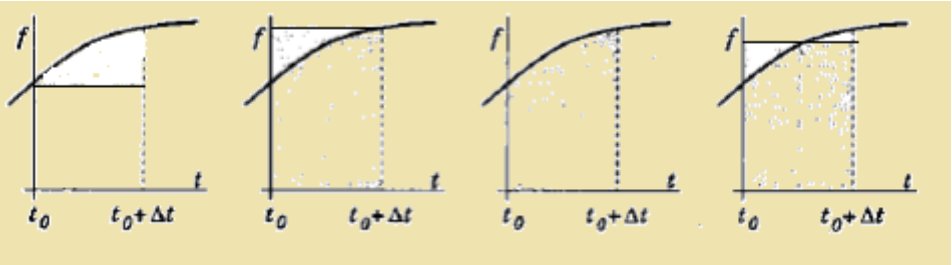

Figure 16: Integrals calculation for the methods presented above (from left to right: explicit Euler, implicit Euler, trapezoidal rule and the midpoint rule)

Among all these methods only the first one does not need the value of the unknown φ^{n+1} more than once in the procedure of the scheme: this means that for the first method (Euler explicit or forward method) the solution can be found directly without iterating .

For all the other methods, the right hand side cannot be calculated without any other approximation, iterative scheme or procedure.

As all the methods shown before are good approximation of the solution with a small Δt value, but not all the methods have the same behavior in front of problems with great time steps.

As already mentioned in the previous section, numerical instability phenomena can rise, even if the starting differential equation set is well-posed and bounded, if the numerical method does not advance toward bounded and physical solution.

Among the methods presented above, the first one (the explicit Euler) is the only *conditionally stable*. In fact, it requires the imposition of stability conditions:

$$\left|1+\Delta t\frac{\partial f(t,\varphi)}{\partial \varphi}\right|<1 \tag{61}$$

All the other methods are unconditionally stable but each of them should be applied carefully to any problem in order to choose the best method with the requested convergence behavior.

Commonly applied methods, that use the advantage of explicit methods in programming and in computing costs in collaboration with the stability of an implicit method, are called **Predictor-Corrector methods** and they are different from all the other attempts of combining the previously presented schemes because Predictor-Corrector methods focus on the formulation of the conservation equations in a form which extracts pressure from the primary variable solution.

The idea behind this approach is that the solution for mass fluxes based on the momentum equation uses an assumed pressure field, then the pressure field is corrected before the second iteration on the basis of the continuity equation. This process is continued until convergence. This approach is particularly important in case of the solution of the flow equations, where the pressure gradient plays a role in each of the momentum equations and where the continuity equation should calculate the pressure and be coupled to the velocity field in order to assure the mass conservation.

In these methods a Poisson equation in terms of pressure is obtained after imposing the continuity equation.

Several different predictor-corrector methods have been developed, among which the **ICE** (Harlow and Amsden, 1971), **SIMPLE** (Patankar and Spalding, 1972).

The first method, often defined *the* predictor-corrector method, predicts the solution at a new time step with the explicit Euler:

$\varphi_{n+1}^{*}=\varphi^{n}+f(t_n,\varphi^{n})\Delta t$ where the symbol * indicates that the corresponding value is not the final solution at t_{n+1} because the solution is then corrected by applying the trapezoid rule using:

$$\varphi^{n+1} = \varphi^{n} + \frac{1}{2}\left[f(t_n, \varphi^{n}) + f(t_{n+1}, \varphi^{*}_{n+1}) \right] \Delta t \,. \tag{62}$$

In explicit time stepping (forward Euler) the corrector step computes directly the entire pressure field via the Poisson equation.

Instead, the SIMPLE method and its improved variants, are based on an implicit or semi-implicit procedure for Pressure equation solution. The scheme in its original version is based on three steps, as shown in Figure 17, with the pressure gradient not incorporated into the source term:

- STEP A: Research of the solution of the momentum equations with a guessed (from the first step) or a previously computed pressure field;
- STEP B: Solution of the Poisson equation to compute the pressure correction variable p' at the new iteration step;
- STEP C: Correction of the velocity field with the pressure correction variable and improving the conservation equation;
- RETURN to STEP A.

The SIMPLE algorithm was originally designed for steady state solutions on collocated grids (Caretto et al., 1972), but can be extended to unsteady problems.

A first proposed improvement is the **SIMPLER** method developed by Patankar (1980). A second version is the **SIMPLEC** procedure (Van Doormal and Raithby, 1984). The presentation of the PISO algorithm (Issa, 1986) follows in order to enhance the velocity of convergence and the stability of the original SIMPLE scheme.

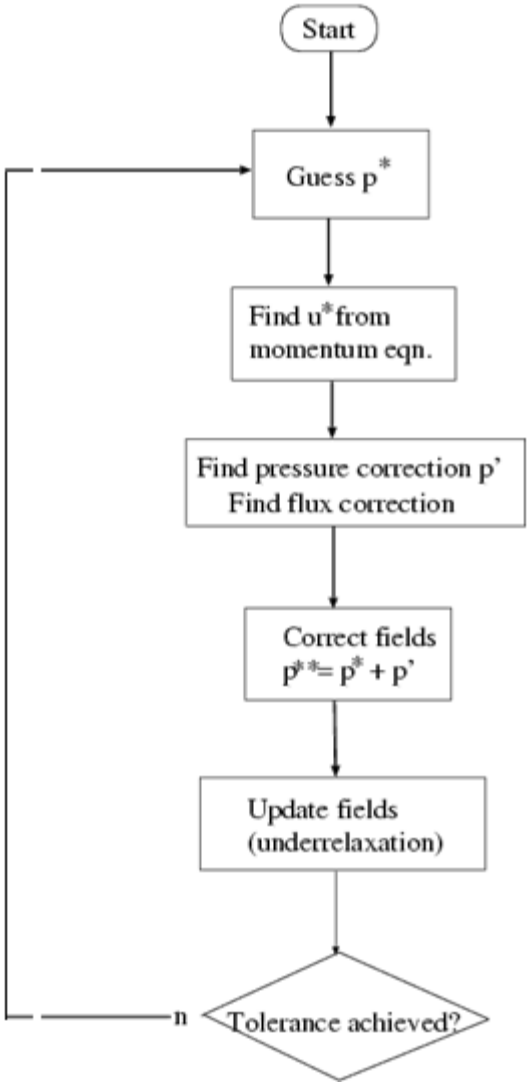

Figure 17: SIMPLE algorithm flow chart

The flow chart of the PISO algorithm is shown in Figure 18 and it performs the following steps:

- STEP A: an initial value for p is guessed from the previous time step;
- STEP B: the linearized algebraic equations are solved to obtain the velocity fields;
- STEP C: the pressure-correction equation is assembled and solved to obtain the corrected pressure value p';
- STEP D: the velocities are corrected and another pressure-correction equation is computed for the second time;
- RETURN to STEP A and continue until convergence.

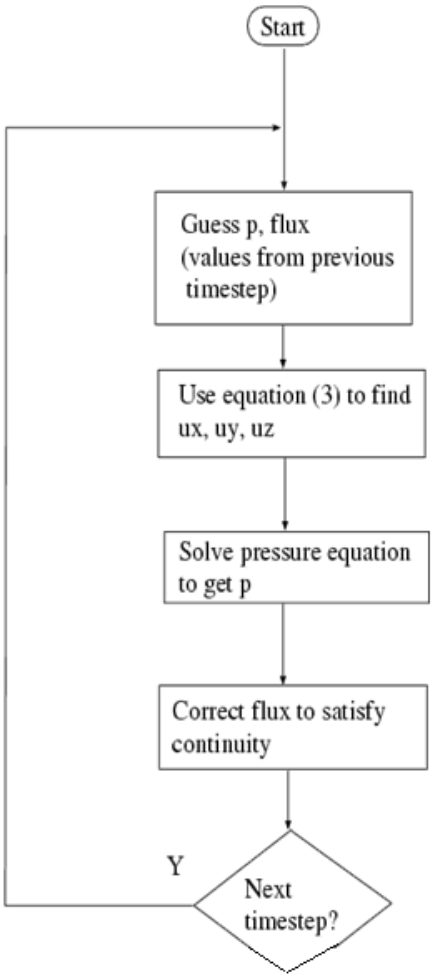

Figure 18: PISO algorithm flow chart

Another predictor-corrector approach was developed by Spalding, (1979) and is called the **IPSA** algorithm: it uses the momentum balance to estimate the velocities and then an implicit coupling between pressure and volume fraction is performed. The correction is then done restoring the balance between the pressure equation and the volume fraction computed through continuity.

For the predictor-corrector method the highest accuracy possible is second order. If a more generic approach is needed, that could be extended to unsteady problems and to all cases that require higher-order approximation **Fractional Steps methods** could be applied: among them the **multipoints**-, the **Runge-Kutta**-like methods and the **Crank-Nicolson** (Crank and Nicolson, 1947) scheme.

In Chapter 3 all these considerations will be applied to the peculiar case of the "four-field" model implemented in the MAST code.

2.4 The role of the stratified and slug flow in horizontal pipes

In Oil&Gas industry the purpose of any multiphase transportation pipeline is the supply to main distribution stations with hydrocarbons in liquid and/or gas phase. Often the mixtures of both phases, sometimes containing water too, are directly extracted from the well and transported via very long on-shore or off-shore pipelines.

In this peculiar application, the most frequently encountered flow patterns are the stratified and the slug flows, see Figure 19. If the first one represents the mixture behavior during normal operating conditions, the slug flow is a serious danger for the pipeline integrity and can be originated as a consequence of abnormal operating conditions (hydrodynamic slug, severe slug) or naturally induced by the pipeline layout (terrain induced slug).

Figure 19: The most important flow patterns in long transportation pipes

The flow maps already presented in Section 2.2 help to understand the link between the two flow patterns, the stratified and the slug flow, and that if the liquid velocity is low, the regime is stratified, or stratified-wavy with small 2D waves at the interface; if the liquid flow rate grows, the transition between stratified and hydrodynamic slug flow is probable even at low gas flow rates.

The hydrodynamic slug is characterized by medium and low slug lengths, of limited impact on the hydrocarbon transportation pipeline integrity, if not made worse by possible onset of severe slug, characterized by a long pressurized plug of liquid accumulated along the line.

After the transition between stratified and slug flow patterns, the onset of the long slug sub-regime could take place (Kadri, 2009). This is a situation during which slow, 3D waves merge together and liquid plug length (ls) could reach values of about ls=400D, as it will be discussed in details in Chapter 4.

The **stratified flow pattern** will be presented in detail in Chapter 5, where attention will be dedicated to its stratified-wavy sub-regime and to the formulation of accurate closure laws able to enhance the prediction of the transition to slug flow.

The slug flow is investigated in the following sections of this chapter, taking into account the most important existing models and numerical codes dedicated to the prediction of slug flow properties. The phenomenon of long slug will be explained in the next Chapter 4 where a more detailed analysis will be dedicated to it and to available prediction tools.

2.4.1. Slug flow occurrences

The slug flow can be originated by different phenomena, occurring in a transportation pipeline:

- hydrodynamic instability;
- pipeline geometrical features, called the terrain induced slugging;
- transient operation in wells exploitation.

The *hydrodynamic slugging* can exist in horizontal or near-horizontal pipelines when the flow conditions are such that stratified flow regime is abandoned, because of interfacial instabilities, and suction forces over the wave crests, due to the gas flow, help the waves to grow and touch the upper part of the pipe cross section: a plug of liquid is formed. Because of the velocity difference between the gas and liquid and between the front and tail of the slug, a pressure difference that moves the plug is created.

The sequence of the hydrodynamic slug onset is described by Dukler and Hubbard, (1975) and shown in Figure 20:

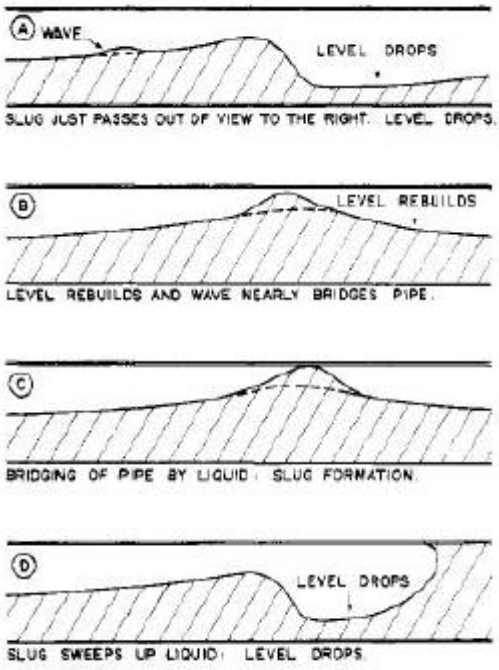

Figure 20: The steps of the hydrodynamic slug formation (Dukler and Hubbard, 1975)

In case of steep variations of the pipeline inclination, due in most cases to the terrain morphology, the *terrain induced slugging* might be induced.

In particular, if after a long downwardly inclined part of the pipeline a upwardly inclined one follows, the liquid accumulates in the valley between the two pipeline segments until a plug of liquid is driven by the increased pressure upstream and the gravitation and the friction losses are overcome.

The characteristic of a terrain induced slug is to be much longer than a hydrodynamic slug and that it can cause severe damaging to the transportation facility.

This second category of slugs can be avoided with correct design of pipelines and good flow assurance analysis.

More interesting from the physical point of view is the analysis of slug flow in a near-horizontal pipeline due to *flow regime transition* occurring naturally from stratified flow.

Once the flow conditions are known, the flow maps, as seen in previous section, could help in predicting the transition if the gas and the liquid flow rates, or their superficial velocities, are known.

To understand which are the conditions that influence the onset of interfacial instabilities, supposed to cause the transition between stratified and slug flow (Barnea and Taitel, 1994), the Kelvin-Helmholtz instability analysis can be used.

In particular, as already described in the previous section, if a stable stratified flow with two fluids having different densities and velocities is perturbed by a linear small disturbance, from the resolution of the system of equations for the perturbed liquid level the flow conditions responsible for that instability could be evaluated in terms of relative velocity between the gas and the liquid phase: the so called Kelvin-Helmholtz critical velocity.

The instability due to the difference in velocities is bounded by surface tension and gravity. The critical velocity can be obtained for viscous and inviscid flows. In particular, as already mentioned, if the inviscid Kelvin-Helmholtz condition coincides with well-posedness of the system of equations, the **Viscous Kelvin-Helmholtz** guarantees well-posedness even if the flow experiences interfacial instabilities. It predicts, in fact, in the opinion of some authors, a different transition point within still well-posed flow conditions (Lin and Hanratty, 1986) that identify the transition between stratified/stratified-wavy regime and slug flow, if see Barnea and Taitel, (1993) and Holmas et al.,, (2008).

These considerations, and those that will follow in next section, are relevant in this thesis because they summarized the background to understand the new "slug capturing" model implemented in the MAST code presented in Chapter 3.

2.4.2. Slug flow modeling

The first steady state slug model proposed was the *unit-cell model* (Dukler and Hubbard, 1975), already described in Figure 4 where there the basic definitions useful for the slug body and tail description were reported:

- Slug length: l_s;
- Liquid film region: l_f;
- Turbulent mixing region l_m;
- Slug unit length: $l_U = l_s + l_f$.

It is well known that the slug moves in the pipe at the slug translational velocity U_T of the slug front; but a lot of other velocity values are needed to describe the behavior of each different part of the slug cell:

- average gas velocity in the bubble: U_G;
- velocity of the area between the front of the bubble and the tail of the slug: U_B;

Average liquid film velocity: U_{Lf}; Average velocity of the liquid in the slug: U_{LS}.

2.4.2.1.The "steady state" models

This first slug model assumes a no-slip condition in the slug between the gas bubbles and the liquid, horizontal flow, already stable slug flow regime and it needs as input two important flow conditions: the slug frequency and the liquid volume fraction in the slug ε_{LS}.

This model has the goal to predict the pressure losses and the liquid content in the line and starts with the calculation of the pressure losses across the slug unit ΔP_S, after having assumed that the pressure losses across the liquid film and the slug bubble are negligible:

$$\Delta P_S = \Delta P_a + \Delta P_{fr} \tag{63}$$

where ΔP_a are the pressure losses caused by the acceleration of the picked up liquid film and ΔP_{fr} are the pressure losses caused by the frictional shear stress. They are given respectively by:

$$\Delta P_a = \frac{\chi}{A}(U_S - U_f) \tag{64}$$

and

$$\Delta P_{fr} = \frac{2 f_s [\rho_L \varepsilon_{LS} + \rho_G (1-\varepsilon_{LS})] U_S^2 (l_s - l_m)}{2D} \tag{65}$$

where χ is the liquid pickup and shedding rate, f_S is the fiction factor.

The slug velocity U_S, as presented by Dukler and Hubbard, (1975), can be obtained from the initial gas and liquid flow rates Q_L and Q_G, as:

$$U_S = 1/A(\frac{Q_L}{\rho_L} + \frac{Q_G}{\rho_G}) \tag{66}$$

The translational velocity can be obtained from

$$U_T = U_S + \frac{\chi}{\rho_L A \varepsilon} \tag{67}$$

if the pickup and shedding rate was known, but that is not the case, yet.

Dukler tried obtained χ in an analytical form but proposed an approximate correlation, too:

$$\chi = \varepsilon_{LS} \rho_L A U_S - \int_0^{r_P} 2\pi r \rho_L u dr \tag{68}$$

where r_p is the pipe radius,

$$C = \frac{\chi}{\varepsilon_{LS} \rho_L A U_S} = 0.021 \ln(\mathrm{Re})_S + 0.022 \tag{69}$$

where *C* is the ratio between the mass pickup to the mass flow in the slug.

Then the liquid film velocity as a function of the ε_{Lf} can be obtained by a mass balance:

$$U_{Lf} = U_S \left[1 - C \frac{\varepsilon_{LS} - \varepsilon_{Lf}}{\varepsilon} \right] \tag{70}$$

By applying a momentum balance over the control volume, the liquid film volume fraction ε_{Lf} can be evaluated and the proposed equation from Dukler and Hubbard, (1975) needs to be solved iteratively from a guessed value of l_f is the following:

$$\int_{\varepsilon_f}^{\varepsilon_S} W(\varepsilon_{Lf}) d\varepsilon_{Lf} = \frac{l_f}{D}.$$

All the other characteristic lengths and properties could then be obtained.

The calculation procedure proposed in the work of Dukler and Hubbard, (1975), is shown in Figure 21.

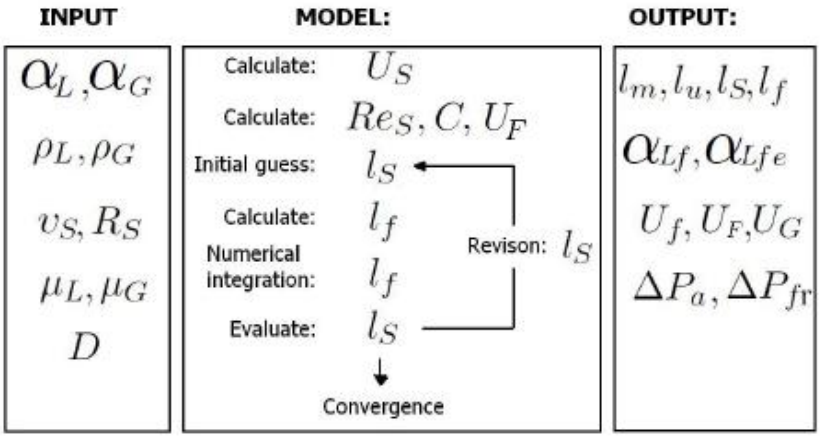

Figure 21: The solution procedure of the slug unit cell model (Dukler and Hubbard, 1975)

Another "steady state" model for the slug flow, presented as an improved version of the slug unit cell model, was proposed by Taitel and Barnea, (1990a; 1990b), and called the *"Equivalent Slug Unit"*.

The definitions introduced by their model are presented in Figure 22, where the control volumes for the gas and the liquid phases are defined:

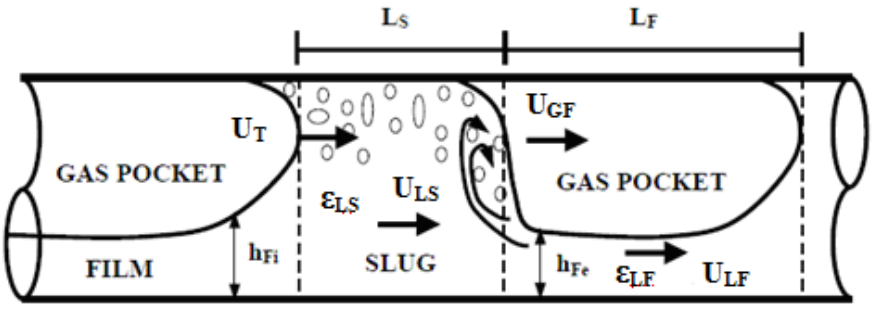

Figure 22: The "equivalent slug unit" model of (Taitel and Barnea, 1990b)

This model consists of a slug region of length l_S and a film region of length l_f.

The liquid region may be considered as aerated with dispersed gas bubbles. In this model, the liquid level is still the only phase involved in bridging the pipe.

The volume fraction in the slug region is ε_{LS} and the average liquid velocity in the liquid slug is, again, U_{LS} that coincides with the average axial velocity of the dispersed bubbles in this area.

The liquid film region is represented as a thin liquid film and an elongated, or "Taylor", gas bubble that flows on the upper part of the pipe in the case of horizontal or slightly inclined pipes (this model extended the validity of the unit cell model to inclined pipes).

Again the interface between the bubbles and the slug flows downwardly at a translational velocity U_T, the film with a velocity U_{Lf} and the gas over the film with a velocity U_{Gf}. The two velocities are not uniform because they can vary along the pipe due to the changes in the film thickness h_f.

Taitel and Barnea, (1990b), presented different cases with which they described their model, for instance they assumed a constant liquid film thickness and then calculated all the other parameters. They started from the following film momentum balance:

$$\frac{\tau_F S_F}{A_F} - \frac{\tau_G S_G}{A_G} - \tau_i S_i \left(\frac{1}{A_F} + \frac{1}{A_G}\right) + (\rho_L - \rho_G) g \sin\theta = 0 \qquad (71)$$

where τ_F and τ_G are the liquid and the gas wall shear stresses in the film zone.

The terms S_F, S_G and S_i are the liquid, gas and interfacial wetted perimeters; the A_F, A_G are the liquid and gas flow area; ρ_L and ρ_G are the liquid and gas densities.

The authors proposed a procedure to calculate the liquid film profile, once the geometry and the fluid properties are known:

1. U_{LS} is calculated being equal to the mixture velocity with: $U_{LS} = U_M = U_{SG} + U_{SL}$, where the U_{SG} and U_{SL} are the gas and liquid superficial velocities;
2. The variables U_T and ε_{SL}, the translational velocity and the volumetric fraction of liquid in the slug, are then calculated through the correlations proposed by Bendiksen, (1984) and Gregory et al., (1978):
   $U_T = 1.2U_M + 0.54\sqrt{gD}$ and $\varepsilon_{SL} = \dfrac{1}{1 + \left(\dfrac{U_M}{8.66}\right)^{1.39}}$ where D is the pipe diameter, U_M is the mixture velocity calculated in step 1;
3. then, an iterative procedure was defined starting from a guessed value of h_f, the liquid film height. The values of the geometrical parameters are obtained from a dimensionless analysis and are proposed below:
   $A_f = A\varepsilon_f$
   $A_G = A(1-\varepsilon_f)$
   $S_f = D\left(\pi - \cos^{-1}\left(2\dfrac{h_f}{D} - 1\right)\right)$
   $S_G = D\pi - S_f$
   $S_i = D\sqrt{1-\left(2\dfrac{h_f}{D} - 1\right)^2}$
   $\varepsilon_f = \left(\dfrac{1}{\pi}\right)\left\{\pi - \cos^{-1}\left[2\dfrac{h_f}{D} - 1\right] + \left[2\dfrac{h_f}{D} - 1\right]\sqrt{1-\left(2\dfrac{h_f}{D} - 1\right)^2}\right\}$
4. U_{Lf} and U_{Gf}, that are the velocities of liquid film and bubble and that are then calculated using a mass balance;
5. The friction factors are evaluated with an already known correlation from the literature

6. The estimation of h_f is then tested, a new estimated value could be tried and the loop continues.

This model, as all the other steady-state models, gives the knowledge of only average values, without any information on the longitudinal distribution of the flow and of its transient behavior.

This is the reason why these kinds of models are often replaced with transient ones. Instead, steady state models can be easily used as initial conditions for two-fluid transient models.

2.4.2.2.Slug-tracking models

In order to improve the analysis of the transient behavior of a slug flow, the slug tracking technique was presented firstly by Bendiksen et al., (1990). This method allows the tracking of each individual slug, identifying for tail and front of the slug the upstream and downstream velocities independently.

This approach is enabled by the use of a Lagrangian system of coordinates with a front-slug tracking scheme superimposed over a standard Eulerian scheme.

In particular, the advantages over the previous models are due to the fact that the distribution of the slugs in the pipeline is an outcome of the model and not completely imposed by closure laws. Indeed, these models have high computational costs, because sometimes the number of slugs in the line is large.

Usually both the slug tail and the slug front are described with a Lagrangian coordinate system that enables the tracking of each position as a function of time.

Once all the information about slug positions and velocities are known, the information on the mass and momentum terms, managed in an Eulerian approach, is then corrected. So, the slug tracking is applied only to the calculation of the individual slug fronts and tails.

A slug tracking scheme distinguishes between a discontinuity of the slug if it is on its tail or on its front. The difference is in particular in the fact that a slug front usually is a discontinuous interface that entrains gas bubbles. Bendiksen, in fact, defined a term, the bubble nose turning number f_B, that enables the model (Bendiksen et al., 1990) to distinguish between a slug tail and front:

$$f_B = \frac{U_f}{g\cos\theta D(1-\varepsilon_G)^{0.5}}\left(\frac{\lambda(\pi-\delta)}{2(1-\varepsilon)}\right)^{0.5} \tag{72}$$

where λ is the Darcy wall fiction coefficient. So the slug front can be treated as a slug nose depending on the sign of f_B.

A nose interface is treated as a Taylor bubble propagating into the liquid slug.

The bubble nose velocity is:

$$U_B = C_1 U_{LS} + U_{br} \tag{73}$$

where C_1 is a constant (0.9-1.2) which is dependent on the inclination of the pipe, U_{LS} is the liquid slug velocity and U_{br} is the bubble rise velocity in the stagnant liquid.

The slug front and tail velocities, defined respectively U_F and U_B, are obtained from volumetric balances:

$$U_F = U_{SM} + W_G + W_d + W_L \tag{74}$$

$$U_B = U_{SM} - W_G - W_d - W_L \tag{75}$$

where U_{SM} is the total superficial slug mixture velocity, W_G is the volumetric flux of gas, W_d is the droplet volumetric flux and W_L is the liquid volumetric flux.

The slug mixture velocity and the volumetric fluxes are:

$$U_{SM} = (U_{SL} + U_{SG}) = U_{LS}\varepsilon_{LS} + U_{GS}(1-\varepsilon_{LS}) \tag{76}$$

where U_{LS} and U_{GS} are respectively the liquid and the gas velocity in the slug;

$$W_L = (1-\varepsilon_{Gf} - \varepsilon_{Lf})(U_F - U_{LS}) \tag{77}$$

$$W_d = \varepsilon_{Lf}(U_F - U_d) \quad if\ W_d > 0 \tag{78}$$

$$W_G = \varepsilon_{GS}(U_F - U_{SG}) \quad if\ W_G < 0 \tag{79}$$

$$W_G = k_1 \frac{S_i}{D}(U_F - U_{LS}) - k_2 \quad if\ W_G > 0 \tag{80}$$

As a consequence, once the velocities are established, the position of the front and tail are determined after a time interval Δt with:

$$X_{F,new} = X_{F,old} + U_F \Delta t \tag{81}$$

$$X_{B,new} = X_{B,old} + U_B \Delta t \tag{82}$$

where $X_{F,new}$ and $X_{B,new}$ are respectively the new positions of the slug front and tail.

The slug length can be then calculated:

$$L_{new} = X_{F,new} - X_{B,new} \tag{83}$$

The slug tracking methods more limiting aspects are due to the fact that they do not predict the onset of the slug flow and that the entire results depends somehow on the flow initialization model. In fact, they need slugs initialization position and length to start the calculation.

Some codes implement transient solution approaches to the slug flow modeling and among them the most important and widely used are the OLGA code (Bendiksen et al., 1991), the TACITE code (Pauchon et al., 1994) and the PLAC code (Black et al., 1990).

The code OLGA was developed by the Norwegian Institute SINTEF and is based on a model solving the continuity equations for the two phases, gas and liquid continuous, and for the liquid droplets; the momentum equations are solved for the liquid, for the gas phase and for the liquid droplets. The energy is accounted by only one mixture equation.

The OLGA code distinguishes between the flow regimes, before selecting the closure laws that match the flow conditions under examination.

In particular, it distinguishes at first between two flow regime groups: the separated (stratified and annular) and the dispersed (bubbly and slug) flow. The criterion used to select between flow regimes is the “minimum slip”: the flow pattern that should be the really expected should have the minimum gas velocity.

In this code, if the flow pattern selected is the slug flow, two different approaches are then used separately for the characterization of the slug flow and of its properties: the liquid film is calculated as a separate flow; the plug of liquid is calculated as a dispersed flow region.

In the case in which a terrain slugging is detected or expected, the OLGA code uses its slug tracking module, implemented as a possible option.

In OLGA code the slug tracking model identifies cells with discontinuities, Figure 23, which are divided into stratified and slug regions. In this way, for each cell the adequate numerical procedure is applied depending on the slug flow type, as shown in (Straume et al., 1992). In this slug tracking model the droplets are not modeled.

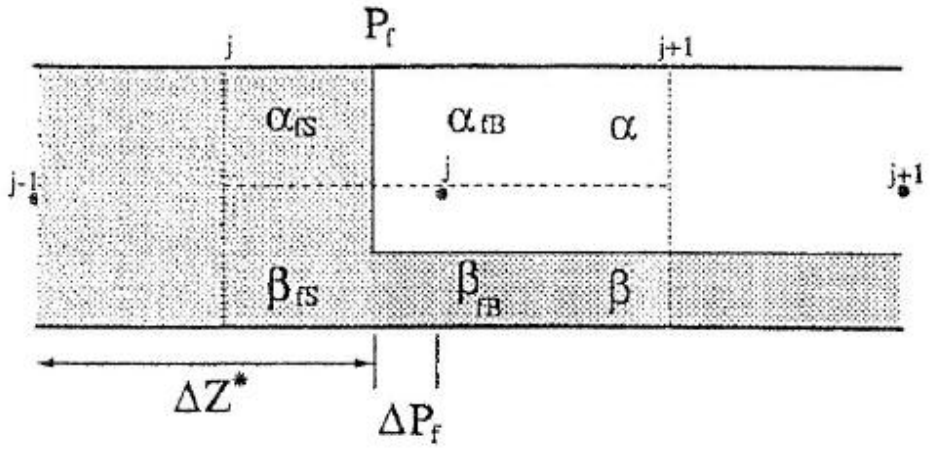

Figure 23: Flow types in the organization of the slug tracking in OLGA (Bendiksen et al., 1990)

In Chapter 3 another solution approach to transient slug flow will be introduced; this method is called "slug capturing" and it is at the basis of the MAST code. This code will be presented in detail in the next chapter where its origin, its set of mass, momentum and energy equations, its numerical methodology and an overview of its performances and validation against experimental measurements are described.

Chapter 3 The “four field” model of the MAST code

3.1 The “slug capturing” technique

3.1.1. Introduction

The slug capturing technique is a method for the resolution of two-phase gas-liquid flow where the slug flow regime is predicted as a mechanistic and outcome of the growth of instabilities at the interface between phases.

The two-fluid model solves mass and momentum conservation equations for each of the simulated phases. The same set of equations is adopted even if different flow patterns will be simulated.

The transitions among the different flow patterns are driven by the growth of instabilities at the interface between the two phases. To make this possible, the mesh size must be sufficiently fine, in the order of the pipe diameter.

The mechanisms that predict the onset of instabilities and its prediction by the set of equations has already been presented in previous sections; here, the application and the validation of this methodology are carried on.

When there is an unbalance between the pressure and inertia at the interface the instabilities appear and the waves grow because of the suction at the wave crest due to the Bernoulli effect.

Once the liquid has reached the upper part of the pipe, the plug of liquid is formed and the slug flow starts; it then develops and grows by the merging of successive slugs or collapses. These mechanisms can be predicted by the solution of the two-fluid model equations.

Other works investigated the capabilities of the slug capturing technique of predicting the flow patterns in case of inclined pipes (Kempf, 1999), (Rippiner, 1998); the same model also predicts the phenomenon of severe slugging (Issa and Abrishami, 1986).

The slug capturing for unaerated two-phase slug flow needs only a few closure laws (the friction factors for the liquid-wall, the gas-wall and the gas-liquid interface) (Issa and Abrishami, 1986).

The numerical code where the slug capturing technique was implemented for the first time was the TRIOMPH code (Issa and Abrishami, 1986).

Its numerical frame is Eulerian, the numerical technique is semi-implicit and a transient solution of the set of equations enables the simulation of the slug flow transient evolution in the pipeline.

Recently a new code, called MAST (Bonizzi et al., 2009), was developed on the basis of the slug capturing technique for the prediction of two-phase gas-liquid flows in the case of a long transportation pipeline.

In particular, the MAST code, as it will be presented hereafter in this chapter, implements a "four-field" model approach so it does not enable only the transition between stratified and slug flow (based on the slug capturing approach) but, thanks to the modelization of both liquid and gas continuous and dispersed fields, it enables the investigation of four reference flow patterns (stratified-slug-annular-bubbles) and the transitions among them. This is the reason why MAST should be classified as a DYNAMIC PATTERN RECOGNITION model. Further details will be added in next sections.

3.1.2. Previous experiences with slug capturing models

In the TRIOMPH code (Issa and Abrishami, 1986) a two fluid model for the gas and the liquid phases, in a transient 1D form was adopted.

The equations are the same as those presented in Chapter 2 for the gas and liquid phase only. Omitting any symbols for area-averaged properties, they are presented below for the gas continuity equation, the liquid continuity equation, the gas momentum equation and the liquid momentum equation in a uniform cross section pipe:

$$\frac{\partial(\rho_G \varepsilon_G)}{\partial t} + \frac{\partial(\rho_G \varepsilon_G u_G)}{\partial x} = 0$$

$$\frac{\partial(\rho_L \varepsilon_L)}{\partial t} + \frac{\partial(\rho_L \varepsilon_L u_L)}{\partial x} = 0$$

$$\frac{\partial(\rho_G \varepsilon_G u_G)}{\partial t} + \frac{\partial(\rho_G \varepsilon_G u_G^2)}{\partial x} = -\varepsilon_G \frac{\partial p}{\partial x} - \varepsilon_G \rho_G g \sin\theta - \frac{\tau_{wG} S_G}{A} - \frac{\tau_i S_i}{A}$$

$$\frac{\partial(\rho_L \varepsilon_L u_L)}{\partial t} + \frac{\partial(\rho_L \varepsilon_L u_L^2)}{\partial x} = -\varepsilon_L \frac{\partial p}{\partial x} - \varepsilon_L \rho_L g \frac{\partial h}{\partial x} \cos\theta - \varepsilon_L \rho_L g \sin\theta - \frac{\tau_{wG} S_G}{A} - \frac{\tau_i S_i}{A}$$

These are the non-linear, first order, partial differential equations for transient, isothermal flow without mass transfer between phases; where ρ, u, p, h, θ are respectively the density, the velocity, the pressure, the liquid height and the pipe inclination. S_k is the geometrical wetting perimeter of the phase k.

As already mentioned, the closure laws really needed for unaerated slug flow simulations are those for the friction factors necessary to calculate the shear stresses τ_{wk} (phase-wall friction) and τ_i (friction between phases).

Of particular interest is the interfacial pressure difference term, added to the standard two-fluid model in order to improve the prediction of pressure variations in the cross section:

$$P_C \frac{\partial \varepsilon_L}{\partial x} = \varepsilon_L \rho_L g \frac{\partial h}{\partial x} \sin\theta \tag{75}$$

This term was not used in early two-fluid models and it was introduced in the TRIOMPH code and investigated by Bonizzi et al., (2001) in order to improve the hyperbolicity of this system of equations and the prediction of gravity waves from the stratified flow pattern.

Another name of this term is the hydrostatic pressure and its derivation is proposed in Bonizzi, (2003), see Figure 24: the hydrostatic term is negligible for the gas phase at atmospheric conditions and so it is usually dropped from the gas momentum equations.

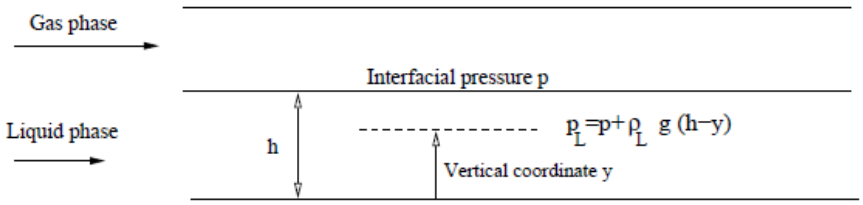

Figure 24: Approximation of the pressure term with the shallow water approach (Wallis, 1968)

Bonizzi, in particular, derived the pressure correction term starting from the value of the local pressure

$$p_L = p + \rho_L g (h - y) \sin\theta \tag{76}$$

and then integrating in the pipe cross section, where y the dimension orthogonal to the pipe axis and p is the pressure term derived by the two-fluid model equations. Its complete expression assumed in the model is:

$$-\varepsilon_L \frac{\partial p}{\partial x} - \varepsilon_L \rho_L g \cos\theta \frac{\partial h}{\partial x} \tag{77}$$

The analysis of closure laws that could better complete the set of equations, improving the prediction of flow conditions and of flow pattern transitions, was performed by Issa and collaborators (Issa and Kempf, 2003; Issa et al., 2006).

They tested in particular some correlations from literature, chosen among the best ones presented by Rippiner, (1998). Among them there are Taitel and Dukler, (1976), Andritsos and Hanratty, (1987), Hand, (1991), Kowalski, (1987). They will be presented in details in Chapter 5.

The influence of the chosen liquid-wall friction factor on the solution has been presented in Bonizzi, (2003). In the same publication, the hyperbolicity of the system of equations, together with the role played by the pressure correction term are examined. In particular, Bonizzi, (2003), stated that when the numerical solution of a set of equations is considered there are three different aspects that will affect the solution and its physical meaning: the ill-posedness of equations, the physical damping due to missing interchanging phenomena between phases (i.e., momentum interfacial transfer phenomena as the interfacial pressure differences and the virtual mass force) and the damping due to the discretization steps, depending on the scheme adopted (Stewart and Wendroff, 1984).

These three aspects are at the basis of the "slug capturing" technique that allows for the prediction of flow pattern transition between stratified and slug flows, with the automatic detection of physical instabilities that appear at the interfaces between gas and liquid. This could be done through the simple solution of the system of equations.

That means, as confirmed in the work of Stewart and Wendroff, (1984), that before the limit of ill-posedness, for some operating conditions, the numerical solution could represent real instabilities if the description of interfacial phenomena is improved (this is the case of the pressure correction term) and if a finer mesh is used.

In the evaluation of the physical meaning of results obtained with the "slug capturing" technique, an important role is played by the numerical method adopted to find the solution. In fact, if the ill-posed character of the standard two-fluid model may cause the growth of unbounded instabilities, obtained by the solution of the set of equations, the chosen numerical method can suppress the high frequency instabilities, while the interfacial transfer terms can help to damp the low frequency instabilities (Issa and Woodburn, 1998).

The investigations performed on the nature of the instabilities, linked to this approach, show that the improvement of the analytical formulation of the two-fluid model, through the addition of closure laws , but only if in differential form such as the interfacial pressure difference and the virtual mass force terms, that better describe the interaction between phases at their interface, is the only way to obtain an hyperbolic set of equations beyond the limit imposed to the well-posedness of the standard two-fluid model by the Inviscid Kelvin-Helmoltz condition. The well-posedness of the standard two-fluid model has

already been discussed in Chapter 2 as depending on the eigenvalues obtained by the characteristic equation of the balance equations.

Through the addition of the pressure correction term, in fact, a different formulation for the criterion for hyperbolicity of the set of equations was proposed by Bonizzi, (2003) for a two-phase flow with compressible gas phase, characterizing conditionally well-posed conditions

In the case of the two-fluid model adopted in Issa and Abrishami, (1986), composed by a set of first order non-linear partial differential equations, the solution is obtained by a numerical approach, where the differential terms are approximated with discretized formulas in space and time, before being solved, with a finite volume methodology presented in Chapter 2 for a generic variable φ.

As already said, the upwind scheme is a highly diffusive technique, being a first order discretization method; so, a fine mesh size enables the model to reach sufficient accuracy. Typical meshes recommended in Rippiner, (1998) should satisfy the condition $0.25 \le \frac{\Delta x}{D} \le 0.5$.

The TRIOMPH code (Issa and Abrishami, 1986) is based on an implicit time discretization technique and solves its set of equations through the application of an iterative algorithm.

The solution vector is, then, composed by the gas void fraction ε_G the two phase velocities and the pressure:

$$\varphi = [\varepsilon_G, u_L, u_G, p]^T \tag{87}$$

The TRIOPMPH model was also characterized by the solution of an overall continuity equation:

$$\frac{\partial \varepsilon_L}{\partial t} + \frac{\partial (\varepsilon_L U_L)}{\partial x} + \frac{1}{\rho_G^{ref}} \left[\frac{\partial (\varepsilon_G \rho_G)}{\partial t} + \frac{\partial (\rho_G \varepsilon_G U_G)}{\partial x} \right] = 0 \tag{88}$$

where ρ_G^{ref} is a reference density. This equation becomes a typical equation as a function of pressure once the velocity U_L and U_G are substituted here from the momentum equations.

The pressure equation in then solved in the TRIOMPH code through the implementation of the PISO algorithm (Issa, 1986) as presented in Figure 25.

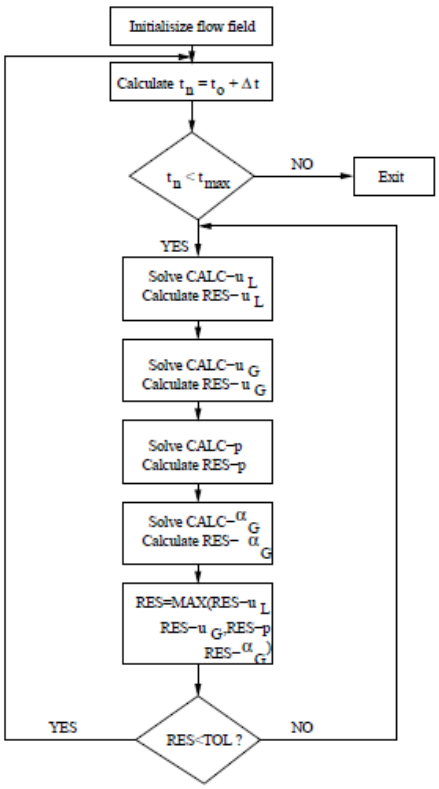

Figure 25: Flowchart of the TRIOMPH code (Issa and Abrishami, 1986)

In this way, the model is unconditionally stable and the information can travel upstream and downstream the flow field.

The well-posed initial value problem to be solved needs four boundary conditions that can be identified with an imposed holdup value, gas velocity, liquid velocity at the pipe inlet and an absolute pressure value at the pipe outlet.

A detailed validation of the TRIOMPH model was performed by Woodburn, (1998) concerning the slug flow prediction capabilities. This author explains the role of the criterion adopted in the code when a liquid slug is generated. In this description, when the liquid volume fraction increases and the gas volume fraction decreases until the point the gas velocity could assume unphysical values, the cell is considered slugged, the gas momentum equation is suppressed and the gas velocity is forced to zero in that cell. The pressure equation in the same cell is, then, considered as depending only on the liquid phase.

The TRIOMPH code was validated during the last two decades by several authors that assessed its methodology for both unaerated (Manolis, 1995; Odozi, 2000; Hale and Hewitt, 2001) and aerated (Bonizzi, 2003) slug flow against experimental measurements performed on the WASP facility at the Chemical Engineering Department of Imperial College and some empirical

correlations for the prediction of major slug properties; an air-water two-phase flow was used in the experimental facility and the validation of the model capability of predicting slug flow in pipelines with different inclinations was compared with holdup, slug length, slug frequency and slug velocity measurements.

Agreement between the measurements and the code predictions are good, as stated by Bonizzi, (2003), with a maximum error bound of 30%. More details can be found in Issa et al., (2003).

It is important to notice that the slug flow predicted by the code is somehow similar to the physical slug flow, but the results cannot be exactly the same as in the measurements: the "slug capturing" technique, in fact, is based on the assumption that the solution is represented by a value with a statistically random behavior.

Recently, a combination between the slug capturing technique and the slug tracking one has been proposed by Renault, (2007) in a new numerical solver able to capture directly from the system of equations the slug initiation process and to track the motion of every single slug in the slug without the numerical constraints of diffusion.

3.2 The MAST code

The MAST (Multiphase Analysis and Simulation of Transitions) model (Bonizzi et al., 2009) is a new simulator for the prediction of multiphase flows in long transportation pipelines and the prediction of flow pattern transitions with a fine mesh approach.

This model, when applied to slow transient, horizontal or near-horizontal gas-liquid flows in a one dimensional configuration solved with a sufficiently high resolution computational grid, does not need the use of flow maps during the calculation in order to predict the transition between flow patterns.

The transitions could, in fact, be predicted naturally by the solution of the system of equations through the selection of an adequate set of closure laws kept fixed in the computation.

In presence of two-phase gas-liquid flow, in order to improve the prediction of the interactions between the phases, a **"four-field" model** approach was adopted: it is an improved version of the "two-fluid" model where in addition to the gas and liquid phases, the dispersed gas, bubbles, and liquid, droplets, fields are also analyzed.

In previous sections the first and the mostly applied multi-field model, the "two-fluid" model, was presented. Since the '70s, in fact, the conviction that

two-phase flows could be treated by a separate set of equations, one for each distinguishable field, has been extensively discussed and tested (Banerjee and Weaver, 1978).

Nevertheless, during last decades the idea that a two-phase gas-liquid flow could be accurately investigated with only two fields was substituted by the technique to introduce also continuity, momentum and energy equations for the liquid droplets field (Kolev, 2004).

Several codes evolved towards the so called "three-field" models and among them someone is nowadays used in industrial applications: for instance, in the nuclear industry there is the code F-COBRA-TF (Thurgood et al., 1983), in the Oil&Gas industry the code OLGA (Bendiksen et al., 1991). Some commercial computational fluid dynamics codes as PHOENICS, FLUENT, CFX have a module dedicated to three-field model investigations.

The definition of "field" depends on the goal that the developer might reach and could be defined, in general, as a portion of the flow where the velocity and the flow properties are uniform in the cross section.

The idea behind this change is that the higher is the number of the simulated fields, better will be the prediction and the flexibility in describing 3D phenomena, such as slug or annular flow patterns, even in a 1D description.

Any 1D system of equations, based on a multi-field approach has to be averaged in time and in space in order to be solved some information concerning the microscopic interaction between fields through the interfaces are lost (Banerjee and Chan, 1980).

This lost information must be inevitably reintroduced by the so called closure or constitutive laws.

A closure law is typically an empirical or semi-empirical equation that has to be added to the mathematical, rigorous system of equations in order to enable its solution by specifying terms that would be otherwise unknown.

Closure laws are requested for the prediction of shear stresses, heat and mass transfer between phases.

The accuracy of the solution widely depends on the quality of such closure relationships.

3.2.1. The "four-field" model approach implemented in the MAST code

The "four-field" model considers both dispersed and continuous gas and liquid phases.

The choice of the model implemented in the code is of major importance for the assessment of a one-dimensional flow when the capacity of capturing fluid properties in the cross section, in a better way than the two-fluid model does, could influence the prediction of the transition between flow patterns.

With a four-field model approach the most important flow patterns could be composed by the distribution of the different fields in the cross section (Bonizzi et al., 2009).

So, as discussed in detail in Section 3.2.4, the slug flow could be seen as a continuous gas phase, that may contain some liquid droplets, and an intermittent liquid phase containing gas bubbles. A stratified gas-liquid flow, may be represented as the flow of separated gas and liquid phases, with a limited presence of the dispersed phases. The bubbly flow, in a similar way, should be composed by a continuous liquid phase with an important presence of dispersed gas bubbles.

In the limit of this idealized representation of gas-liquid flow patterns, the annular flow could be described as the condition for the existence of a continuous gas phase, containing entrained liquid drops, and a limited amount of a liquid phase, possibly containing some gas bubbles.

As Bonizzi et al. (2009) stated, in a one dimensional framework the distinction between the stratified and the annular flow is difficult to define in a rigorous way, for the simple reason that an annular flow, as other more complicated gas-liquid flow patterns with physical evidence, is not a one-dimensional phenomenon and so other techniques are needed if a detailed description of liquid film distribution on the pipe wall is requested.

But, as in the case of the MAST code for the design of long hydrocarbon transportation pipelines, if the framework of application is well defined, the inconveniences of this limitation are bounded and the level of accuracy reached by the model has been demonstrated being satisfactory by Bonizzi et al., (2009), in applications for which it was developed and tested.

Several authors previously investigated the multi-field model approach, for instance Ishii, (1975) and Banerjee and Chan, (1980), but the MAST code is the first that proposes the four-field model in an organic way, with each field treated separately if continuous or dispersed, in the Oil&Gas industry.

The four-field model propagates the interfacial area, even if the area is subdivided into continuous and dispersed fields. This is an important property for the application of interfacial transfer phenomena and closure laws at the interfaces.

In MAST, each field volume fraction is estimated through computations of their conservation equations, where ε_L, ε_G, ε_l, ε_g, ε_d, ε_b are respectively the total liquid, total gas, liquid continuous, gas continuous, liquid dispersed and the dispersed gas volume fractions respectively.

The total gas and liquid fields are defined as the sum of the continuous and the dispersed fields:

$$\varepsilon_L = \varepsilon_l + \varepsilon_d \tag{89}$$

$$\varepsilon_G = \varepsilon_g + \varepsilon_b \tag{90}$$

and so $\varepsilon_L + \varepsilon_G = 1$.

The required equations in the case of isothermal flow are: four continuity equations, four momentum equations; in case of non isothermal flow, one energy equation is solved for both the liquid and gas phase in thermal equilibrium.

Two momentum equations are written for the two dispersed fields and two for the gas and liquid layers. The liquid layer is defined as the liquid continuous and the gas dispersed; the gas layer is defined as the gas continuous and the liquid dispersed, identified respectively by the index 1 and 2.

The definition of volume fractions and densities of the two layers are:

$$\varepsilon_1 = \varepsilon_l + \varepsilon_b \tag{91}$$

$$\rho_{1=} \frac{\varepsilon_l \rho_l + \varepsilon_b \rho_g}{\varepsilon_l + \varepsilon_b} \tag{92}$$

$$\varepsilon_2 = \varepsilon_g + \varepsilon_d \tag{93}$$

$$\rho_{2=} \frac{\varepsilon_g \rho_g + \varepsilon_d \rho_l}{\varepsilon_g + \varepsilon_d} \tag{94}$$

where 1 identifies the liquid continuous+gas dispersed layer and 2 the gas continuous+liquid dispersed layer.

The mass balance equations for each of the four fields (liquid continuous, gas continuous, liquid dispersed and gas dispersed) are presented below:

$$\frac{\partial(\varepsilon_l \rho_l)}{\partial t} + \frac{\partial(\varepsilon_l \rho_l U_l)}{\partial z} = -\Phi_e + \Phi_d \tag{95}$$

$$\frac{\partial(\varepsilon_d \rho_l)}{\partial t} + \frac{\partial(\varepsilon_d \rho_l U_d)}{\partial z} = \Phi_e - \Phi_d \tag{96}$$

$$\frac{\partial(\varepsilon_g \rho_g)}{\partial t} + \frac{\partial(\varepsilon_g \rho_g U_g)}{\partial z} = -\phi_e + \phi_{de} \tag{97}$$

$$\frac{\partial(\varepsilon_b \rho_g)}{\partial t} + \frac{\partial(\varepsilon_b \rho_g U_b)}{\partial z} = \phi_e - \phi_{de} \tag{98}$$

where l, g, d, b are the continuous liquid, the continuous gas, the dispersed liquid and the dispersed gas contributions.

To account for the exchanges between fields, due to mass transfers, some source terms are considered in the equations: the bubbles entrainment rate ϕ_e, the bubbles disengagement rate ϕ_{de}, the droplets entrainment Φ_e and deposition rates Φ_d respectively. The velocities U_d and U_b are the droplets and the bubbles ones respectively.

The mass balance equations for the two layers are then obtained from previous equations as:

$$\frac{\partial(\varepsilon_L \rho_l)}{\partial t} + \frac{\partial(\varepsilon_l \rho_l U_l)}{\partial z} + \frac{\partial(\varepsilon_d \rho_l U_d)}{\partial z} = 0 \tag{99}$$

$$\frac{\partial(\varepsilon_G \rho_g)}{\partial t} + \frac{\partial(\varepsilon_g \rho_g U_g)}{\partial z} + \frac{\partial(\varepsilon_b \rho_g U_b)}{\partial z} = 0 \tag{100}$$

The momentum equations for the two layers are presented below, written in terms of the centre of mass velocity of the two mixture fields:

$U_1 = \dfrac{c_b \rho_g U_b + (1 - c_b)\rho_l U_l}{\rho_1}$ for the field 1, and

$U_2 = \dfrac{c_d \rho_l U_d + (1 - c_d)\rho_g U_g}{\rho_2}$ for the field 2,

where $c_{b=} \dfrac{\varepsilon_b}{\varepsilon_b + \varepsilon_l}$ and $c_{d=} \dfrac{\varepsilon_d}{\varepsilon_d + \varepsilon_g}$ are the ratio of each dispersed field volume fraction to the mixture volume fraction of the liquid and gas layer respectively;

where $\rho_{1=} \dfrac{\varepsilon_l \rho_l + \varepsilon_b \rho_g}{\varepsilon_b + \varepsilon_l}$ and $\rho_{2=} \dfrac{\varepsilon_g \rho_g + \varepsilon_d \rho_l}{\varepsilon_g + \varepsilon_d}$.

Then, the momentum equations for layer 1 and 2 are:

$$\frac{\partial(\varepsilon_1\rho_1 U_1)}{\partial t}+\frac{\partial(\varepsilon_1\rho_1 U_1^2)}{\partial z}+\frac{\partial}{\partial z}\left[\left(\frac{\rho_g\rho_l c_b(1-c_b)\varepsilon_1}{\rho_1}\right)\right]U_{S1}^2=-\varepsilon_1\frac{\partial P}{\partial z}-\varepsilon_1\rho_1 g\cos(\theta)\frac{\partial h}{\partial z}$$

$$-\varepsilon_1\rho_1 g\sin(\theta)+(-\frac{\tau_{w1}S_{wp1}}{A})+\frac{\tau_i S_i}{A}-\Phi_e U_l+\Phi_d U_d+\phi_e U_g-\phi_{de}U_b$$

and

$$\frac{\partial(\varepsilon_2\rho_2 U_2)}{\partial t}+\frac{\partial(\varepsilon_2\rho_2 U_2^2)}{\partial z}+\frac{\partial}{\partial z}\left[\left(\frac{\rho_g\rho_l c_d(1-c_d)\varepsilon_2}{\rho_2}\right)\right]U_{S2}^2=-\varepsilon_2\frac{\partial P}{\partial z}-\varepsilon_2\rho_2 g\cos(\theta)\frac{\partial h}{\partial z}$$

$$-\varepsilon_2\rho_2 g\sin(\theta)+(-\frac{\tau_{w2}S_{wp2}}{A})-\frac{\tau_i S_i}{A}+\Phi_e U_l-\Phi_d U_d-\phi_e U_g+\phi_{de}U_b$$

where it is important to notice that the indices 1, 2, U_{S1}, U_{S2}, l, *g*, *d*, *b* represent respectively the layer 1, the layer 2, the slip velocity between bubbles and continuous liquid, the slip velocity between droplets and continuous gas, liquid continuous, gas continuous, droplets and bubbles.

In both expressions, ε is the volume fraction, U is the velocity, g is the gravity acceleration, P is the pressure at the phase interface, h is the liquid height, τ is the shear stress, ρ is the density and A, S_{wp1}, S_{wp2}, S_i, θ are the geometrical parameter for area, wetted perimeter and the pipe inclination.

The terms τ_{w1}, τ_{w2}, τ_i and are the shear stresses defined in the classical way:

$$\tau_{w1}=\frac{1}{2}f_{wk}\rho_k|U_k|U_k \quad \text{where } k=l,g \tag{101}$$

$$\tau_i=\frac{1}{2}f_i\rho_g|U_g-U_l|(U_g-U_l) \tag{102}$$

Then, a special consideration is needed for the two momentum equations for the dispersed fields:

$$\frac{\partial(\varepsilon_m\rho_m U_m)}{\partial t}+\frac{\partial(\varepsilon_m\rho_m U_m^2)}{\partial z}=-\varepsilon_m\frac{\partial P}{\partial z}$$
$$-\varepsilon_m\rho_m g\sin(\theta)+\Omega_e U_k+\Omega_{de}U_m+F_{drag} \tag{103}$$

where the subscript m denotes both the dispersed liquid and the gas fields;

Ω_e and Ω_{de} represent the entrainment and disengagement for both dispersed fields: they are respectively the droplets, or the bubbles, entrainment and deposition rates;

the term F_{drag} accounts for the drag of the dispersed fields acting on their interfaces.

The peculiarity of the defined momentum equations for the dispersed fields is that they were simplified in the form of algebraic equations by the authors because their left hand side, together with the virtual mass and Basset forces, the lift force, the hydraulic head term are small compared to their right hand side.

This approach has been validated (Bonizzi et al., 2009), evaluating the contribution of inertial terms and verifying that dispersed fields contribution do not alter the behavior of the characteristics of the set of equations.

In order to enable the solution of the previously defined system of equations a full set of closure laws has to be added.

3.2.2. The role of closure laws

As already said, the use of a "multi-field" approach does not prevent from the need of full sets of closure laws, as many as the number of involved fields.

Closure laws are necessary for friction factors for the phase-wall and phase-to-phase friction prediction.

A list of references and additional closure laws are given by the authors (Bonizzi et al., 2009) and are presented below in Table 2 and Table 3.

The closure laws taken as reference were selected because they are well known in literature or because they were applied in many test cases performed for validation purposes.

Additional closure laws were tested as well and they could be applied for peculiar applications, e.g. in case the roughness of the pipe plays an important role, or a sensitivity analysis is requested.

Most of the correlations will be presented in detail in Chapter 5 and they will not be introduced here.

Correlation	Reference	Equation and condition for application
Liquid-wall	(Taitel and Dukler, 1976)	$f_{lw} = 16/\mathrm{Re}_l \text{ for } \mathrm{Re}_l < 2100$
		$f_{lw} = 0.046(\mathrm{Re}_l)^{-0.2} \text{ for } \mathrm{Re}_l \geq 2100$
Gas-wall	(Taitel and Dukler, 1976)	$f_{gw} = 16/\mathrm{Re}_g \text{ for } \mathrm{Re}_g < 2100$
		$f_{gw} = 0.046(\mathrm{Re}_g)^{-0.2} \text{ for } \mathrm{Re}_g \geq 2100$
Gas-liquid	(Taitel and Dukler, 1976)	$f_i = 16/\mathrm{Re}_i \text{ for } \mathrm{Re}_i < 2100$
		$f_i = 0.046(\mathrm{Re}_i)^{-0.2} \text{ for } \mathrm{Re}_i \geq 2100$

Table 2: MAST code reference closure laws for friction factors

In Table 2 the gas and liquid Reynolds number were defined in a classical way as

$$\mathrm{Re}_k = \frac{\rho_k U_k D_k}{\mu_k} \tag{104}$$

and the interfacial Reynolds number has been defined as:

$\mathrm{Re}_i = \dfrac{\rho_g \left| U_g - U_l \right| D_2}{\mu_g}$ with $D_2 = \dfrac{4A_2}{S_{w-P2} + S_i}$ that is the hydraulic diameter of the layer 2.

Similarly, the hydraulic diameter of the layer 1 is

$$D_1 = \frac{4A_1}{S_{w-P1}} \tag{105}$$

In Table 3 the Reynolds number for superficial liquid velocity is

$$\mathrm{Re}_{sl} = \frac{\rho_l U_{sl} D}{\mu_l} \tag{106}$$

And the modified Froude number in the Andreussi and Persen (…) correlation is

$$F = (U_g - U_l)\sqrt{\frac{\rho_g}{\rho_l - \rho_g}\frac{\dfrac{dA_1}{dh_1}}{A_2}\frac{1}{g\cos\theta}} \tag{107}$$

In Table 4 other closure laws needed by the code are presented. They are necessary to describe all the mass transfer phenomena between phases thought as interpenetrating continua, see Banerjee and Chan, (1980) and Dinh et al., 2003.

In particular, correlations for bubble entrainment and disengagement, droplets entrainment and deposition rate, droplets size and bubbles size, drag forces acting on the bubbles and the droplets are listed.

U_{wave} is the velocity of a solitary wave flowing downward, σ_{gl} is the gas-liquid surface tension, the coefficient K is the bubble disengagement rate and is usually taken equal to 0.28.

k_d is the deposition velocity that should be taken as 0.1 m/s; the droplets entrainment constant k_e is taken equal to $7.7E-8$.

In the above correlations ,the following Reynolds number and the Eotvos number for droplets and bubbles are defined as:

$$\mathrm{Re}_d = \frac{\rho_g |U_g - U_d| d_d}{\mu_g},\ \mathrm{Re}_b = \frac{\rho_l d_b |U_l - U_b|}{\mu_l} \text{ and } Eo = \frac{g(\rho_l - \rho_g) d_d^2}{\sigma_{gl}}.$$

At present an extensive comparison among all different existing mass exchange term closure laws when applied in the code versus experimental measurements does not exist. The equations reported in Table 4 are, then, the reference ones, suggested by the authors and used during their validation tests.

Further details on these correlations can be found in the related literature.

Correlation	Reference	Equation and condition for application
Liquid-wall	(Spedding and Hand, 1997)	$f_{lw} = 24/\mathrm{Re}_l \text{ for } \mathrm{Re}_l < 2100$ $f_{lw} = 0.0262(\varepsilon_1 \mathrm{Re}_{sl})^{-0.139} \text{ for } \mathrm{Re}_l \geq 2100$
Liquid-wall	Moody eq. (Hall, 1957)	$f_{lw} = 16/\mathrm{Re}_l \text{ for } \mathrm{Re}_l < 2100;$ $f_{lw} = 0.001375\left[1+\sqrt[3]{\frac{2\cdot 10^4 \cdot k}{D_1}+\frac{10^6}{\mathrm{Re}_l}}\right]$ $\text{for } \mathrm{Re}_l \geq 2100$
Gas-wall	Moody eq. (Hall, 1957)	$f_{gw} = 16/\mathrm{Re}_g \text{ for } \mathrm{Re}_g < 2100;$ $f_{gw} = 0.001375\left[1+\sqrt[3]{\frac{2\cdot 10^4 \cdot k}{D_2}+\frac{10^6}{\mathrm{Re}_g}}\right]$ $\text{for } \mathrm{Re}_g \geq 2100$
Gas-liquid	(Andreussi and Persen, 1987)	$f_i = f_{gw} \text{ for } F \leq F_0 = 0.36;$ $f_i = 1 + 29.7\,(\mathrm{Fr} - 0.36)^{0.67}\left(\frac{h_1}{D}\right)^{0.2}$ $\text{for } F \geq F_0 = 0.36$
Gas-liquid	(Andritsos and Hanratty, 1987)	$f_i = f_{gw} \text{ for } \varepsilon_2 U_2 < U_{G,crit} = 5\sqrt{\frac{\rho_{g0}}{\rho_g}};$ $f_i = f_{gw}\left(1+15\left(\frac{\mathrm{U}_2\varepsilon_2}{U_{G,crit}}-1\right)\left(\frac{h_1}{D}\right)^{0.5}\right)$ $\text{for } \varepsilon_2 U_2 \geq U_{G,crit} = 5\sqrt{\frac{\rho_{g0}}{\rho_g}}$
Gas-liquid	(Cohen and Hanratty, 1968)	$f_i = 0.014$
Gas-liquid	(Wallis, 1968)	$f_i = 0.005\left[1+75\varepsilon_1\right]$

Table 3: MAST code reference closure laws for friction factors

Correlation	Reference	Equation and condition for application
Bubble entrainment	(Nydal and Andreussi, 1991)	$\phi_e = \rho_g A\left[0.076\frac{S_i}{D}(U_{wave}-U_l)\right]-0.15$
Bubble disengagement	(Andreussi et al., 1993a), (Andreussi et al., 1993b)	$\phi_{de} = -\rho_g K\left[1.8\frac{\sigma_{gl}g(\rho_l-\rho_g)}{\rho_l^2}\right]^{0.25} S_i(1-\varepsilon_l)$
Drag on bubble	(Tomiyama et al., 1995)	$C_D = \max\left[\frac{24}{\mathrm{Re_b}}(1+0.15\cdot \mathrm{Re}_b^{0.687}), \frac{8}{3}\frac{E_0}{E_0+4}\right]$
Bubble diameter	(Andreussi et al., 1999)	$d_b = \frac{\sigma_{\mathrm{gl}}}{\frac{1}{2}f_{lw}\rho_l U_1^2} We_{crit}^0(1+51.7\varepsilon_b^{1.5}), We_{crit}^0 = 1.05$
Droplet entrainment rate	(Pan and Hanratty, 2002)	$\Phi_e = \frac{4}{\pi D}\frac{k_e}{\sigma_{gl}}\sqrt{\rho_g\rho_l}U_g^2\left(\frac{\rho_l A U_l \varepsilon_l}{D}-100\mu_l\right)$
Droplet deposition rate	(Pan and Hanratty, 2002)	$\Phi_d = \frac{4}{\pi D}k_d\frac{\varepsilon_d}{\varepsilon_g}\rho_l$
Drag on droplet	(Alipchenkov et al., 2004)	$C_D = \frac{18.5}{\mathrm{Re}_d^{0.6}},\ 2<\mathrm{Re}_d<500$ $C_D = 0.44,\ \mathrm{Re}_d > 500$
Droplet diameter	(Sarkhi and T.J., 2002)	$d_d = \frac{1}{\mathrm{U}_{\mathrm{sg}}^{1.1}}\left[4.848\frac{\pi\Phi_e D}{\rho_l U_{sg}}+0.0038\right]$

Table 4: MAST code reference closure laws for friction factors

3.2.3. The numerical solution procedure adopted in the MAST code

The MAST code numerical solution method is based on a standard pressure-velocity coupling scheme, similar to the one recommended in Ferziger and Peric, (1999) in the case of two-fluid models, revisited for its new "four-field" model and optimized from the point of view of CPU time performances. In MAST the pressure equation have been parallelized with the OpenMP library to be computed on multi-cores PC. In MAST code the Poisson equation is solved to obtain the pressure equation and the velocity fields are corrected only once, as better described hereafter.

In particular, this procedure is based on the idea of coupling phase velocity and pressure fields in order to enable information to travel upstream and downstream the pipeline. In fact, for the calculation of mass fluxes through the cell faces, the phase densities need to be corrected with the velocity fields, to keep into account the new pressure value influence (Demirdzic et al., 1993).

In fact, once the mass conservation equations for continuous liquid and gas, for dispersed liquid and gas, and for the total layer 1 and 2 are solved, the volume fraction of each field is obtained.

The combination of the mass equations for the total liquid and gas, divided by the respective densities, used to obtain the pressure equation has the form:

$$\frac{1}{\rho_l}\left[\frac{\partial(\varepsilon_l \rho_l U_l)}{\partial z}+\frac{\partial(\varepsilon_d \rho_l U_d)}{\partial z}\right]+\frac{1}{\rho_g}\left[\frac{\partial(\varepsilon_g \rho_g U_g)}{\partial z}+\frac{\partial(\varepsilon_b \rho_g U_b)}{\partial z}\right]+ \frac{\varepsilon_G}{\rho_g}\frac{\partial \rho_g}{\partial t}+\frac{\varepsilon_L}{\rho_l}\frac{\partial \rho_l}{\partial t}=0 \quad (108)$$

The pressure equation is the only implicitly integrated equation of the model for stability reasons, but the choice of an explicit discretization for all the other equations enables good calculation performance. The stability of the computation is granted by the respect of the Courant number limitation:

$$C=\frac{U_{\max}\partial t}{\partial t}<1 \quad (109)$$

where $U_{\max}$ is the maximum phase velocity.

All the other equations of the model, as the mass, momentum and energy balance equations, are solved through the Thomas' algorithm applied to a tridiagonal coefficient matrix without iteration loops.

The explicit approach avoids computationally expensive calculations because all the problem variables are calculated only on the basis of the old time step values.

Then, the implicit solution of the pressure equation with a pressure velocity coupling starts and a single correction step is necessary to correct the phase velocities previously calculated on the basis of the pressure field. The advection and viscous terms are explicitly computed only once each iteration on the velocity fields.

This procedure is claimed to enforce the mass conservation of not only the total liquid and gas phases, but also of the two dispersed fields (gas bubbles and liquid droplets).

Concerning the discretization method, a finite volume scheme on a staggered grid arrangement was chosen.

3.2.4. The validation of the MAST model

Several tests have been proposed by the authors (Bonizzi et al., 2009) in other to validate the capability of the code to capture the transition between different flow patterns, in addition to the correct prediction of pressure losses and liquid level in the pipeline.

The validation was done on the basis of the MAST code criteria for the identification of flow regimes that are listed below.

In fact, it was shown that the MAST code predicts the transition from a flow pattern to another on the basis of the predicted characteristics of the four field distribution in the control volume.

So, each field contributes to the description of each flow pattern in a way that will be presented below:

- Stratified flow: both stratified gas and liquid layers, with a low concentration of dispersed gas phase (the difference between wavy or smooth interface is not captured);
- Annular flow: both stratified layers with an important presence of void (the way the code describes the annular flow could be easily identified with the stratified flow);
- Slug flow: there are both stratified layers, with the liquid one that could bridge the pipe, causing very thin, or zero, stratified gas layer;
- Bubbly flow: The pipe is fully bridged by the liquid layer without any gas layer.

In Bonizzi et al., (2009) the agreement between the transition conditions found by the MAST code and the transition curves of the Taitel and Dukler map (Taitel and Dukler, 1976) was proposed, see Figure 26.

The results obtained are quite good and the criteria they used to state the presence of the investigated flow patterns were already presented.

The authors reproduced with MAST model the transition boundary between different flow patterns in a horizontal 80 mm ID pipeline, 30 m long, with air and water flowing at atmospheric pressure, paying particular attention to the transition between the stratified and the slug flow, because of the importance of the prediction of slug flow properties in the Oil&Gas field framework, as already explained in previous sections.

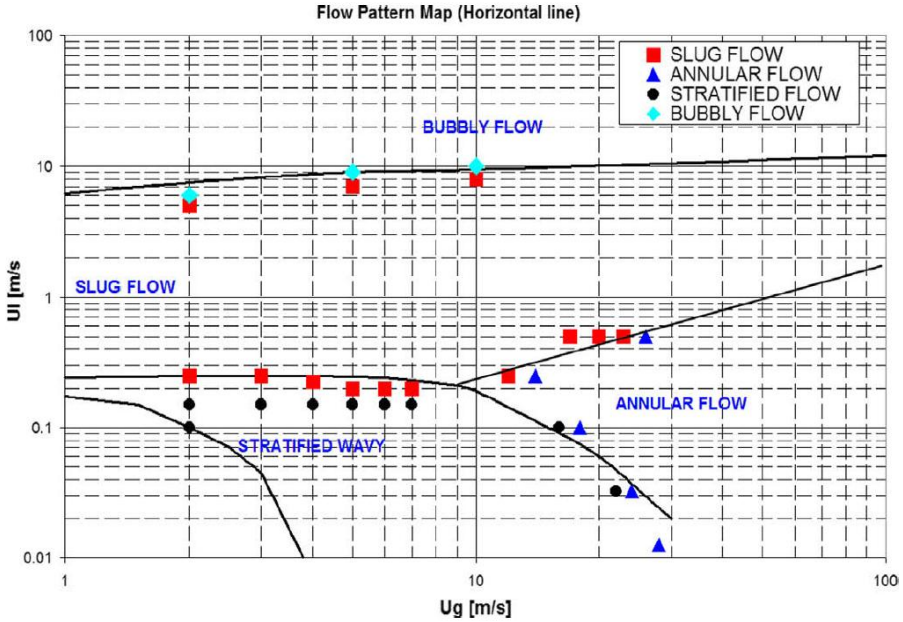

Figure 26: Comparison between prediction of the transition between flow patterns and the Taitel and Dukler flow map (Bonizzi et al., 2009)

Several slug flow properties were, in fact, compared against experimental measurements and closure laws, as briefly discussed below.

The slug bubble velocity predicted by the four-field model has been compared with the closure laws proposed by Bendiksen (1984), obtained from his experimental measurements in an air-water flow at high pressure, in a 3" pipe, see Figure 27, and good agreement was obtained:

$$u_B = C_0 u_{mix} + u_0$$

$$C_0 = \begin{cases} 1.05 + 0.15\sin^2\vartheta & Fr \le 3.5 \\ 1.2 & Fr > 3.5 \end{cases}$$

$$u_0 = \begin{cases} (0.35\sin\vartheta + 0.54\cos\vartheta)\sqrt{gD} & Fr \le 3.5 \\ 0.35\sqrt{gD}\sin\vartheta & Fr > 3.5 \end{cases} \qquad (110)$$

Further validation work was performed (Bonizzi et al., 2009); for the mean slug body length, predictions were compared with measurements of Nydal et al., (1992) in a horizontal pipeline of 0.05 m ID, with air-water flow at atmospheric pressure. MAST code performance is presented in Figure 28

It is important to notice that in Bonizzi et al., (2009) an aspect that was extensively pointed out was the fact that the model implemented in the MAST code was created to investigate 1D phenomena and that it cannot add information about 3D flow properties.

This is the reason why this model cannot distinguish between annular flow and stratified flow with high frequency waves at the interface. In this case, the distribution of the liquid film on the pipe cross section perimeter may not be observed by the code because of its multidimensional nature.

In any case, the transient nature of two-phase flows is correctly captured through the variation of phase distribution in the cross section. In particular, the transition between stratified and slug flow is captured in high detail and the slug flow main properties predicted are in good agreement with physical evidence. It is important to notice that the flow pattern of arrival, after the transition, depends on the flow properties and the boundary conditions but it does not depend on the flow pattern of departure.

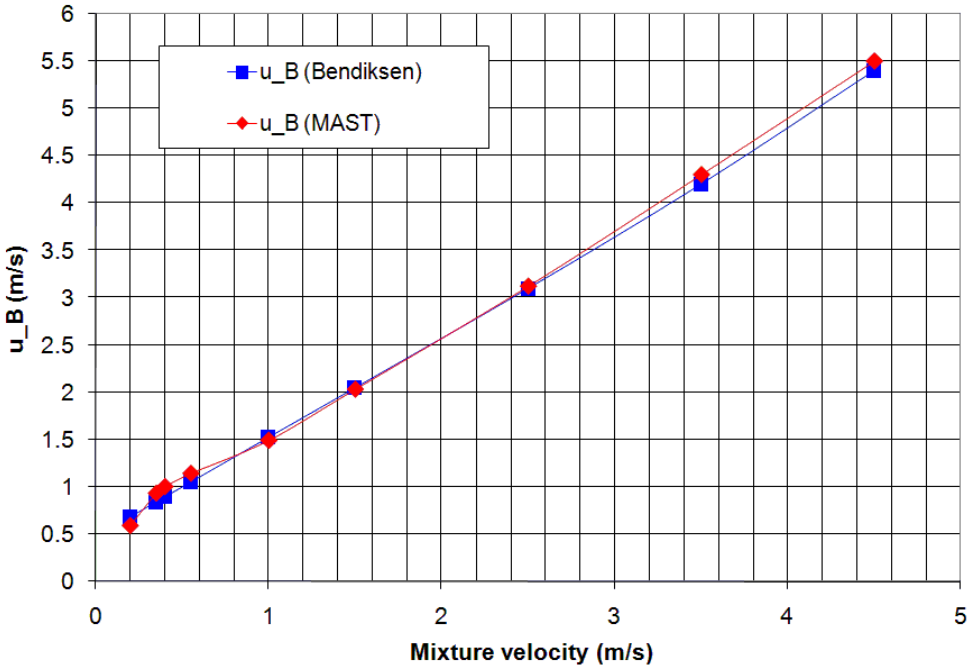

Figure 27: Bubble velocity predictions versus measurements (Bonizzi et al., 2009)

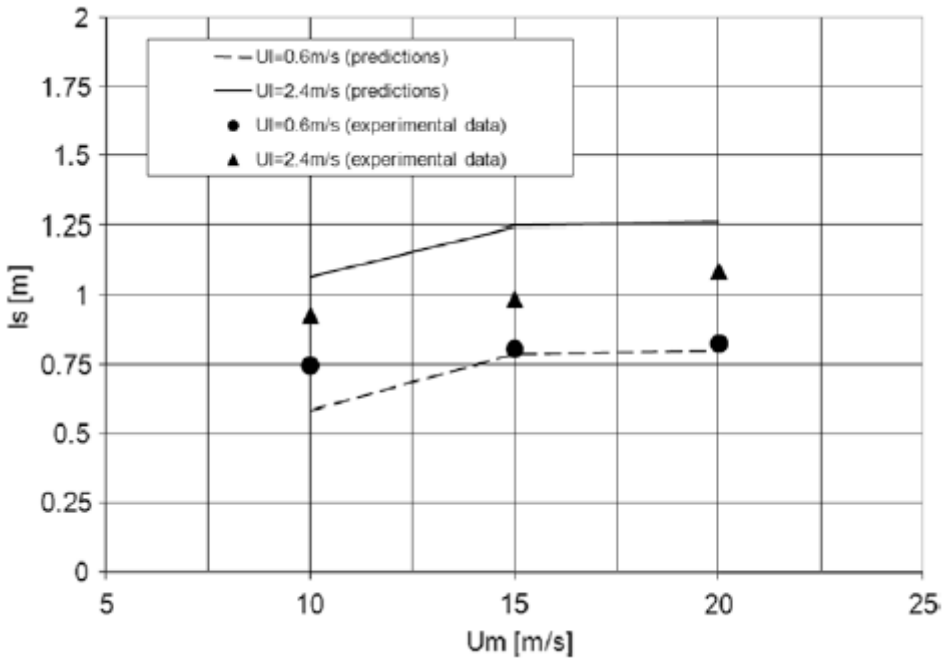

Figure 28: Comparison between code predictions and experiments for mean slug body length (Bonizzi et al., 2009)

An extensive validation of the slug flow predictability by the MAST code has been presented in (Andreussi et al., 2008). In this work, the authors proposed the comparisons between the code predictions and a measurement campaign obtained in the BHR Large Pipeline Test Facility. This test loop enables measurements of slug flow properties reproducing operational conditions close to real field conditions.

The facility is 375 m long with 0.203 m ID and a water-air flow at atmospheric pressure was adopted in this campaign.

The line presents a small vertical riser of 1.4 m at the end of the horizontal part.

The experiments presented include measurements of slug velocity, slug length, slug frequency, pressure losses and mean liquid holdup.

Five runs were performed with different inlet gas mass flow rates, see Table 5.

RUN	Water mass flow rate [kg/s]	Gas mass flow rate [kg/s]
1	26.15	0.057
2	26.15	0.11
3	26.15	0.16
4	26.15	0.24
5	26.15	0.35

Table 5: Mass flow rates for tests of BHR facility (Andreussi et al., 2008)

Comparisons between experimental measurements and MAST code predictions, presented in Andreussi et al., (2008), are re-proposed here from Figure 29 to Figure 33.

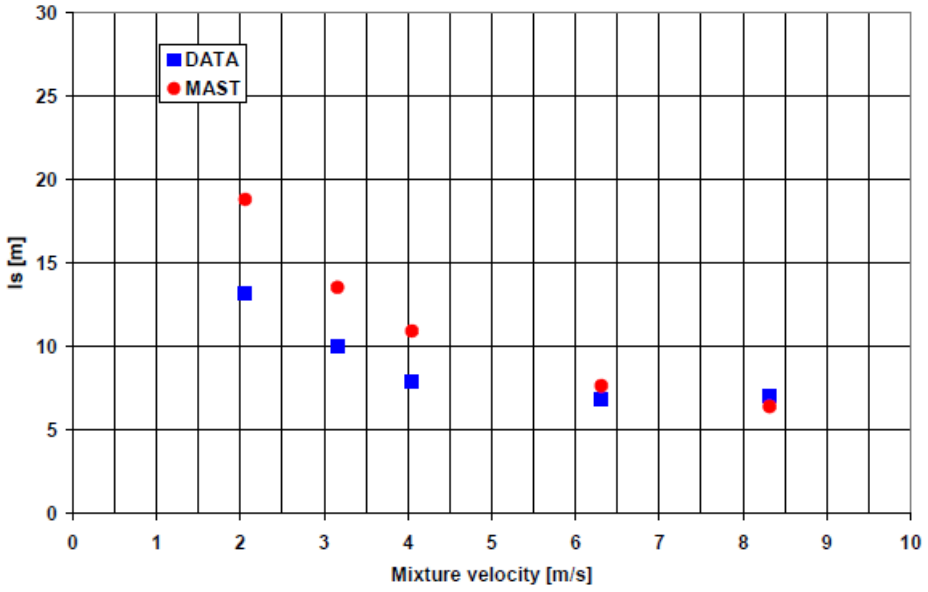

Figure 29: Comparison of slug body length between MAST and the BHR experimental data (Andreussi et al., 2008)

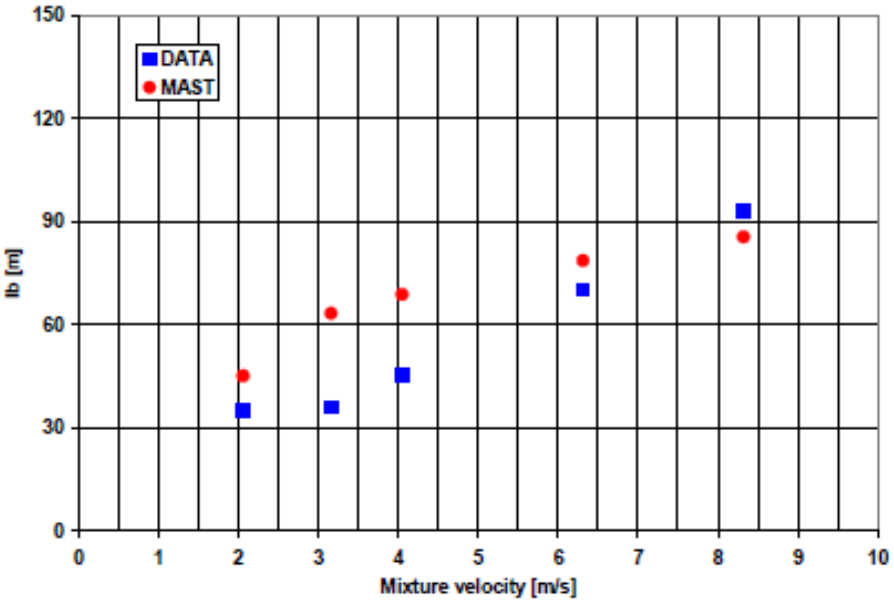

Figure 30: Comparison of bubble length between MAST and the BHR experimental data (Andreussi et al., 2008)

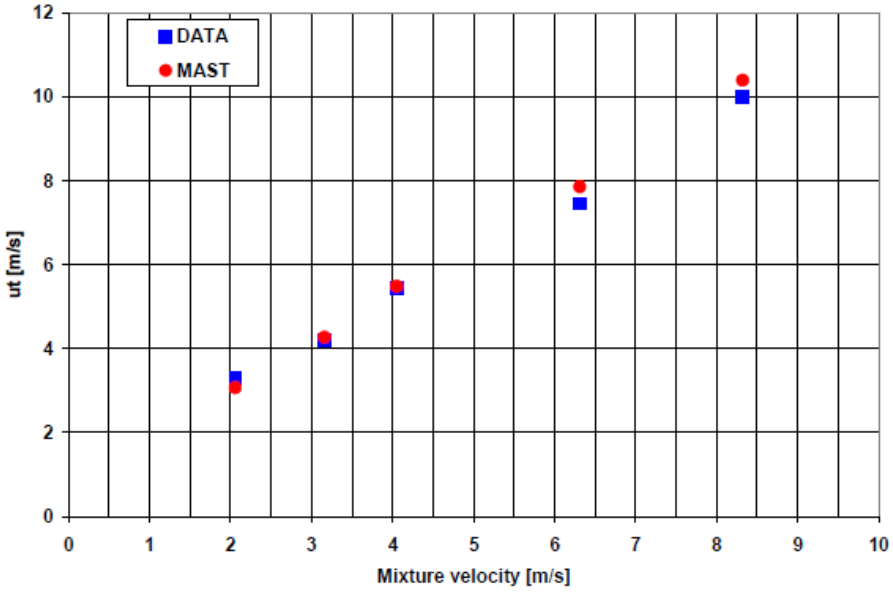

Figure 31: : Comparison of slug velocity between MAST and BHR experiments (Andreussi et al., 2008)

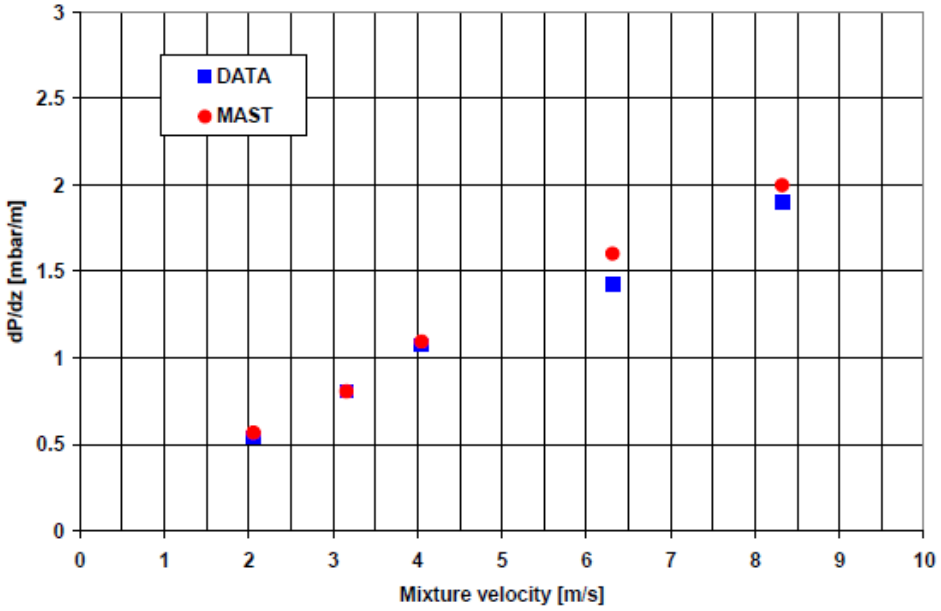

Figure 32: Comparison of pressure gradient between MAST and BHR experimental data (Andreussi et al., 2008)

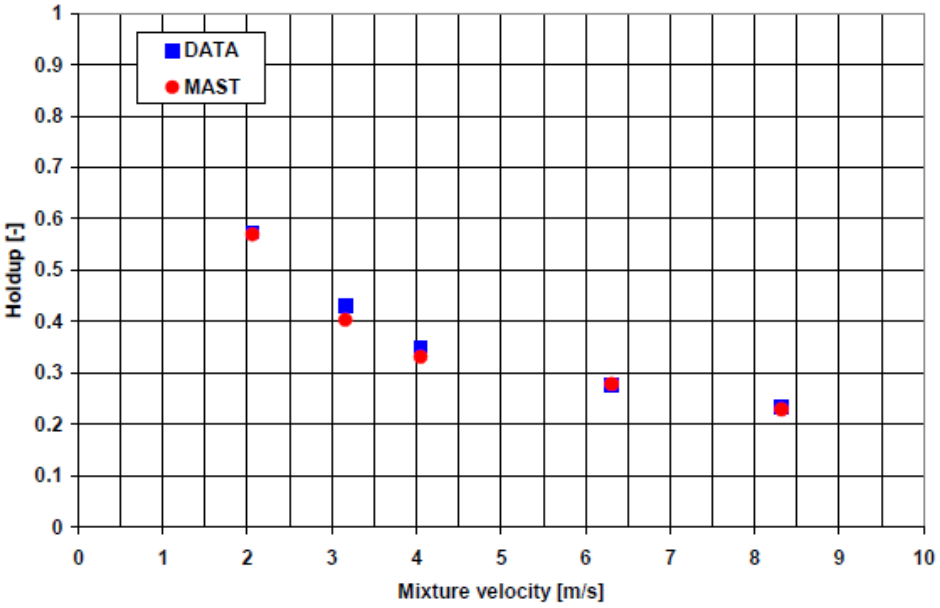

Figure 33: Comparison of liquid holdup between MAST and BHR experimental data (Andreussi et al., 2008)

Further validation of the MAST model has been performed by other authors during the last years. Among them, there is the comparison made by U. Kadri (Kadri, 2009) where his wave transition model from stratified to slug flow or roll-waves has been tested against the MAST model, see Figure 34 that represents the comparison between the theoretical predictions, the code calculations and the experimental measurements of the time formation of slugs and roll waves. The time formation is the time needed by the first

hydrodynamic slug, or roll wave, to grow from stratified flow condition imposed at the inlet of the test facility. The model and the code prediction were evaluated on the basis of experimental measurements coming from a 137 and 16 m long air–water horizontal pipe flows with diameters of 0.052 and 0.06 m

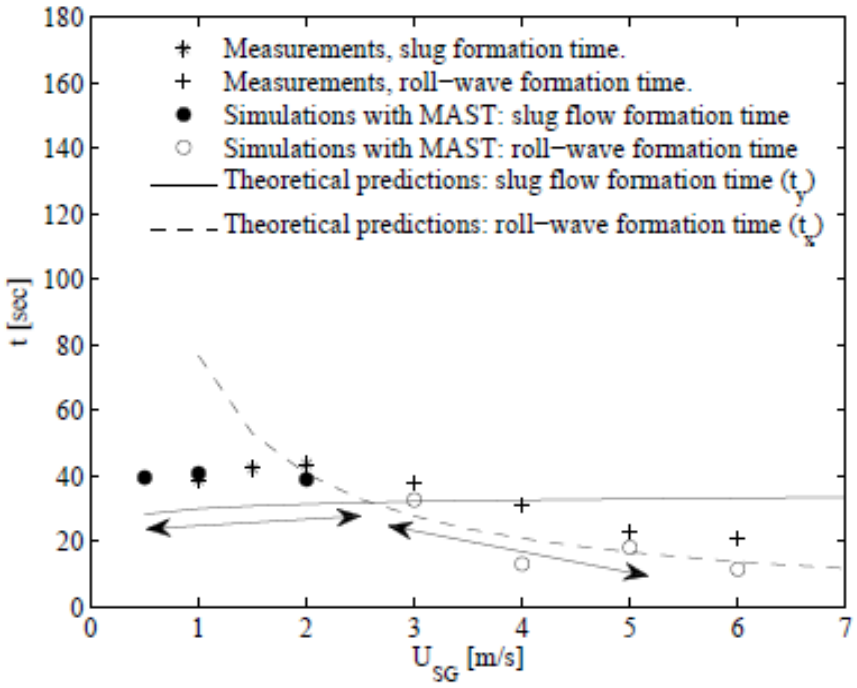

Figure 34: Theoretical predictions of time formation for slug flow (t_y) and roll-waves (t_x) in a horizontal 0.06 m ID pipe with air and water flowing at atmospheric pressure

At the beginning of this doctoral work, the results obtained in the validation of the MAST code in (Bonizzi et al., 2009) in each of the predicted flow patterns was reproduced, applying different boundary conditions at the same pipeline and analyzing the code behavior in any operating conditions considered in term of output information.

The capability of the code of evaluating the growth of interfacial disturbances from an imposed initial stratified flow has been considered simulating a 500 m long, ID 0.079 m, horizontal pipeline where air and water flow at atmospheric pressure, during a transient of 500 s. The inlet conditions were kept constant during the same simulation, but different gas and liquid mass flows have been reproduced.

In the following Figure 35 and Figure 36 the behavior of the code in capturing the transient variation of all different field volume fractions is presented for the most important flow pattern transitions: stratified, slug and annular.

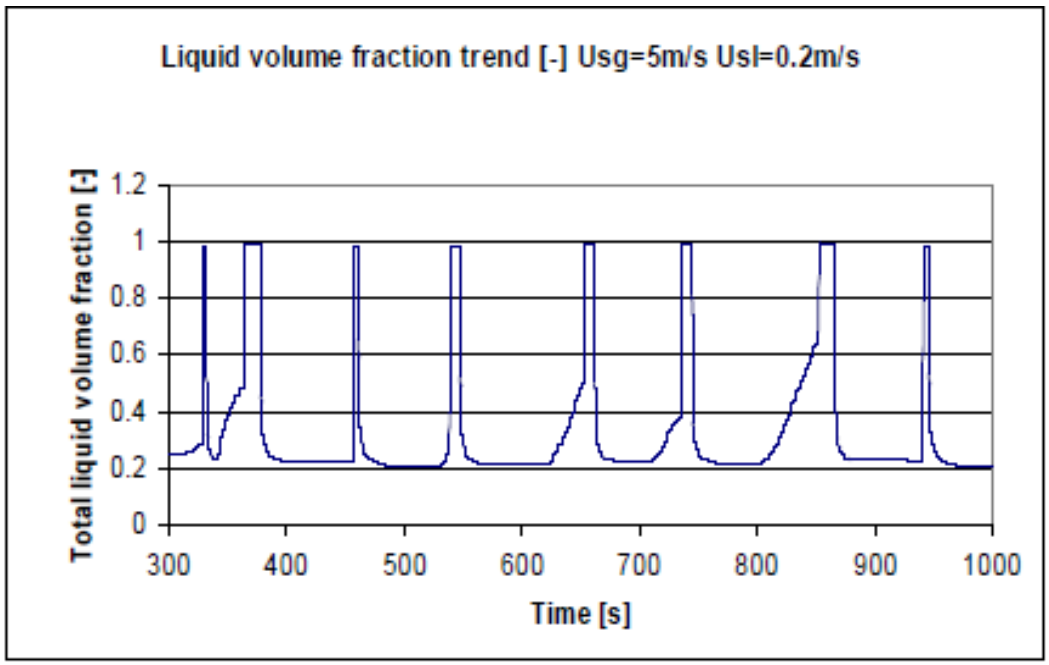

Figure 35: The liquid volume fraction during slug flow pattern as predicted by the MAST code

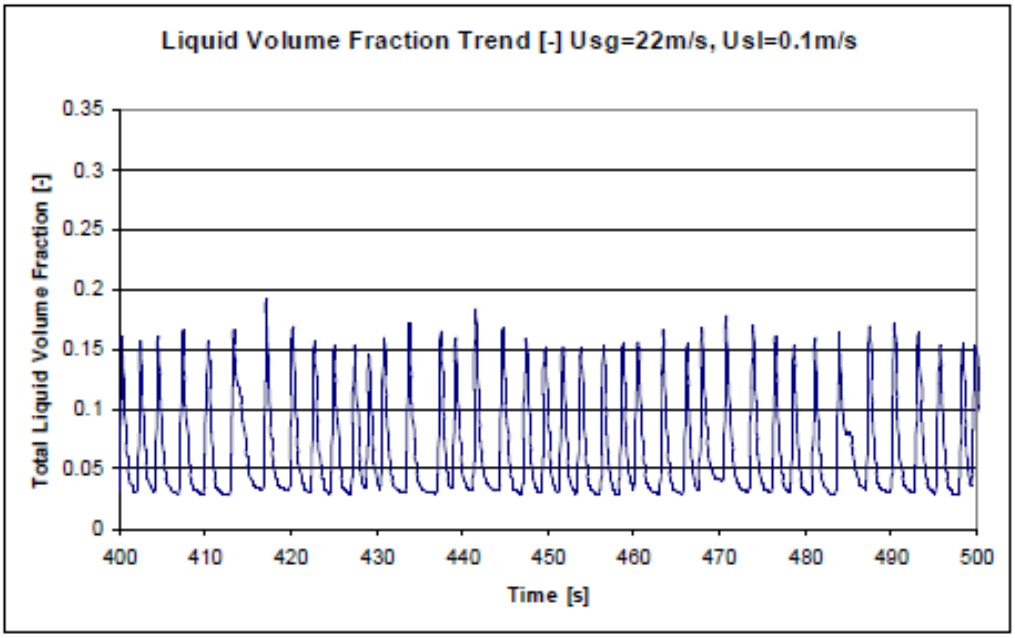

Figure 36: The liquid volume fraction during annular flow pattern as predicted by the MAST code

Chapter 4 Slug flow sub-regimes

4.1 Introduction

The objective of the present chapter is to illustrate the application of the MAST code in the investigation of the slug flow sub-regimes and, in particular, the transitions between the long and the hydrodynamic slug flow regimes, as described by Kadri et al., (2009a). It is shown that MAST is able to capture the correct transition boundaries between these slug flow sub-regimes identified by Kadri, (2009) and to predict with good accuracy the resulting length of the slugs exiting the line.

Slug flow data are taken from several experiments conducted in a 137 m long (L/D=2740) TU Delft facility (ID= 0.052m) by M. Zoeteweij, (2007) and in a 217 m long (ID=0.069m) SINTEF facility in Trondhenim, Norway, by O. Kristiansen, (2004).

More details will be given in next sections. These data were compared against MAST code predictions at different gas and liquid flow rates, at low (atmospheric) and medium (12 bar and 23 bar) pressure conditions.

Several authors investigated the physical mechanisms at the basis of the onset of 3D roll waves and of slug flow from the stratified and stratified-wavy gas-liquid flow. For instance, Taitel and Dukler, (1976), suggested a simple approach to the prediction of the transition from stratified to intermittent flow based on the differential gas-liquid velocity: the transition coincides with the balance between gravity and the pressure difference existing between a wave crest and trough. In literature, other approaches that could be found are: the non-linear inviscid Kelvin-Helmholtz instability analysis (IKH) as shown by Milne Thomson (1968); the linear viscous instability analysis (VKH) of a stratified flow, as reported by Lin and Hanratty, (1986); the slug stability criteria as suggested by Dukler and Hubbart, (1975), Hulburt and Hanratty, (2002), and others. Woods and Hanratty, (1999) added the investigation of growth mechanisms of a liquid slug in different flow rate conditions.

Numerical codes addressing such models are based on slug, or wave, tracking techniques or on experimental flow maps. As already said in previous chapters, this is the case of the many multi-field models used in several nuclear or Oil&Gas industry computer codes. They, in fact, improved the resolution of separate sets of balance equations for each field, but continued to use flow maps.

As said, the “four field model”, as implemented in MAST, cannot distinguish between stratified and stratified-wavy flow patterns, but can predict the growth

of roll-waves simply solving the balance equations, on the basis of the disequilibrium between inertia and pressure forces differences at the gas-liquid interface, see Figure 37. Finally, when the waves grow enough to close the duct, a slug has been detected and simulated by the code.

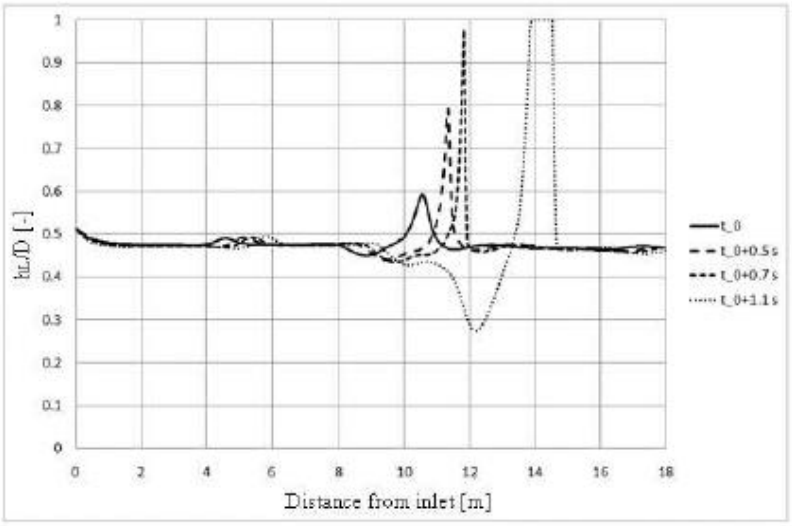

Figure 37: Evolution of hydrodynamic instabilities captured by MAST in a 30 m long pipeline, 0.08 m ID when air and water flow at atmospheric pressure

The computational method implemented for solving the "four-field" model approach remains stable near the ill-posedness condition (Liao et al., 2008) while, within a range of gas-liquid slip velocities, disturbances and roll waves grow in time and space.

The **slug flow** pattern consists of an elongated gas bubble traveling along the tube transporting a plug of liquid. The **stability** of this flow regime is based on the balance between the rate of liquid adjoined from the slug front or detached from the slug tail (Woods and Hanratty, 1996).

The relation among slug types, length, growth rate of waves and stability has been described by Woods and Hanratty, (1996; 1999) and by Woods et al., (2006), with a detailed assessment of the liquid level and of the Froude numbers upstream and downstream the liquid slug. They theorized the existence of slug sub-regimes with different occurrences and supported their model with an experimental flow regime map showing the transitions between them, proposed in Figure 38. In long pipes, in presence of relatively small gas and liquid flow rates, low frequency long liquid slugs form because of roll wave coalescence.

This slug flow subregime is identified with the area numbered I in the figure; it is characterized by low Froude numbers ($Fr < 1$) and the location of its formation is far from the entrance ($L/D > 40$). The line A represents the

transition between stratified and slug flow. Higher frequency and smaller slug lengths can be observed with higher gas and liquid flow rate conditions, area called III, characterized by high flow Froude numbers (Fr > 1) and which form within a length L = 40D from entrance. The zone II has intermediate behavior.

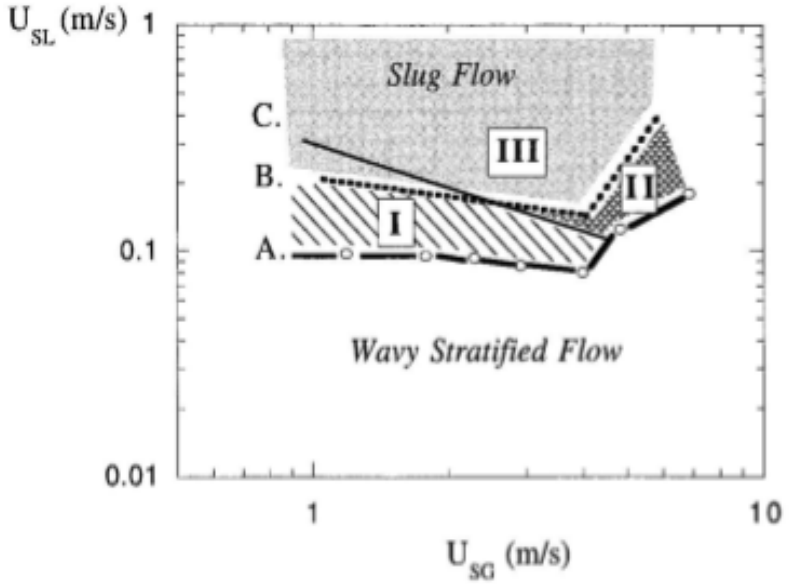

Figure 38: Slug flow sub-regime map Woods and Hanratty, (1999)

4.1.1. Experimental measurements

The measurements at atmospheric pressure used in the present analysis were done by Zoeteweij, (2007) in a U-shaped facility, 137 m long horizontal pipeline with an internal diameter of 0.0525m and a wide turn at 68m from the inlet, presented in Figure 39 and Figure 40. Experiments were performed in a Plexiglas transparent tube that enables visual observation. The test fluids were air and water.

In order to mitigate inlet flow conditions, the two phases are mixed in a Y-shaped section with the gas phase entering from the top. The measurements were performed along the whole line.

The measurements provide a detailed flow map of the long slug regime and sub–regimes.

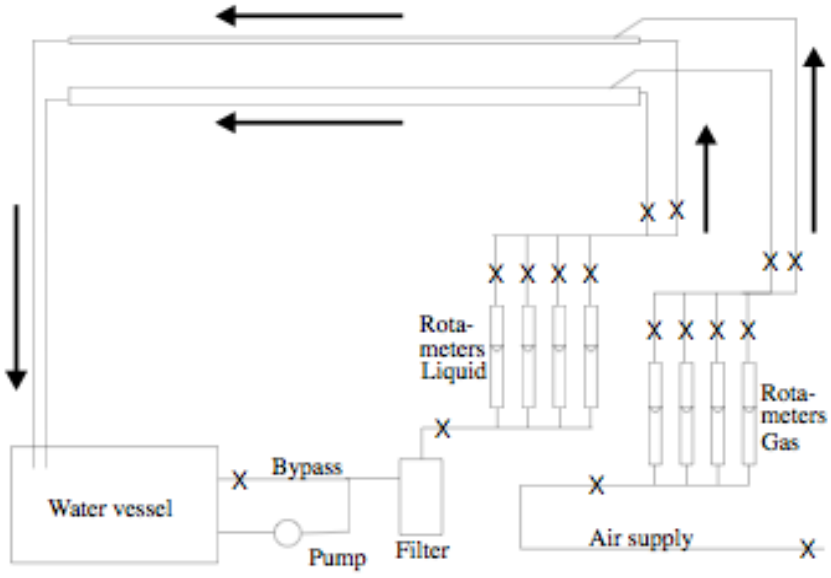

Figure 39: Layout of the TU Delft Facility

8 conductive double point probe sensors (separated by 70 cm) to measure the length and velocity of slugs

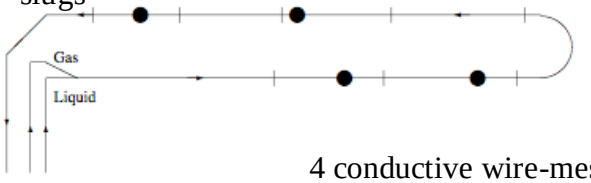

4 conductive wire-mesh sensors which measure the structure of slugs (Prasser et al.,1998)

Figure 40: Low pressure experimental set-up

Similar experiments, conducted at medium pressure conditions, have been performed by Kristiansen, (2004), who investigated the transition from stratified to slug flow in a near-horizontal pipe 217 m long with a 0.069 m internal diameter. The actual test section is 10 3m long, with an inclination of -0.1°. The schematic view of the facility layout is presented in Figure 41. In order to simulate higher pressure conditions, the gas used in the experiments was sulphur hexafluoride, which is a dense gas with density approximately 5.5 times that of air.

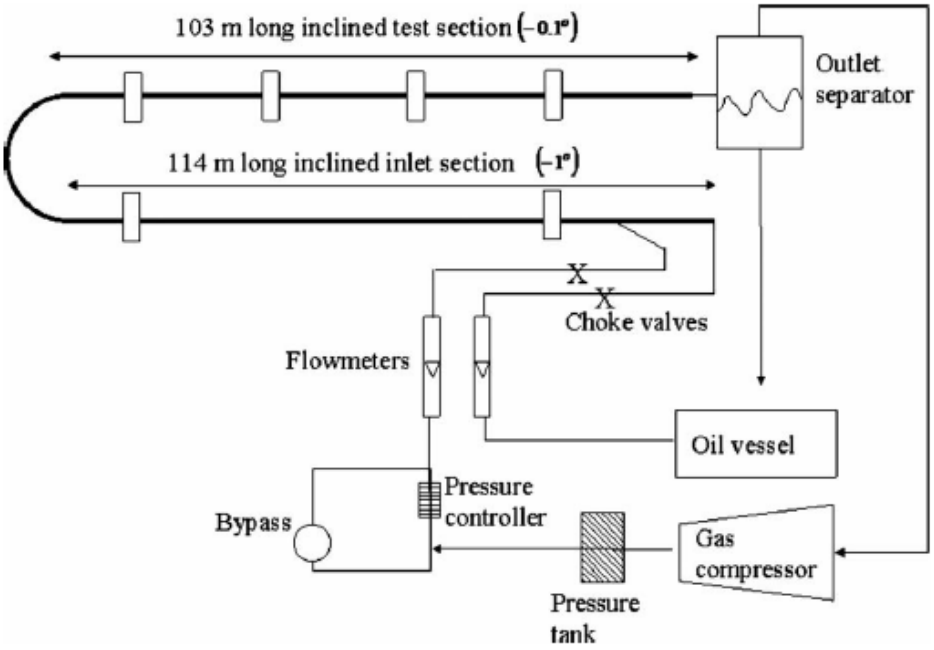

Figure 41: SINTEF laboratory experimental facility layout

The liquid used was ExxsolD80 oil. The range of gas and liquid superficial velocities was 0.2-08 m/s and 0.05-0.5 m/s, respectively. The experimental measurements were taken at operating pressures of 1.5 and 3 bara respectively, giving an effective gas density of, respectively, 9 and 18.5 kg/m^3, simulating therefore operating pressures relative to the gas density of air of 12 and 23 bar, respectively.

Kristiansen, (2004) measured slug sizes that varied depending on the gas and liquid loadings. Kadri in (Kadri et al., 2010) gave their own interpretation of these experimental observations based on their model and on the work of Woods and Hanratty, (1999). Slugs of type I, II and III, classified on the basis of the liquid excess in the slug, were identified in the flow pattern maps generated by Kristiansen, (2004) and presented in Figure 42 for the case of the lower pressure (1.5 bar) series of experimental measurements from Kadri et al., (2010).

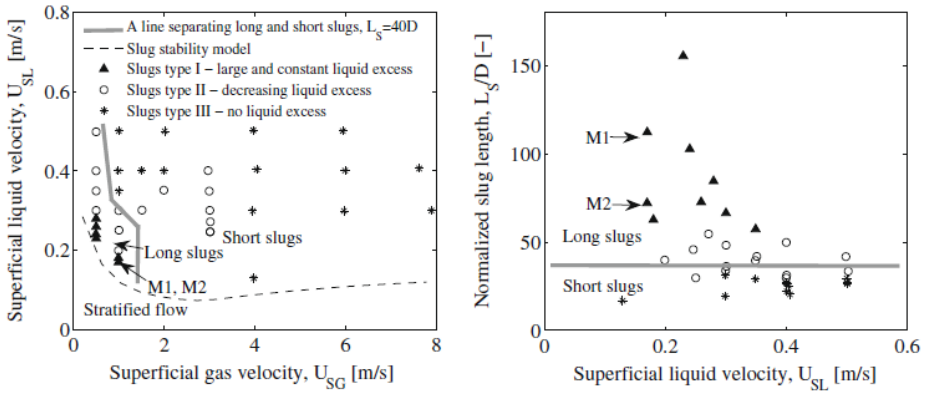

Figure 42: Slug flow sub-regime experimental observations for pressure operating conditions of 1.5 bar and an effective gas density of 9 kg/m^3

Kadri et al., (2010) stated that at higher operating pressure slugs of type I (which are deemed to be the longest that might be generated under slug flow conditions) ceased to exist, and only slugs of type II and III can be detected, as it could be observed in Figure 43 for higher pressure operating conditions.

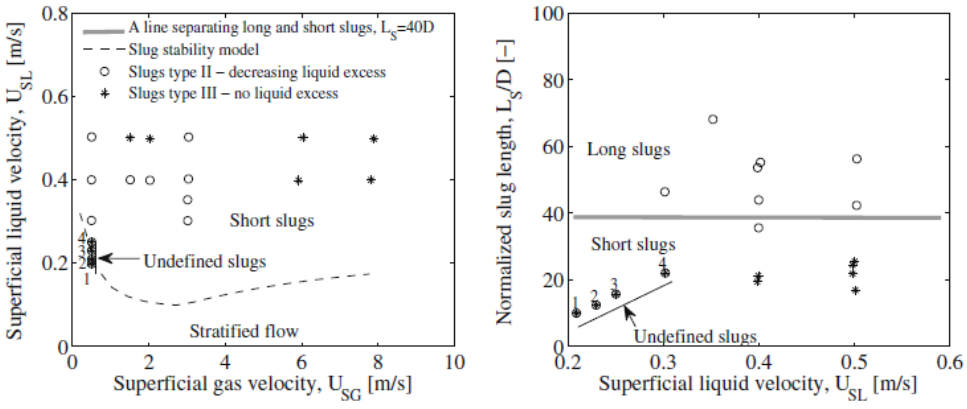

Figure 43: Slug flow sub-regime experimental observations for pressure operating conditions of 3 bar and an effective gas density of 18.5 kg/m^3

The operating pressure has a strong effect on the slugs that are generated and, in particular, higher pressures tend to shrink the long slug flow regime region in the map.

4.1.2. Slug length predictive model

The experiments carried out by Zoeteweij, (2007) showed that, at low gas and liquid loadings and at relatively low pressures, long liquid slugs reaching several hundred pipe diameters may appear for gas-liquid two-phase flow in horizontal and near-horizontal pipes. The slug flow regime was therefore divided in sub-regions making distinction between hydrodynamic and long slugs.

According to the identification criteria adopted by Zoeteweij, hydrodynamic slugs have a typical length around 40 pipe diameters, while long slugs have a typical length around 500 pipe diameters. Kadri et al., (2009a) analyzed the flow patterns observed by Zoeteweij and derived a simplified model for the prediction of flow properties in the long slug region. This model calculates the average slug length from a volumetric liquid balance, between the liquid rates that is added to the slug at the front, and the change in liquid level at the tail of the slug.

In their derivation, Kadri et al., (2009a) addressed the formation of slugs from growing waves. It has to be remarked that the developed model is dependent on some closure laws that are required in order to close the derived set of equations. In particular, the model requires a closure equation to calculate the wave celerity, closures to compute the waves and slug frequencies, and a closure for the propagation velocity of the gas bubble at the rear of the slug. On this basis, the model is able to predict the resulting slug length which will then fall in one of the slug flow sub-regimes identified by Kadri et al., (2009a) depending on the average liquid excess, defined as the difference between the liquid height $h_{L\max}$ for the equivalent stratified flow at the given gas and liquid loadings and the liquid height $h_{L\min}$ at the slug neutral stability:

$$h_L = h_{L\max} - h_{L\min} \tag{111}$$

According to this model, at low gas and liquid flow rates, where the slug frequency is relatively low, a slug which is about to form is far enough from a second slug downstream, and, as a result, the liquid height at the front is not affected by the presence of the second slug.

This slug belongs to the family of the long growing slugs (type I), and for this kind of slugs the actual liquid excess exactly corresponds to that expressed by Eq. (111). For increased but still intermediate gas and liquid flow rates, the slug frequency increases and the liquid height at the front of the slug is affected by another slug downstream. In this case, Kadri et al., (2009a) argue that the liquid excess is roughly half that of Eq. (111).

Slugs characterized by such liquid excess belong to type II, and can be considered long stable slugs. For higher flow rates the number of slugs in the line increases; a forming slug reaches neutral stability immediately after the formation and a short hydrodynamic slug will form. These slugs belong to type III, and, owing to the attained neutral stability condition, the liquid excess will vanish.

Kadri et al., (2009a) has established the long to hydrodynamic slug transition boundary at the value of slug length equal to L_s = 40 D, as shown in Figure 44.

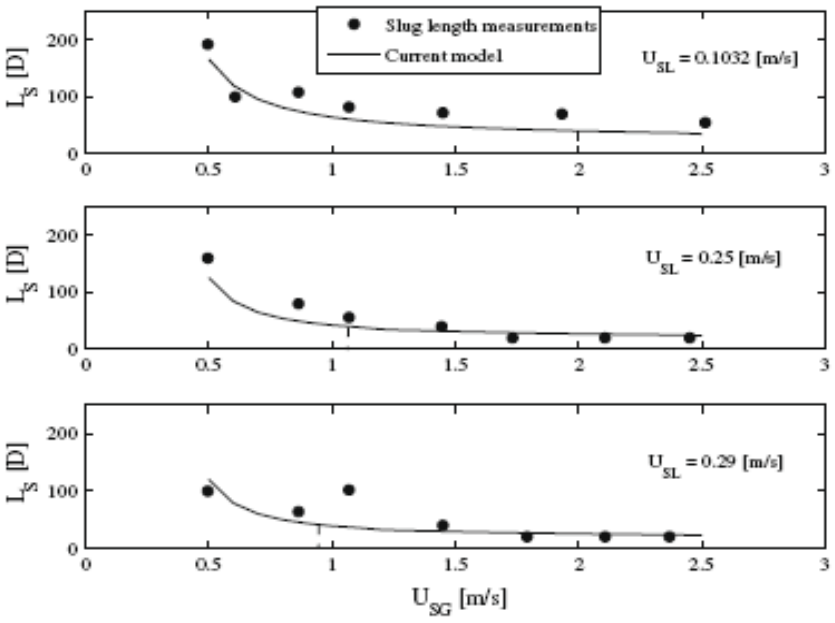

Figure 44: Air-water theoretical predictions and measurements of slug length as a function of gas velocity in a horizontal pipe, 0.052 ID at atmospheric pressure (Kadri et al., 2009a)

Concerning MAST, it was shown that, provided that a fine mesh resolution is adopted, the model is able to predict the transition among the various flow regimes in an automatic way. Bonizzi et al., (2009) demonstrated that the code has the capability not only to predict flow regime transitions, but also to predict the relevant dynamic features of the resulting flow regime.

Hence when slugging occurs, the information related, for instance, to the slug velocity or length, which is required as an input by other transient codes or by the mechanistic model developed by Kadri et al., (2009), is instead an output of this code, altogether with all the other quantities specific to the slug flow regime (pressure gradient and hold-up) . For the purpose of the present work, it is therefore interesting to check if MAST is able to predict the values of the slug length reported by Kadri et al., (2009), at varying gas and liquid flow rates.

4.2 Numerical simulations with the MAST code

The long liquid slug phenomenon occurs at low and medium liquid flow rate, with liquid slug size reaching more than 100 L/D. During the exploitation of an oil and gas field such long liquid slug can cause abrupt fluctuations of supply and variations of the flow rates, producing operating limitations.

So the prediction of slug flow and the capability to distinguish between hydrodynamic and long slug flow have a major importance in the design of long pipelines.

In the following figures, the mechanistic model by Kadri et al., (2009) and the predictions of the transient multi-phase flow simulator (Bonizzi et al., 2009) are compared with the experimental data.

To the author's knowledge, at present the MAST code is the reference tool for the automatic prediction of flow regime transition without the use of any flow pattern map. After the mesh refinement process to one diameter length, arranged in a staggered grid nodalization, the computational procedure, using the explicit scheme for discretized differential terms in time but not in pressure, solves the full set of balance equations until convergence is reached.

For mesh sizes of this order or less, no effect of the mesh size on the computed results was detected.

Figure 45 shows this comparison for the experimental data by Zoeteweij, (2007). In this figure, the average slug body length normalized with respect to the pipe diameter is plotted for a prescribed liquid velocity as a function of the gas velocity.

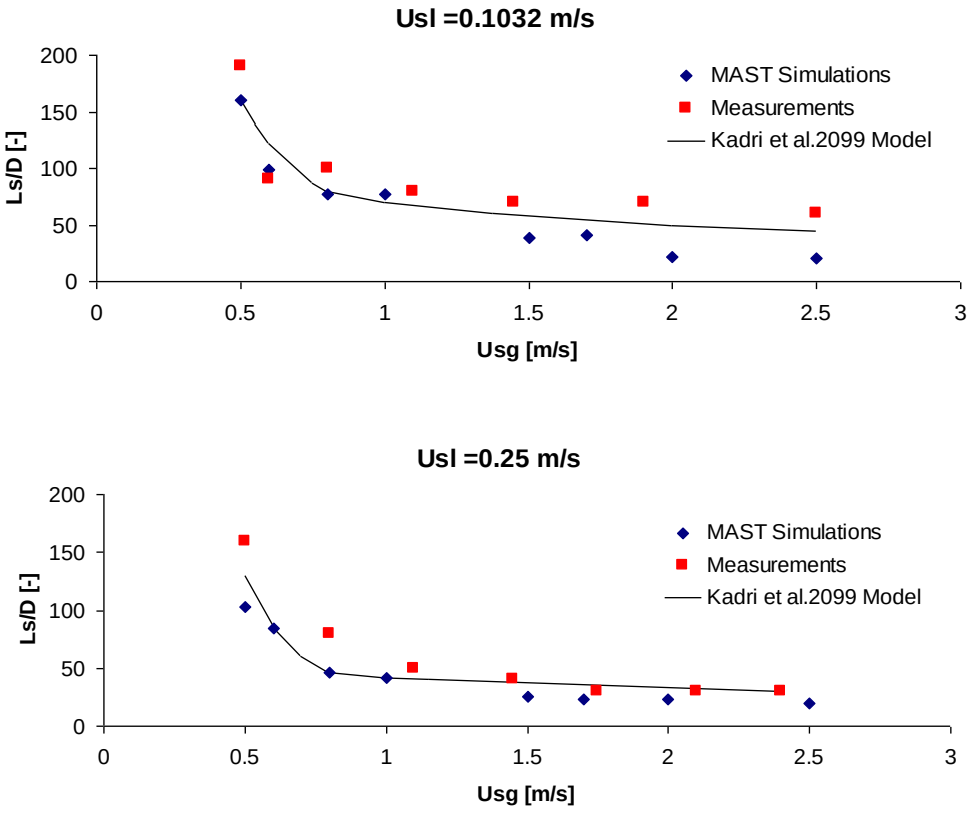

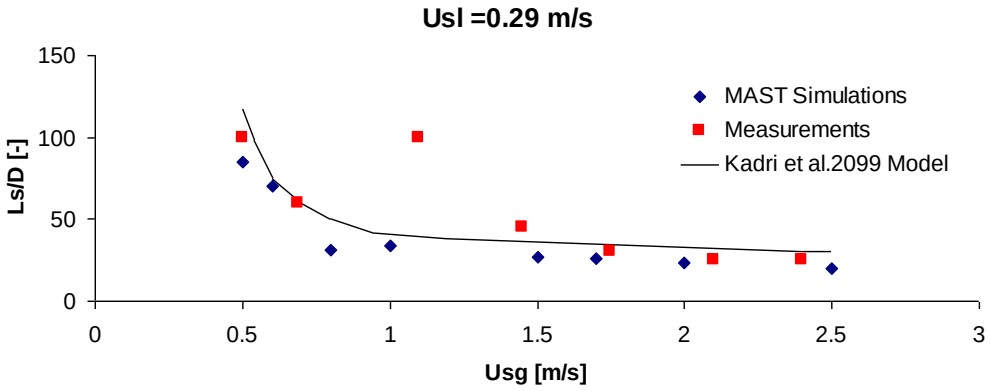

Figure 45: Comparison between MAST simulations, Kadri et al., (2008) model and slug length measurements for three different liquid superficial velocity (0.10 m/s, 0.25 m/s, 0.29 m/s)

This figure shows that both models predict the correct trend, where not only do the slug size decrease at increasing gas superficial velocities, but also the maximum slug size, of the order of hundreds of pipe diameters, is obtained at the lowest mixture velocity. It is interesting to notice that, if one takes the boundary between long and short hydrodynamic slugging to occur for average slug sizes of around 40 pipe diameters, such transition takes place at higher gas velocities when the liquid loading decreases.

The good agreement between the code predictions and the mechanistic model highlights the fact that the numerical methodology (provided that a fine mesh resolution is adopted) captures the physical effects which are the basis for the mechanistic model developed by Kadri et al., (2009a).

Figure 46 shows the comparison between the experimental measurements by Kristiansen, (2004) and the code predictions for the equivalent 12 bar case, with the SINTEF facility that is working actually at 9 bar but using a denser gas, SF6, than the air as explained in §4.1,1. with the gas superficial velocity set at 1.5 m/s. Figure 47 illustrates the comparison for the equivalent pressure case of 23 bar, with the gas superficial velocity fixed at 1.5 m/s.

Both Figure 46 and Figure 47 show a good agreement between the experiments and the code predictions. This confirms the capability of the numerical methodology to predict the formation of slugs of different length even at higher pressure conditions. In particular, this trend confirms the formation of longer slugs at lower superficial liquid velocity.

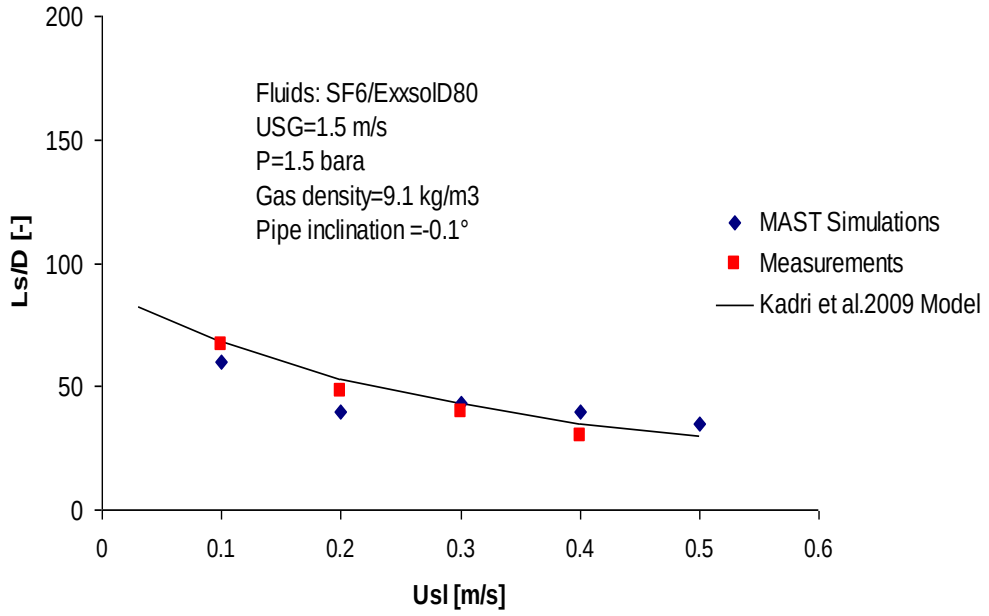

Figure 46: Comparison for average slug sizes between 1D MAST code simulations and experimental measurements by Kristiansen, (2004) for the equivalent 12 bar pressure case

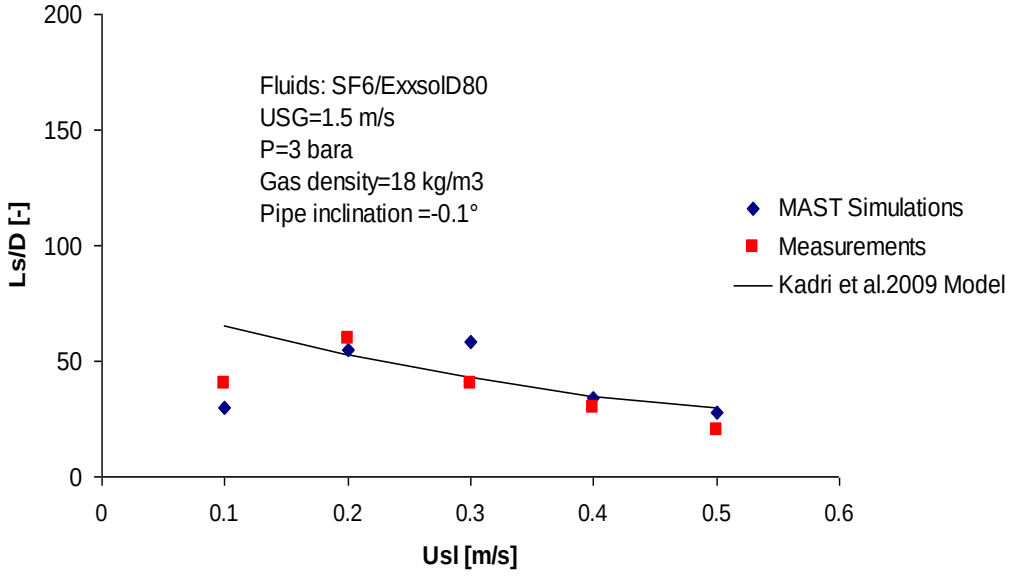

Figure 47: Comparison for average slug sizes between 1D MAST code simulations and experimental measurements by Kristiansen, (2004) for the equivalent 23 bar pressure case.

Considering the good predictions obtained for small pipe diameters at various pressures, it was decided to investigate the possible existence of the long slug

flow regime at larger pipe sizes, typical of industrial production lines and at even higher pressures.

In this regard, a pipe diameter of 0.2 m was considered, with different gas and liquid flow rates and physical properties equivalent to those of the Kristiansen experiments at a pressure of 36 bar.

The results are summarized in Figure 48, where the average slug size is plotted against the gas superficial velocities for different liquid velocities. It is interesting to notice that also at larger diameters the long slug flow regime occurs.

As it results from experimental evidence, the transition between stratified and slug flow occurs at higher liquid loadings than the ones verified at lower pressure operating conditions. As shown in Figure 48, slugs with an average size up to 100 diameters are predicted at the lowest mixture velocities.

Once the gas velocity significantly increases, the slug length tends to values which are typical of the hydrodynamic slug flow regime (around 20-30 diameters).

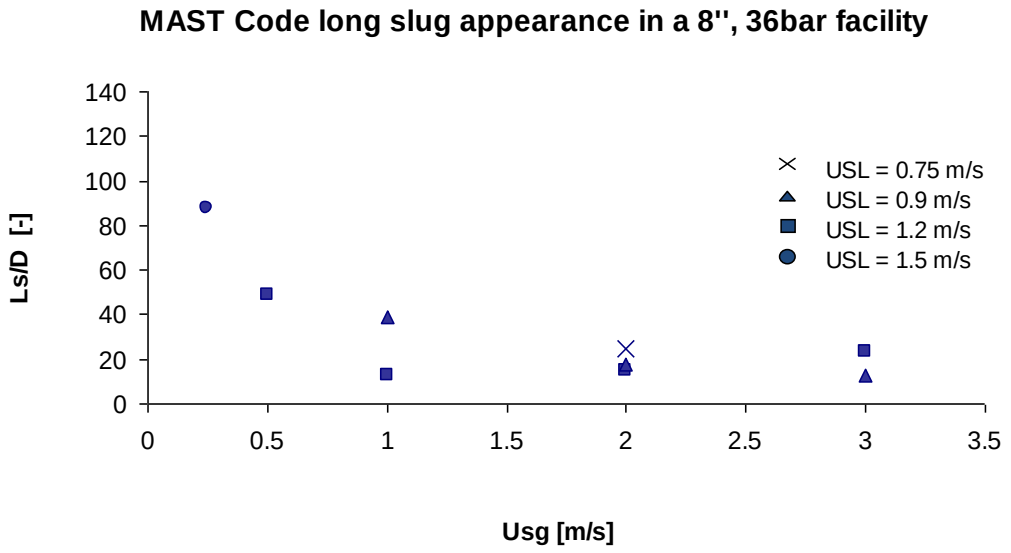

Figure 48: Predictions of slug body length for gas-liquid flow in a 8'' pipe diameter at 36 bar

In conclusion, the MAST code (Bonizzi et al., 2009) allows the prediction of the formation of long slugs in horizontal or near-horizontal pipes to be predicted with good accuracy. Comparing the code results with available experimental data at different pressures, it is found that the code is also able to predict the transition from the long to the short hydrodynamic slug flow

regime. In this comparison, the standard version of the code, with no ad-hoc correlations, has been adopted.

The mechanistic model proposed by Kadri et al., (2009a), based on volumetric balances between the front and the rear of the slug, is also found to be adequate in the estimation of the average slug body length. This model relies upon a number of empirical relations and requires the proper choice of some adjustable parameters. Therefore, it seems dangerous to extend the use of this model beyond the range of parameters on which it is based.

Considering the good agreement between the experiments and the predictions obtained with the multi-phase flow simulator, an attempt has been made to use the simulator to predict the formation of long slugs for larger pipe size and gas density. The obtained results confirm the formation of long slugs at low mixture velocities also for cases of industrial interest.

Chapter 5 Two-phase friction factors in near-horizontal stratified gas-liquid flow

The simplest gas-liquid distribution in a near horizontal hydrocarbon transportation pipeline is the stratified flow. Although this flow pattern is the most frequently analyzed in the literature, up to now large uncertainties still exist between experiments and predictions for pressure drops and liquid level estimation.

At low gas and liquid flow rate conditions, the interface is often represented as flat and smooth; but when the gas flow rate increases the interface experiences instability in the form of 2D waves. An increase of the gas velocity brings to large amplitude waves, called “roll waves”, with possible droplets atomization and entrainment of the liquid phase in the gas flow.

These mass and momentum transfers increase the pressure losses: the interface may be represented as a surface that has a high roughness, with all evidence proportional to the gas-liquid shear stress. A further increase in the gas flow rate brings to two different flow patterns, depending on the liquid flow rate. At low liquid flow rate and high enough gas flow rate the dispersed flow regime takes place: a core of gas, with dispersed liquid drops, flows over a wavy thin liquid layers that covers at least the bottom part of the pipe. At higher liquid flow rates and high enough gas flow rate the slug flow may appear: an intermittent presence of liquid plugs covering the entire cross section, moving at large velocities and entraining a certain rate of gas bubbles.

The idealization in gas-liquid flow regimes definition often omits a number of possible flow patterns that may equally occur in the pipe. Nevertheless, the identification of few reference flow patterns, where a continuous gas component, a continuous liquid component, a dispersed gas component (bubbles) and a dispersed liquid component (droplets) coexist with their own mass and momentum balance equations in a 1D approach, is necessary if an analytical description of involved phenomena is needed.

In configurations typical of gas transportation pipelines, with the presence of condensate and water, the reference flow pattern can be classified as a stratified/dispersed flow, in which a thick layer of liquid flows on the bottom of the pipe, due to the gravity effect, and a consistent amount of liquid is entrained by the gas when the gas velocity is higher than a threshold value.

In this context, the minimum requested information includes the liquid holdup, the liquid level distribution on the duct perimeter, the interfacial instability growing effects and its onset conditions, the pressure losses and the friction

factor coefficients, the droplet entrainment and deposition rates and the mechanisms causing the droplet spreading on the pipe surface.

5.1 Formulation of nearly horizontal gas-liquid flow model

In the following, the most commonly and widely used models and procedures for the analytical calculation of holdup and pressure gradient in stratified, stratified-wavy flows will be presented.

Below the steady state mass and momentum balance equations for a gas and a liquid flowing concurrently in a near-horizontal pipe, modeled as a 0D system, integrated over the cross sectional area, are presented:

$$\varepsilon_k U_k = \frac{Q_k}{A} = U_{sk} \qquad \text{with k = L, G;} \tag{112}$$

$$A_k\left(\frac{dp}{dx} + \rho_k g \sin\theta\right) + \tau_{wk} S_{wk} \pm \tau_i S_i = 0 \tag{113}$$

where ε_k is the volumetric liquid fraction, U_k is the real velocity of phase k, Q_k is the volumetric flow rate of phase k, A is the cross section area, U_{sk} is the superficial velocity of phase k; A_k is the cross sectional area occupied by the phase k, $\frac{dp}{dx}$ represents the pressure gradient, ρ_k is the density of phase k, θ is the pipe inclination with respect to the horizontal axis, τ_{wk} and τ_i are the wall shear stress for phase k and the interfacial shear stress, S_{wk} and S_i are the hydraulic perimeter at the wall of phase k and the interfacial chord length.

The knowledge of the interfacial shape and of the phase volumetric distribution, for both gas and liquid components in the cross section, enables the solution of mass and momentum balance equations.

5.2 Phenomenological modeling of stratified flow

The correct form of all geometrical parameters describing the distribution of each phase in the cross section in stratified flow is easily obtained from the wetted liquid angle δ_l value or, alternatively, from the dimensionless liquid height See Figure 49, where *D* is the internal diameter and A_k the cross section area occupied by each phase.

In particular, the liquid wetted angle is defined as:

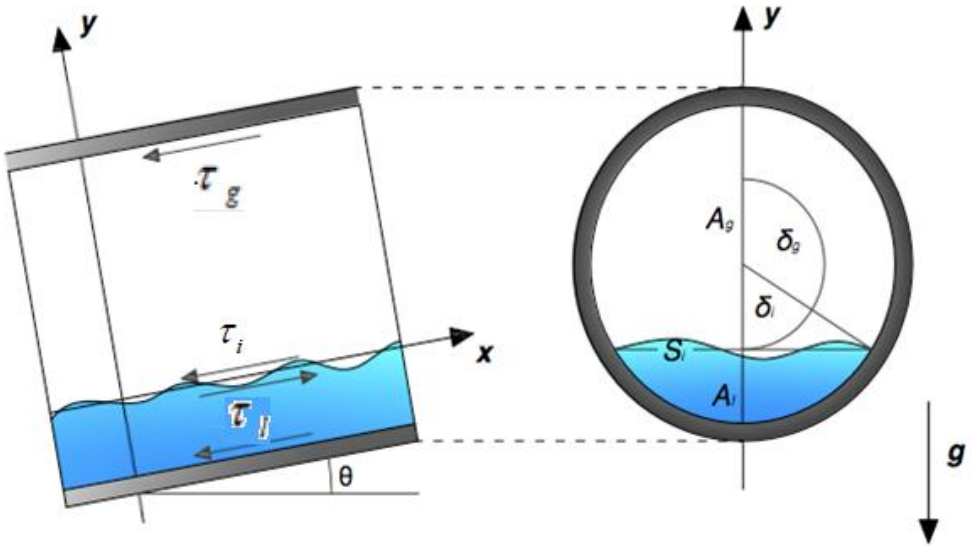

Figure 49: Stratified gas-liquid flow model

$$\delta_L = \arccos(2(\frac{1}{2} - \frac{h_L}{D})) \tag{114}$$

The hydraulic perimeter of phase *k* and the interfacial cord length could be expressed as:

$$S_{wk} = D\delta_k, \qquad S_i = D\sin\delta_l \tag{115}$$

The volumetric liquid fraction is:

$$\varepsilon_L = \frac{1}{\pi}(\delta_L - \frac{1}{2}\sin 2\delta_L) \tag{116}$$

The cross sectional area occupied by the phase k is:

$$A_k = \varepsilon_k A \tag{117}$$

Two further equations come from the "jump condition" of shear stress continuity at the interface and from the geometrical correlation between volume fractions:

$$\sum_{k=L,G} \tau_k^i = 0, \qquad \sum_{k=L,G} \varepsilon_k = 1 \quad . \tag{118}$$

Equation for gas-wall, liquid-wall and interfacial shear stresses are also required in order to find the complete solution for the stratified gas-liquid flow, in terms of holdup and pressure gradient estimation.

The gas-wall and liquid-wall shear stress are defined as:

$$\tau_k = \frac{1}{2} f_k \rho_k U_k |U_k| \tag{119}$$

The interfacial shear stress is:

$$\tau_i = \frac{1}{2} f_i \rho_G (U_G - U_L) |(U_G - U_L)| \tag{120}$$

The f_k and f_i coefficients are the gas-wall, liquid-wall and interfacial friction coefficients, necessary to the 1D numerical solution of the problem.

The unresolved and weakest points of this model are the friction factors because these coefficients are strongly dependent on the gas and liquid velocities, mixture properties and geometrical parameters. In particular, to optimize the interfacial friction factor correlation the interfacial instabilities have to be taken into account; the liquid-wall friction factor has to include the interfacial shear stress effect. These theories were presented in open literature by Hanratty and collaborators (Hanratty, 1976; Andritsos and Hanratty, 1987; Hurlburt and Hanratty, 2001) and have been recently reproposed by the working group of Biberg and colleagues (Biberg, 1999; Biberg, 2005). But a full set of friction factor correlations, liquid-wall and inerfacial gas-liquid, with these features for the prediction of shear stresses in operating condition typically encountered during the design of hydrocarbon long transportation pipelines, is not yet available in literature.

The objective of the present work is, then, the development of a new set of friction factor correlations, based somehow on previous theories, but optimized on a wider range of experimental measurements with low, medium and high pressure operational conditions.

5.3 Available friction factor correlations

A literature search on available friction factor correlations accounting for interfacial instabilities, in the form of both small or roll waves, has been performed. None of the correlations analyzed has been based on a sufficiently complete high density and high viscosity data set, and their field of application is limited.

In closure law definition, two different approaches could be distinguished: the empirical models, based on a collection of data and a subsequent correlation of those data with purely empirical, or weakly physical approaches; the phenomenological model, based on "a priori" definition of geometrical parameters and interfacial shape in order to obtain analytical phenomena formulations.

These two different types of models have important limitations: the former do not take into account peculiar gas-liquid distributions in the cross section; the latter have extremely limited validity range.

Another important classification is between standard models, born to cover the entire range of gas-liquid flow rates, and specific models, realized to describe a peculiar gas-liquid geometrical distribution.

5.3.1. Available friction factor correlations: standard models

The most used among existing models of general application is the Taitel and Dukler, (1976), which is based on a Blasius type correlation:

$$f_{k,w} = c_k (\mathrm{Re}_k)^{-n_k} \quad , \tag{121}$$

This model provides a complete formulation for phase-wall and interfacial friction factors:

$$(c_k, n_k) = \begin{cases} (16,1), \textit{for } \mathrm{Re}_k \le 2100; \\ (0.046,0.2), \textit{for } \mathrm{Re}_k > 2100; \end{cases} \tag{122}$$

where $$\mathrm{Re}_k = D_k U_k / \nu_k \tag{123}$$

and $$D_L = 4\frac{A_L}{S_L}, \qquad D_G = 4\frac{A_G}{S_G + S_L} \tag{124}$$

For the interfacial friction factor it is assumed $f_i = f_{wg}$, hypothesizing that $U_{SG} >> U_{SL}$.

Later, in the work of Andritsos and Hanratty, (1987) **,** a new approach for the stratified gas-liquid flow closure laws was proposed, with an accurate assessment of interfacial friction factor at stratified smooth and rough surface transition, in presence of two different liquids (water and air; water-glycerol and air) and two different pipe diameters (0.0252 m; 0.0953 m), flowing at atmospheric pressure.

The interfacial friction factor experiences a strong increase, proportional to gas superficial velocity, when disturbance waves appear at the gas-liquid interface. Assuming a flat interface, the proposed correlation is:

$$\frac{f_i}{f_G}=\begin{cases}1,\ for U_{SG}\le U_{SG,c}\\ 1+15(\frac{h_L}{D})^{0.5}(\frac{U_{SG}}{U_{SG,c}}-1),\ for U_{SG}>U_{SG,c}\end{cases} \tag{125}$$

where $U_{SG,c}=(5m/s)(\rho_{G0}/\rho_G)^{0.5}$ and ρ_{G0} is the gas density at atmospheric pressure.

In the work of Andreussi and Persen, (1987) the shape of interfacial waves and the appearance of disturbance waves were analyzed in depth. Different pipe inclinations and different liquid viscosities were taken into account.

The following correlation, tested on a limited experimental data set, has been proposed by these authors:

$$\frac{f_i}{f_G}=\begin{cases}1,\ for F\le F_0\\ 1+29.7(F-F_0)^{0.67}(\frac{h_L}{D})^{0.2},\ for F>F_0\end{cases} \tag{126}$$

where the dimensionless group F is the Froude number, comparing the inertial and gravitational forces

$$F=U_G(\frac{\rho_G}{\rho_L-\rho_G}\frac{1}{A_G}\frac{dA_L}{dh_L}\frac{1}{g\cos\beta})^{0.5} \tag{127}$$

and F_0 is the value of the Froude number for which the appearance of small waves starts; this is usually assumed to have a value between 0.36 and 0.5. The authors stated in their publication that the Blasius correlation could not estimate properly the liquid-wall friction factor.

Kowalski, (1987) in his work analyzed a measurement campaign of wall shear stress that he used to determine a new liquid-wall friction factor correlation and to extrapolate a new gas-liquid interfacial friction factor. He collected data from two circuits circulating air or Freon 12 with water as liquid.

The proposed liquid-wall friction correlation is:

$$f_{w,L} = 0.263\left[\varepsilon_L \, \mathrm{Re}_L^+\right]^{-0.5} \tag{128}$$

where $\mathrm{Re}_L^+ = (j_L D)/\nu_L$.

The proposed interfacial friction factor is the one presented below:

$$f_i = 7.5\times10^{-5}\,\varepsilon_L^{-0.25}\,\mathrm{Re}_G^{-0.3}\,\mathrm{Re}_L^{0.83} \tag{129}$$

where its validity domain is

$22{\cdot}600 \le \mathrm{Re}_G = (U_G D)/\nu_G \le 430{\cdot}600$ and

$8800 \le \mathrm{Re}_L = (U_L D)/\nu_L \le 47{\cdot}800$.

In the work of Spedding and Hand, (1997) a new correlation was presented, with the difference that this correlation was based on a wide experimental data base, with different pipe inclinations, different internal pipe diameters (between 0.025 m and 0.0953 m) and different liquid viscosities (between 1cP and 100 cP).

The proposed correlation for the liquid-wall friction factor is:

$$f_{SL} = 0.0262(\varepsilon_L \, \mathrm{Re}_{SL})^{-0.139} \tag{130}$$

where $\mathrm{Re}_{SL} = \dfrac{U_{SL} D \rho_L}{\mu_L}$.

The proposed interfacial friction factor is:

$$\frac{f_i}{f_{SG}} = \begin{cases} 1.76 + \left(\dfrac{U_{SG}}{6}\right) + k_i \end{cases} \tag{131}$$

where $k_i = 2.7847 \log_{10}(\beta_L)_r + 7.8035$ and $(\beta_L)_r = \dfrac{U_{SL}}{U_{SL}+6}$.

An new attempt towards two-phase flow phenomenological modeling was proposed by **D. Biberg**. His approach was based on a classical turbulence model and on the definition of a "capillary number" or a "mixing length" at the interface, derived from the "eddy viscosity" concept and the Prandtl's theory (Biberg, 1999). Through these parameters, Biberg could express the interfacial roughness in terms of an interfacial turbulence.

Biberg, by a careful elaboration of an approximation for the turbulent velocity profile in both the liquid and the gas fields, was able to express the gas-wall and liquid-wall friction factors with a Colebrook like approach, adding a typical gas and liquid hydraulic diameter evaluation and the contribution of the interfacial shear stress.

The proposed phase-wall friction factor shape is:

$$\frac{1}{\sqrt{\lambda}_k} = -1.8\log_{10}\left(\frac{6.9}{\mathrm{Re}_{D_{ki}}} + \left(\frac{k_s}{3.7D_k}\right)^{1.11}\right) \mp 2\log_{10}\left(1+\frac{S_i}{S_{wk}}\right) sign\left(\frac{\tau_i}{\tau_k}\right)\left(\left|\frac{\tau_i}{\tau_k}\right|\right)^{0.5} \quad (132)$$

The interfacial friction factor correlation presented in Biberg, (1999) is:

$$\frac{\tau_i}{\tau_G} = \frac{\frac{S_{wG}}{S_{wG}+S_i} KC_a f(\delta_G)}{1-\frac{S_i}{S_{wG}+S_i} kC_a F(\delta_G)} \quad (133)$$

where K = 750, $C_a = \frac{\mu_m U_r}{\sigma}$ is the "capillary number" and U_r, σ are, respectively, the slip between phases and the surface tension.

$\mu_m = \frac{\mu_G \mu_L}{(\mu_G \delta_L^* + \mu_L \delta_G^*)}$ is the mixture viscosity, function of phase viscosities and of liquid holdup. The dependence from the liquid holdup is defined with the functions δ_f^*,with f representing both the liquid and the gas phases, for which the author gives the values represented in Figure 50.

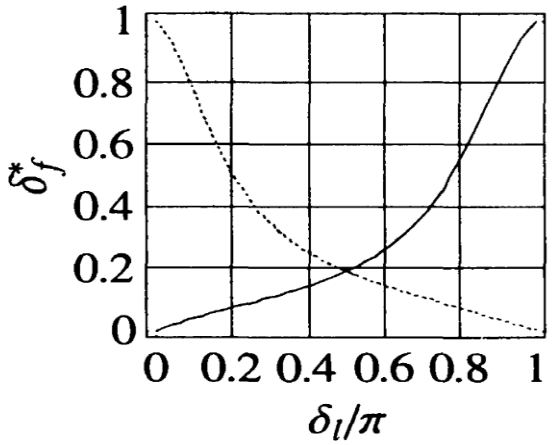

Figure 50: Functions defined versus the liquid wetted angle for liquid (solid line) and gas (dashed line) (Biberg, 1999)

The complete Biberg theory will not be discussed here, but it can be found in his publication (Biberg, 1999), where the author explained that the numerical coefficients, that are the closure values of his models, were obtained from a limited experimental data base Espedal (Espedal, 1998).

In conclusion, a gas-liquid flow can approximately be represented as a stratified, flat interface flow in a wide range of applications in presence of a

large pipe diameters (> 50 mm) and/or low gas flow rate (< 15 m/s), but a good interfacial friction factor has to take into account also the growth of interfacial instabilities.

All the correlations and models presented above are a starting point for the development of a better model, possibly based on enough experimental data measurements at typical natural gas transportation pipelines operational conditions.

5.3.2. Important specific models

A set of models specifically derived for relative high gas velocities and low liquid loading have been developed to describe annular/stratified flow in small diameter pipes, then in transition between stratified and annular flow.

Wallis, (1968) proposed a modified version of the Nikuradse (Nikuradse, 1933) sand roughness friction correlation in order to quantify the liquid film roughness. Wallis correlation has been widely used both in low level liquid stratified flow and in annular flow. Several improvements and modifications were proposed through the years to this correlation, keeping fixed only the friction factors and the dimensionless liquid height relationship (Dobran, 1987, Whalley and Hewitt, 1987 and Fernandes et al., 2004); the boundary of validity of this kind of correlations is small and covers the conditions between "large" dimensionless liquid level $\frac{h_L}{D}$ (≈ 0.03) and "small" dimensionless liquid level $\frac{h_L}{D}$ (≈ 0.005).

The horizontal or almost horizontal pipe configuration is characterized by non-uniformity of liquid film thickness around the channel circumference when the transition between stratified and annular flow pattern occurs; in fact, the liquid thickness at the bottom is greater due to the gravitational force. This phenomenon highly increases the difficulties in liquid height or liquid wetted perimeter prediction in terms of systems parameters.

Among the several specific models developed during the last few years considering a non-planar gas-liquid interface, the most important ones are due to Hart et al., (1989) (ARS Model) and Grolman et al., (1997) (MARS Model); the Chen et al., (1997) and Meng et al., (1999) (Double Circle Model) correlations add, respectively, the pipe inclination effect and the presence of liquid droplets in the gas phase. A validity extension assessment is necessary if applied to medium-large diameter pipes (≥ 4'') and to high pressure operating conditions or high viscosity liquids.

Badie et al., (2000) compared and improved all the specific models presented above and observed an air-water and air-oil annular flow in a 0.079 m diameter pipe, in medium-high gas flow rate and low liquid loading conditions. In their conclusion, it was observed that pressure gradients were significantly under

predicted by previous models for air-oil flow data, whereas better agreement was obtained for air-water flow data.

Chapter 6 Experimental measurement databases

This research has been developed in the framework of a collaboration between TEA Sistemi S.p.A. and ENI E&P, with the support of the University of Pisa and DIMNP for the characterization of advanced models for two-phase flow analysis.

In this context, an experimental campaign, called SESAME project, was carried out at TEA Sistemi lab of Ospedaletto, Pisa (Italy) in order to investigate the behavior of gas-liquid two-phase flow, in different operating conditions and with different fluid properties, in an experimental facility 70 m long and 0.079 m ID.

The present doctoral work started in conjunction with the experimental measurement activities. Though this contributed to determine a delay in the availability of reliable experimental measurements at different gas and liquid flow rates and pressure, on the other hand this work supported the experimental campaign with some tests of the measurements in free-falling liquid (water) conditions and gas (nitrogen) – liquid (both oil and water) two-phase flow conditions. The comparison with some existing models for the prediction of pressure losses and liquid levels was in this case performed.

During this preliminary analysis, in order to enlarge the number of available experiments, the investigation of nearly-horizontal stratified gas-liquid flow model began with the search in the literature of available pressure loss and liquid level measurements for two-phase flow.

This activity allow to collect some experimental databases, presented in §6.2 that were used for comparison with the new ones and that extend the SESAME project experimental database.

6.1 The SESAME project

The SESAME project aims at the investigation of two-phase flow properties, geometrical features of the liquid and the gas phases in order to understand their distribution in the cross section as a function of the operating conditions, such as:

- pressure gradient;
- liquid film thickness around pipe wall;

- liquid film flow rate;
- entrained liquid flow rate;
- rates of droplet entrainment and deposition;
- droplet size distribution.

During the present doctoral activity, only part of these data were made available and only stratified nitrogen-water experiments were considered for the development of new friction factor correlations. The dispersed liquid field investigation will be carried on by TEA Sistemi in a near future.

The experimental facility, shown in Figure 51, has a nominal 4" pipe diameter, XXS schedule, with an internal diameter, ID, of 80 mm. The test involves different physical properties of the fluids (gas density, liquid viscosity and surface tension) and different gas and liquid flow rates in the annular and stratified fields of two phase flow.

Figure 51: Panoramic view of the SESAME project facility

The fluids adopted are nitrogen as gas and oil or water as liquid. A small set of tests will be performed with a water-organic alcohol mixture, able to reproduce the physical properties of a light hydrocarbon mixture, in particular for the value of the surface tension.

The oil to be used for the experiments is the D120, with a density of 832 kg/m^3, viscosity of 4.94 cSt (centistokes) at 25°C, and a superficial tension of 28.2 mN/m.

The alcohol mixture is made of about 7% of ethylic alcohol, 7% of butilic alcohol and 86% of water. This mixture has a surface tension of about 25 mN/m, and this is the most important parameter to be taken under control.

In addition, another relevant aim of the project is the development of physically based closure laws for:

- gas-liquid interfacial friction factor;
- liquid film hold-up and wetted perimeter;
- rates of droplet entrainment and deposition;
- mean droplet size.

The sensor system has been developed in order to give real-time information about the local thickness of the liquid layer, the distribution of a possible annular flow condition at the pipe wall and of the mean liquid hold-up.

6.1.1. Description of SESAME experimental facility and measurements devices

A simplified chart of the multiphase flow loop installed at the TEA Sistemi Laboratory is shown below in Figure 52.

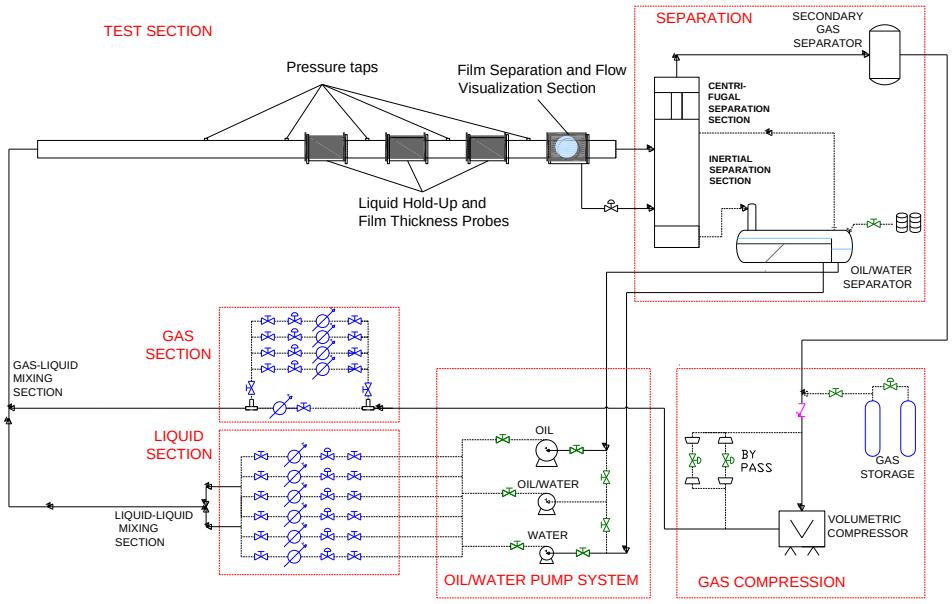

Figure 52: Layout of experimental loop

The loop is divided into four main sections. The gas (industrial nitrogen) is circulated in the loop through a volumetric compressor, which allows a maximum head of 5 bar with a flow rate of 400 m^3/h, at 25 bar-a. A set of three

pumps working in parallel with maximum flow rates of 5, 30 and 65 m^3/h and a head of 5 bar permits a wide range of operating conditions, also in terms of water-cut, that is the water content of oil, (0-100%).

Single phase gas and liquid streams pass through dedicated sections of the test facility, where the volumetric flow rates are measured and controlled by regulation valves, and pressures, temperatures and densities are measured.

The standard instrumentation is constituted by magnetic flow meters, Coriolis and orifice meters for the liquid phase, Venturi, vortex and orifice meters for the gas phase. Different instrument diameters allow measuring a wide range of flow rates

In Table 6 and Table 7 the main flow loop parameters are given.

Specifications	values
Loop Operating Pressure	2 – 40 bar
Loop Operating Temp.	2° - 40° C
Pipeline ID	80 mm
Length of Test Section	25m
Loop Max Pressure Drop	5 bar
Max. Superficial Gas Velocity	22 m/s (30 bar)
Max. Superficial Liquid Velocity	5.5 m/s (Single Phase)
Installed Power	400 kWatt

Table 6: Experimental loop main specifications

Fluid	DN, Type	Accuracy
Oil	1”, Coriolis Meter	0.3 %
	3”, Orifice Meter	1.5 %
Water	¼”, ½”, 1”, 3”, Magnetic Flowmeters	0.5 %
Gas	1”, 3”, Venturi Meters	1.5 %
	3/8”, Orifice Meter	1.5

Table 7: Reference flow meter

6.1.2. Description of the test section

A scheme of the test section is shown in Figure 53, reporting also the position of different devices needed for the experiments:

- conductance probes, designed for the measurement of the liquid hold-up, the film thickness distribution and the local tracer concentration;
- tracer injection system, that will be part of the measurement method for the measurement of droplet entrainment and deposition;
- liquid film separation section, equipped with glass windows for droplet flow visualization and droplet size measurement;
- pressure taps, for the measurement of pressure drop at various locations.

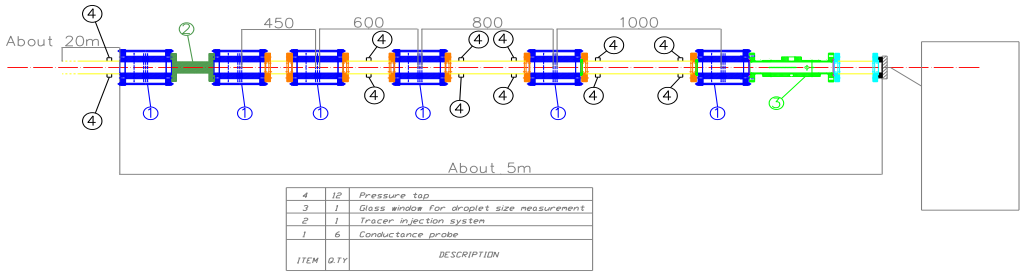

Figure 53: Test section

Ahead of the test section, a straight pipe about 20 m long allows the flow development. All the measuring devices are installed in the terminal part of the pipe, which is approximately 5 m long, for an overall straight pipe length of 25 m. The test section (piping and devices) is machined to an internal diameter of 79 mm with a tolerance of 50 µm and a surface roughness of 1.6 µm. In addition, customized flanges have been adopted in every joint of this section, in order to avoid discontinuity at the internal pipe wall.

The tests are performed in conditions of a straight and horizontal pipe (with a good approximation), with the possibility of a small controlled inclination. A picture of the test section is proposed in Figure 54.

Figure 54: Picture of the SESAME test section

6.1.3. The measurement approach

The fundamental idea of the measurement system described in this manuscript is based on an electrochemical conductive hold up measuring approach. The current flowing in a solution under the influence of a known electric field is related to the geometry of the dielectric boundary that delimits such solution (including the gas in a multi-phase flow) and to the electrical properties of the electrolyte used.

More in detail, the parameter measured by the system is the electrical conductance between thin "needle" electrodes plugged into the wall of a short tube, which is made of a dielectric material (a brand of Polyethylene Terephthalate - PET). Needle shaped electrodes have been chosen in order to minimize the disturbance to the flow under measurement, and, in a multi-electrode scheme, are characterized by a good linearity with a low interference between adjacent electrode pairs.

The configuration of such electrodes is constituted by three parallel planes, normal to the axis of the tube, where three identical arrays of 15 electrodes each (needles), are located. A picture of such configuration is shown in Figure 55, while length and orientation of each electrode can be found in the cross section shown in Figure 56.

The three arrays of electrodes are used according to the following rule:

- the middle one is the one being energized by an excitation signal (all the electrodes are forced to the same potential);
- the two external arrays are formed by electrodes connected in pairs (those carrying the same number), whose signals are fed to the analog front-end electronics. The observable quantity, which is the total current flowing into each pair of electrodes, is measured by said analog electronics.

The excitation signal, supplied to the array of 15 electrodes placed in the middle, is generated by a low distortion sinusoidal oscillator, set to a frequency of 100 KHz.

The two side arrays are connected to dedicated wideband current-input and demodulation circuits that perform simultaneous conversions of all the channels, thus avoiding the slow processing of a multiplexed scheme.

Such current input stages ensure to tie their input potential to the reference potential of the whole electronic front-end, assuming the ideal OP-AMP (OPerational-AMPlifier) approximation for each transimpedance amplifier. Such reference potential corresponds also to the "zero" voltage level of the excitation signal; as a consequence, a known electric field is generated between the middle and the side arrays of electrodes, where the relationship between the

pattern of the liquid electrolyte and the measured currents can be obtained both theoretically (by simulation) and practically (by characterization in controlled conditions).

In addition to that, this virtually equipotential array of current-input electrodes can be placed at the same potential of the other electrically conductive wet surfaces of the experimental set-up (metal ducts and flanges), to minimize unwanted currents flowing between the probe and the rest of the test apparatus.

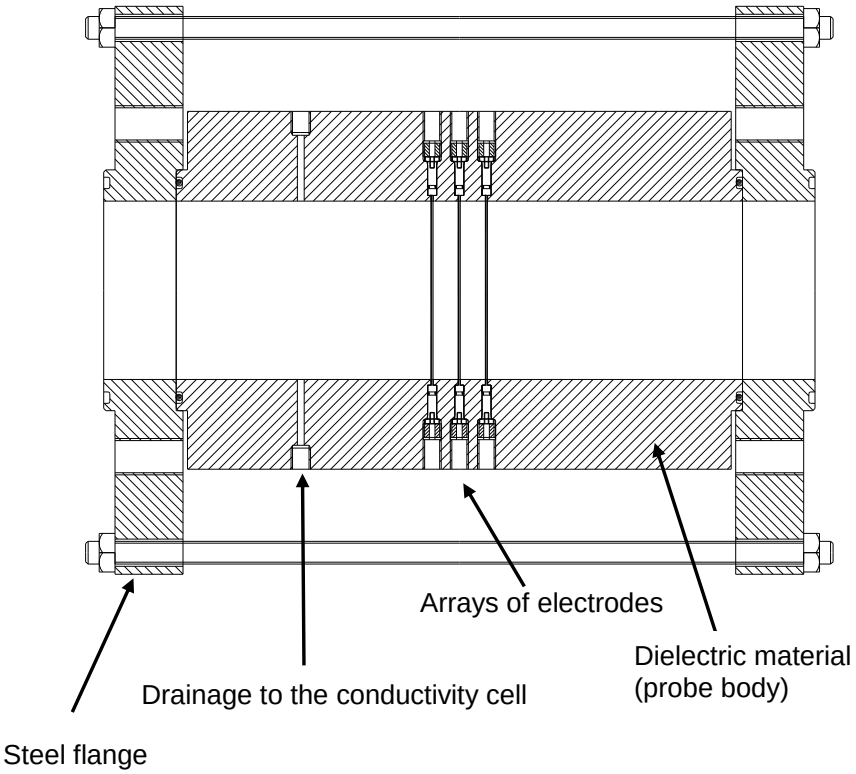

Figure 55: Longitudinal section of one probe

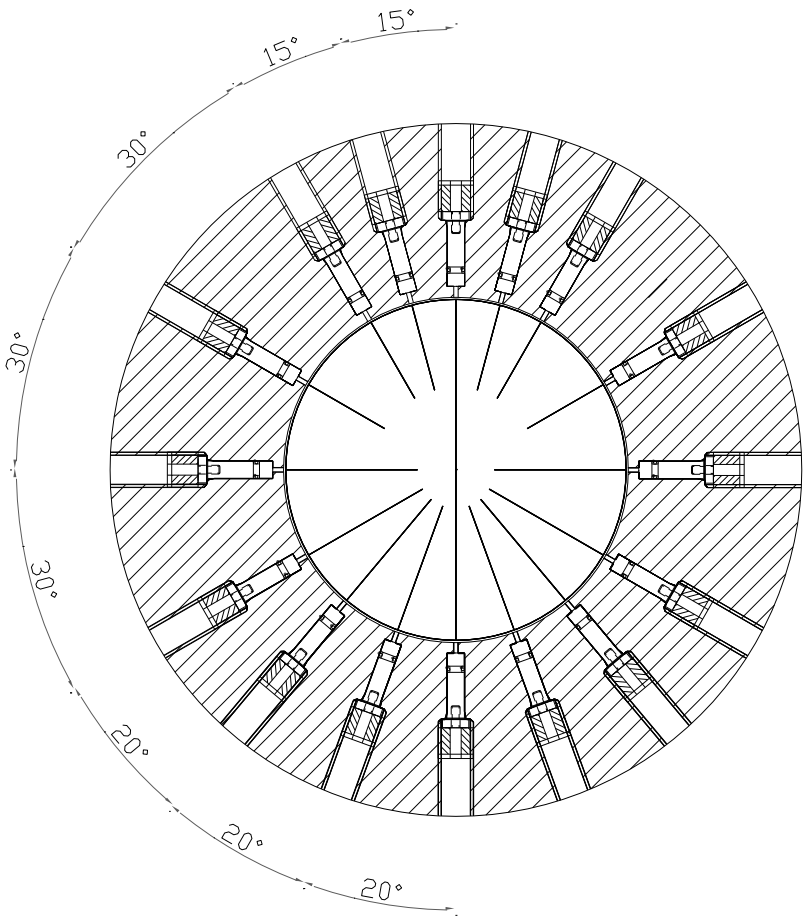

Figure 56: Cross section of one probe. Position and mounting of the electrodes are shown

6.1.4. Preliminary tests and validation of free-falling liquid level measurements

The first series of tests performed in the SESAME facility concerned free-falling liquid (water) measurements of liquid level in the cross section.

The test section with the 6 probes (sensor units), spaced as seen in Figure 57 was set-up. The liquid was fed to the line by a submersible pump, placed in the re-circulation tank, in order to obtain a continuous flow. A functional diagram of the experimental set-up is shown in Figure 58.

Three different tilt angles have been experimented (0.3°, 1.0° and 2.0°) at six different flow values; measurement results and comparison with model data are described below.

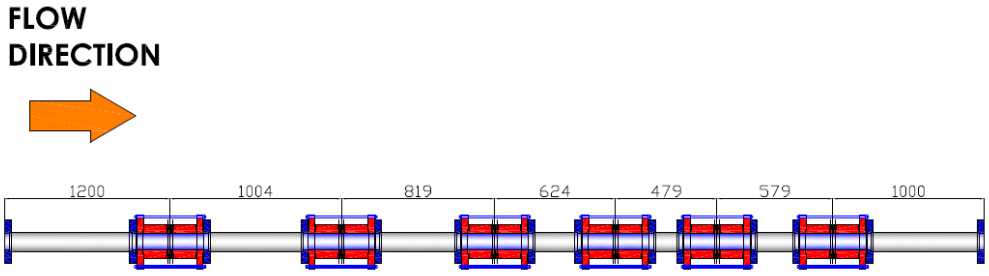

Figure 57: Layout of measurement devices

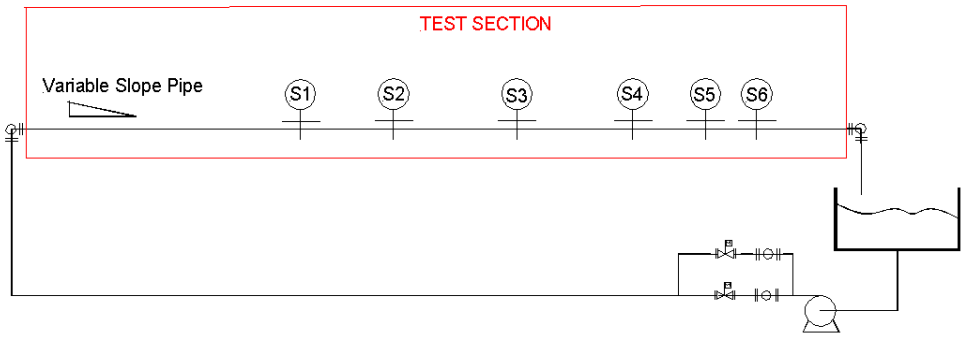

Figure 58: Functional diagram of experimental set-up

These first series of tests at low pressure enabled the verification of the liquid level measurements and the obtained values were then compared with several predictive models from literature.

This activity was performed in the framework of the present doctoral work and was the occasion to simulate in a simple MATLAB routine the operating conditions of the SESAME facility during experiments, to implement for the first time some of the most important and widely adopted liquid-wall friction factor correlations and to predict liquid level in the test cross section.

The operating conditions listed in Table 8 were simulated:

Liquid flow rate [l/min]	T1 Jan 2010	T2 Jan 2010	T3 Jan2010	T4 Feb2010
5.0	1 deg. Incl. downward	0.3 deg. Incl. downward	2 deg. Incl. downward	0.3 deg. Incl. downward
10.0				
20.0				
25.0				
30.0				
40.0				
45.0				

Table 8: Free-falling liquid only operating conditions

The liquid wall friction factor relationships applied for comparisons are the Taitel and Dukler, (1976) correlation, the Spedding and Hand, (1997) one and the Biberg, (2005) liquid-wall friction factor correlation that was defined by an explicit approximation of the Colebrook-White formula.

The Biberg, (2005) liquid only friction factor correlation is the one proposed below:

$$\frac{1}{\sqrt{\lambda}} = \frac{\frac{5.02}{\mathrm{Re}_D\sqrt{\lambda_0}} - 4.6\left(\frac{2.51}{\mathrm{Re}_D\sqrt{\lambda_0}} + \frac{k_s}{3.7D}\right)\log_{10}\left(\frac{2.51}{\mathrm{Re}_D\sqrt{\lambda_0}} + \frac{k_s}{3.7D}\right)}{\frac{5.02}{\mathrm{Re}_D} + 2.3\left(\frac{2.51}{\mathrm{Re}_D\sqrt{\lambda_0}} + \frac{k_s}{3.7D}\right)} \tag{134}$$

where

$$\frac{1}{\sqrt{\lambda_0}} = -1.8\log_{10}\left(\frac{6.9}{\mathrm{Re}_D} + \left(\frac{k_s}{3.7D}\right)^{1.11}\right) \tag{135}$$

is the Haland's formula (Haland, 1983).

The results of comparison are presented below from Figure 59 to Figure 62. In tese figures "Blasius" represents the liquid-wall friction factor correlation from Taitel and Dukler, (1976).

The behavior of measurements with the pipe inclination of 0.3 degrees downward, performed in January 2010, was evaluated as anomalous for liquid flow rate larger than 40 [l/min] and the repetition of this test series was done in

February 2010. The deviation from the predicted values assumed by the test at higher liquid flow rate was then investigated and corrected.

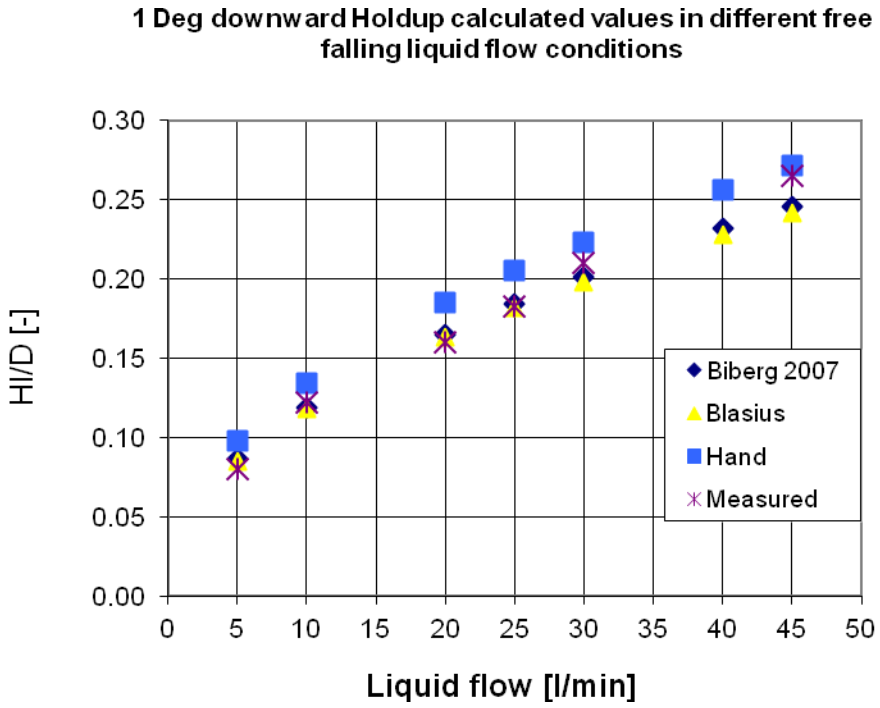

Figure 59: 1° downward inclined pipe free-falling liquid level measurements comparison versus existing models (Jan.2010)

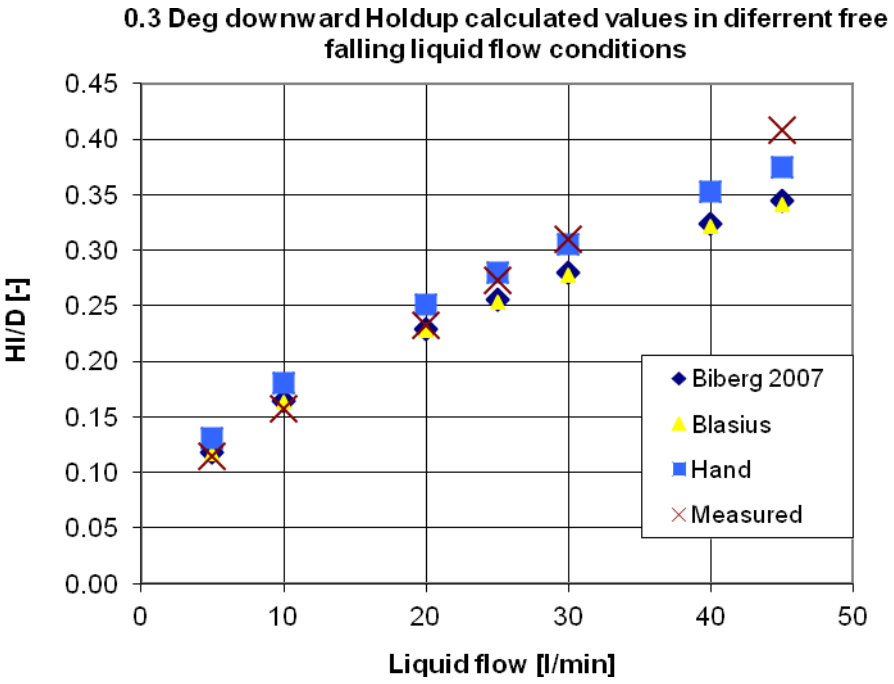

Figure 60: 0.3° downward inclined pipe free-falling liquid level measurements comparison versus existing models (Jan.2010)

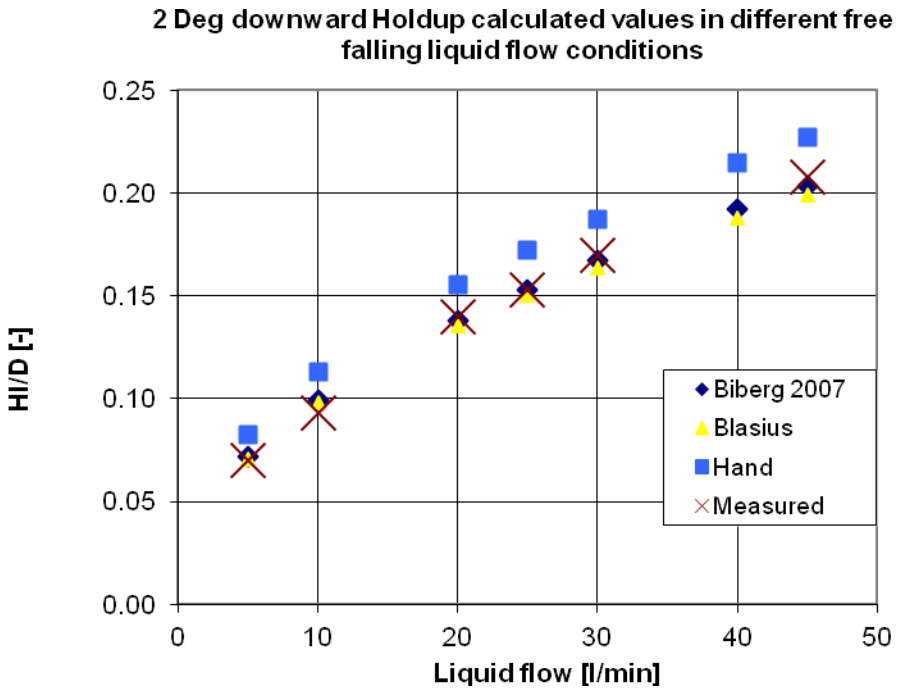

Figure 61: 2° downward inclined pipe free-falling liquid level measurements comparison versus existing models (Jan.2010)

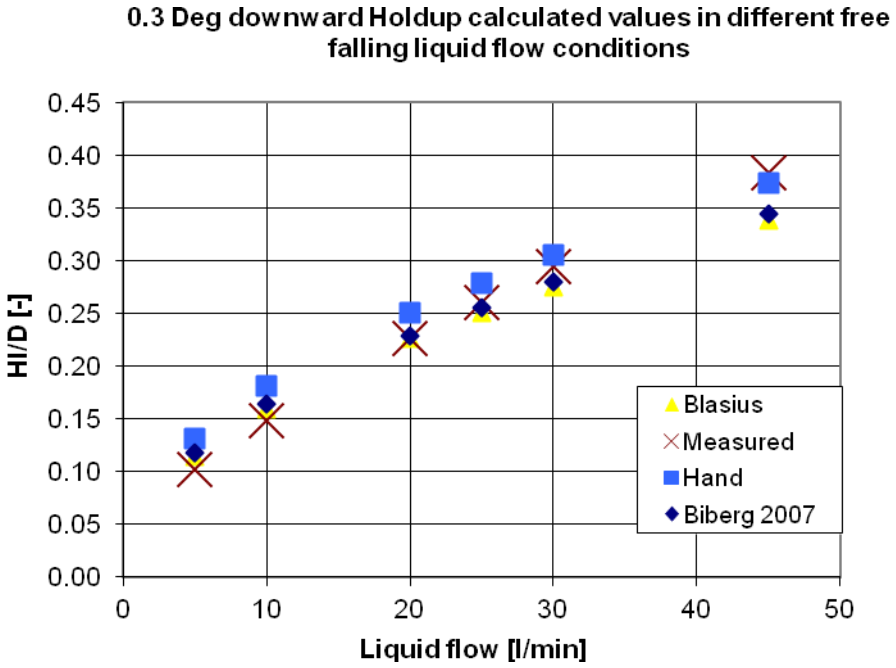

Figure 62: 0.3° downward inclined pipe free-falling liquid level measurements comparison versus existingmodels (Feb.2010)

This first experimental measurements validation activity was a good starting point to gain experience in handling measurements from the SESAME test facility and to start the development of computational tools useful for the calculation of pressure losses and liquid level in a 0D horizontal pipe. The

comparison of measured liquid levels, in different inlet flow rates and pipe inclinations, against predictions from well-known existing models, shows a good agreement between measured and calculated values. This result was a confirmation of the suitability of the SESAME experimental set-up for liquid level measurements. Concerning used models from the literature, the correlation from Taitel and Dukler, (1976), is confirmed to be a good estimator of the liquid-wall friction factor, at least with low and medium liquid flow rates and in case of free-falling liquid simulations.

6.1.5. The nitrogen-water campaign

For the purposes of the present work the experimental data really taken into account for the development of new friction factor correlations were those of the nitrogen-water measurement campaign.

A preliminary campaign with nitrogen-oil at medium pressure conditions was already carried out previously; these tests were not taken into account during the present work, because the results from this preliminary campaign need to be further investigated and confirmed by a repetition of the measurements. These data were therefore partially analyzed during this doctoral activity but not used for the development of new friction factor correlations.

The nitrogen-water experimental campaign was aimed to collect information concerning liquid level and pressure losses in stratified and stratified-wavy flow pattern, with different gas and liquid flow rates and four different operating pressures.

A summary of the considered flow conditions s presented in Table 9.

Gas Sup.Vel. [m/s]	Liq.Sup.Vel. [m/s]	Gas density [kg/m^3]	Inclination [deg]
3-13	0.01-0.14	3	0°
5-13	0.03-0.14	7	
3-9	0.03-0.14	16	
6-9	0.02-0.14	22	

Table 9: Nitrogen-water measurements operational conditions

6.2 Collection of experimental data from literature

A literature search was also conducted in order to find already available experimental measurements for pressure losses and liquid level to be used for the formulation of new friction factor correlations.

In the work of Ottens et al., (2001) a complete set of horizontal gas-liquid flow experimental measurements is presented for pressure losses and liquid level, for air-water and air-water-glycerol flowing in a pipe 0.052 ID, at different pipe inclinations (from -2° to 2°) and at atmospheric pressure conditions. Several gas and liquid flow rates are reproduced.

Badie et al., (2000) proposed a series of pressure gradient and liquid holdup measurements for air-water and air-oil in a horizontal and near-horizontal (from -2° to +2° inclined), 0.079 ID pipe. In their work, the transport of a gaseous hydrocarbon with condensation of the gas phase that results in a thin liquid level flowing at the bottom of the pipe and as droplets into the gas stream was investigated. Both water and oil were adopted as liquid, in presence of air. In the work of Ullmann and Brauner, (2006) these two first series of data were already used for comparison against predictions.

In Andritsos and Hanratty, (1987) a full set of experimental measurements was proposed. Experiments were done in a horizontal gas-liquid flow loop. Plexiglas pipelines of 0.0252 m ID and of 0.0952 m ID were adopted. The liquids used were water and water-glycerine with variable viscosities of 1, 12 and 80 cp for the 0.0952 m ID pipe and viscosities of 1, 4.5, 16 and 70 for the 0.0252 m ID pipe. Different gas and liquid flow rates were then introduced into the pipeline and pressure losses and liquid level were measured using two parallel wire conductance probes.

Another experimental database for pressure losses and liquid level in horizontal stratified gas-liquid flow, for medium and high pressure operating conditions was added to the investigation during the present doctoral work. This contribution comes from the SINTEF laboratory facility and includes measurements at 20, 30, 50, 70, 90 bar, with the investigation of three different liquids: two different kinds of diesel fuel and an oil, having different viscosities, densities and surface tensions. The gases adopted were nitrogen and SF6 in some cases.

From all the presented experimental measurements, both nitrogen-water SESAME data and data from literature, new interfacial and liquid-wall friction factors were obtained once the gas and liquid phase distributions in the pipe cross section were defined.

These “measured” friction factors were then used to obtain empirical friction factor correlations after being analyzed versus different flow properties, in order to evaluate their behavior.

For instance, the effect of the onset of instabilities on the trend of the interfacial friction factor, depending on the superficial gas velocity and the liquid level, was investigated.

In fact, a primary factor affecting the interfacial friction factor, as stated also by Andritsos and Hanratty, (1987), is the superficial gas velocity; the

dimensionless liquid level plays a secondary role and makes the interfacial friction factor to decrease with increasing the liquid level.

Some examples of plots of the interfacial friction factors, divided by the gas-wall friction factor, versus the superficial gas velocity and liquid level are presented for the SESAME data at 16 bar in Figure 63 and Figure 64 and for Ottens data in Figure 65 and Figure 66, for different values of the superficial liquid velocity. Similar results were obtained for all the available experimental databases.

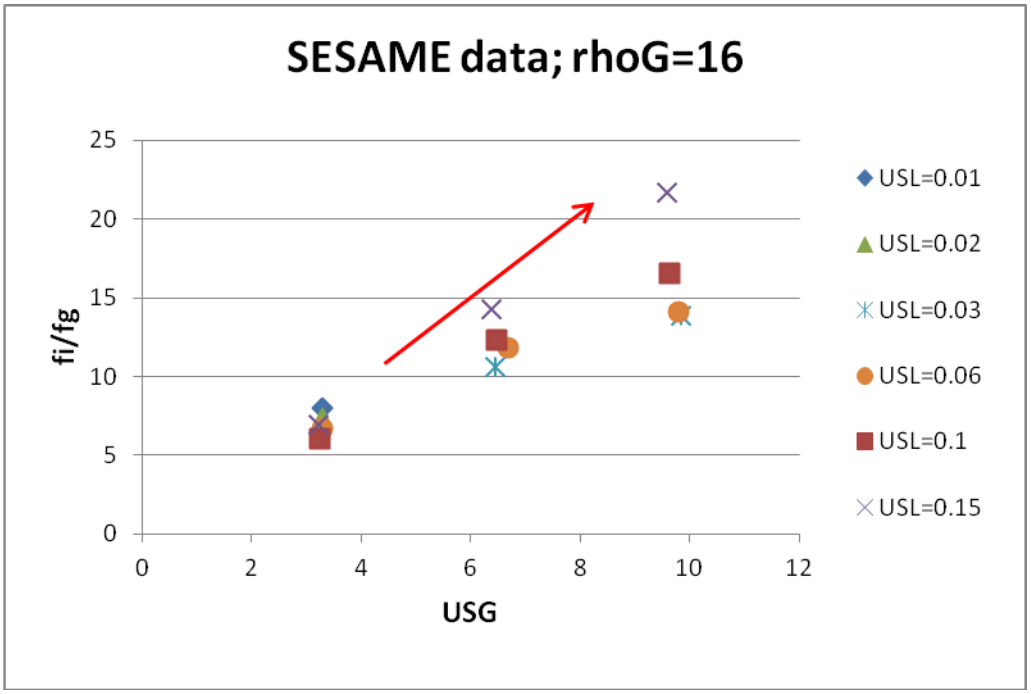

Figure 63: SESAME data for interfacial friction factor as a function of superficial gas velocity U_{SG}

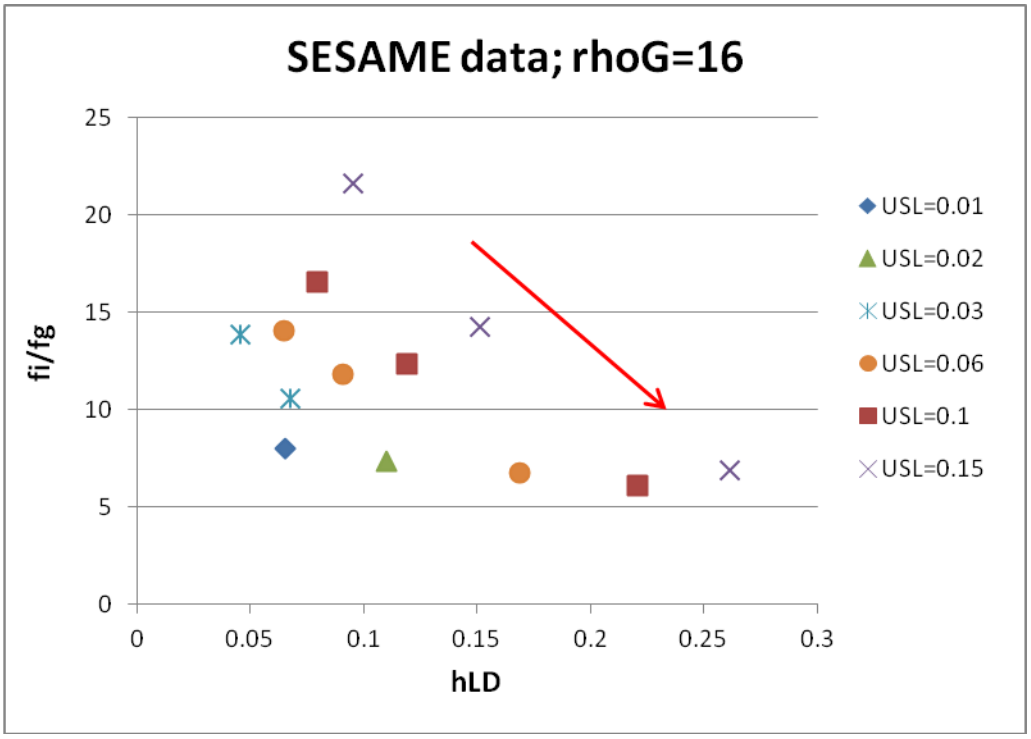

Figure 64: SESAME data for interfacial friction factor sensitivity analysis as a function of dimensionless liquid level h_L/D

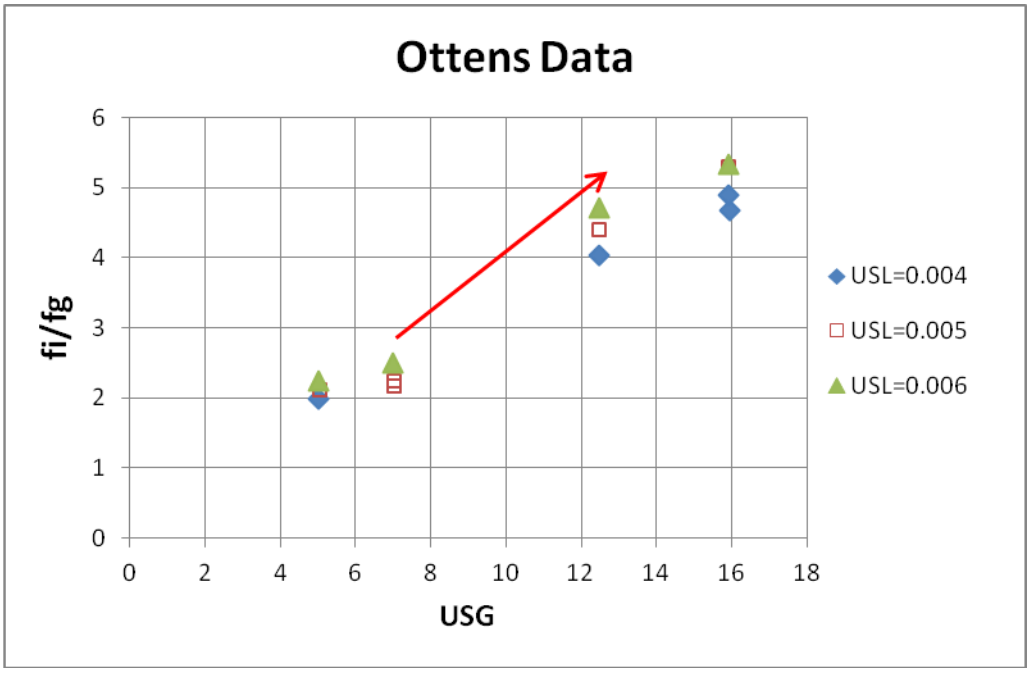

Figure 65: Ottens et al., (2001) data for interfacial friction factor as a function of superficial gas velocity U_{SG}

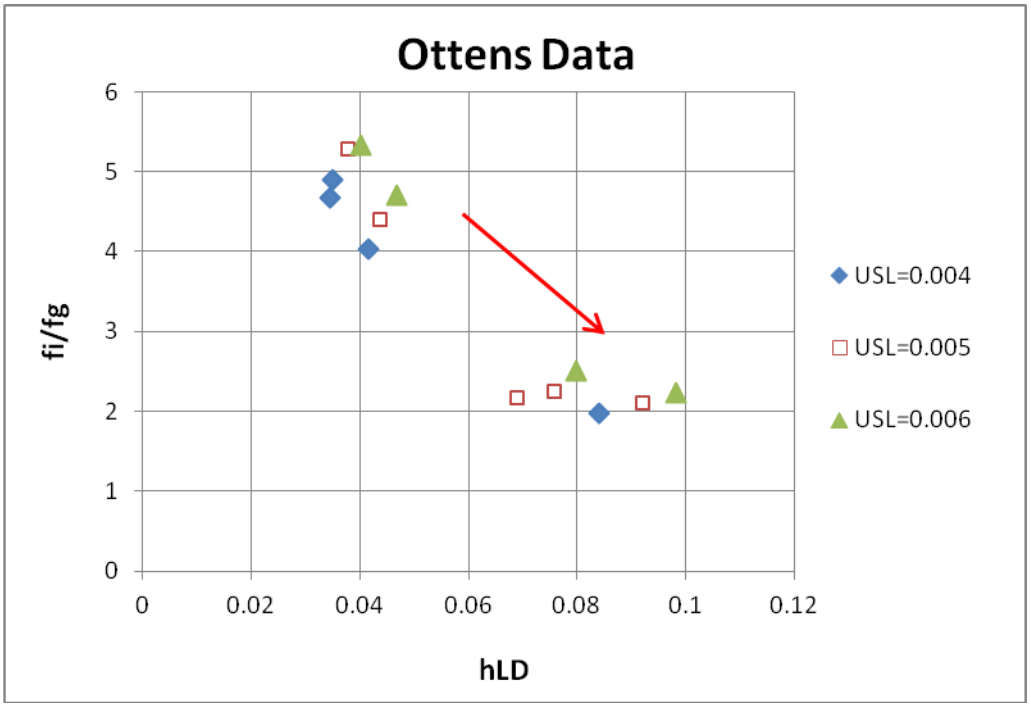

Figure 66: Ottens et al. (2001) data for interfacial friction factor as a function of liquid level h_L/D

6.3 Numerical algorithms for the determination of friction factor correlations

For the determination of the new friction factor correlations several steps must be completed once the reference database is available.

For semi-empirical correlations, the structure that better represents the phenomena to investigate should be defined; in our case, it is referred to the shear stress at the interface and at the phase-wall, also depending on the interfacial instabilities, as it will be shown in Chapter 7.

When the form of the correlation, i.e., the role of the selected dimensionless numbers, is selected, its coefficients and exponentials may be determined by a curve fitting process.

The objective of curve fitting is to find the coefficients of a power law that best describes a set of data.

For empirical correlations determination, a sufficient number of experimental data is requested and the number of unknowns is lower than the number of equations to be satisfied. The resulting-equation system must be therefore solved via a least squares method.

This approach in general is based on the minimization of the summation of squared errors between the results of the equation and the experimental values.

Least squares techniques are subdivided in two categories that are the linear, or ordinary, and non-linear ones.

A linear least squares method allows direct solution; the non-linear methods have to be solved by iterative refinements.

Friction factor correlations proposed in the present work have been determined applying both the linear and the non-linear least squares approach presented in next sections and developing some algorithms to use them.

6.3.1. Linear least square method

A linear least square method has been computed with the QR decomposition algorithm and run within MATLAB^{TM} platform.

This method has the goal of minimizing the value $\|Ax\text{-}b\|_2$, which denotes an Euclidean norm derived from a system of equations such as $Ax = b$, once a matrix A(m x n) with m > n, b(m x 1) and the x(n x 1) that minimizes it are given.

As already said, the system of equations that have to be solved is overdetermined; a QR decomposition algorithm was chosen to solve it.

In the QR factorization approach the matrix A(m x n) is decomposed in an orthogonal matrix Q(m x n) and an upper triangular one R(n x n).

In this way, the linear least squares problem becomes a triangular one and the resolution evolves as follows.

$$A = QR \tag{136}$$

$$QRx = b \tag{137}$$

$$Rx = Q^T b \tag{138}$$

$$x = R^{-1}Q^T b \tag{139}$$

where x is the vector of coefficients.

6.3.2. Non-linear least square method

A second non-linear least squares method was adopted to confirm the results proposed by the linear one and it was implemented in the MATLAB^{TM} platform as well.

The non-linear least squares adopted is based on the Levenberg-Marquardt method and the numerical steps follows the routine *SMarquardt* developed by Nielsen, (1999).

This method applies an iterative approach that is based, on the idea of Levenberg, (Levenberg, 1944) and later Marquardt (Marquardt, 1963), on the use of a damped Gauss-Newton method.

The idea behind this method is quickly presented below for the case of finding the least squares solution x^* of a function $\mathrm{f}:\Re^n \to \Re^m$ with (m > n) where

$$x^* = \arg\min_x F(x) := \left\{ F(x) = \frac{1}{2}\|\mathrm{f}(x)\|_2 \right\} \tag{140}$$

when the components $f_i(x)$ of $\mathrm{f}(x)$ are nonlinear functions, iterations are needed and x_1, x_2,…, have to be computed from a starting point x_0, assuming that the descending condition $F(x_{k+1}) < F(x_k)$ is satisfied.

A descent direction satisfies the condition

$$\mathrm{h}^{\mathrm{T}}\mathrm{F}'(x_k) < 0 \tag{141}$$

where h is the descent direction such as

$$x = x + \alpha \mathrm{h}, \quad \text{with}\,(\alpha > 0) \tag{142}$$

and the gradient $\mathrm{F}'(x_k)$ is

$$\mathrm{F}'(x_k) = \mathrm{J}_{\mathrm{f}}(x)^{\mathrm{T}}\,\mathrm{f}(x) \tag{143}$$

with J_{f} that is the Jacobian matrix defined as

$$(\mathrm{J}_{\mathrm{f}}(x))_{ij} = \frac{\partial f_i}{\partial x_j}(x).$$

The simplest method to define the descent direction h is based on using the *steepest descent direction* $\mathrm{h} = -\mathrm{F}'(x)$, computing α with a line search. This approach is robust even if x is far from x^*, but has poor final convergence.

Another available method is the *Newton's method* where the descent step is found as solution of the equation

$$\mathrm{h}\,\mathrm{F}''(x) = -\mathrm{F}'(x) \tag{144}$$

where

$$\mathrm{F}''(x) = \mathrm{J}_f(x)^{\mathrm{T}}\,\mathrm{J}_f(x) + \sum_{i=1}^{m} f_i(x)\,\mathrm{f}_{\mathrm{i}}''(x) \tag{145}$$

This method has quadratic convergence but is not robust and it has the constraint due to the calculation of second order derivatives.

The *Gauss-Newton method* is based on a descent direction obtained from a Taylor expansion of f:

$$\mathrm{f}(x+h) \cong \mathrm{l}(h) \equiv \mathrm{f}(x) + \mathrm{J}_{\mathrm{f}}(x)\,\mathrm{h} \tag{146}$$

$$\mathrm{F}(x+h) \cong L(h) \equiv \frac{1}{2}\mathrm{l}(h)^{\mathrm{T}}\,\mathrm{l}(h) \tag{147}$$

So, the step is the minimizer of L(h), which is the solution of

$$(\mathrm{J_f}(x)^T\,\mathrm{J_f}(x))\,\mathrm{h} = -\mathrm{F}'(x) \tag{148}$$

The matrix $A = \mathrm{J_f}(x)^T\,\mathrm{J_f}(x)$ is symmetric. If $\mathrm{J_f}$ has full rank, then A is positive definite and h satisfies the condition for descent direction given above.

This method has quadratic final convergence but has often a lack of robustness as well.

The Levenberg-Marquardt (LMA) method was born with the purpose of interpolating between a Gauss-Newton method and a gradient descent approach in order to give to the former more robustness also in cases the procedure starts from values too far from the final x^*.

The difference with pure Gauss-Newton method is in the definition of the equation to solve to find the descent direction:

$$(\mathrm{J_f}(x)^T\,\mathrm{J_f}(x) + \mu\,\mathrm{I})\,\mathrm{h} = -\mathrm{F}'(x) \tag{149}$$

where I is the identity matrix and μ is the damping parameter, a positive scalar. If μ is small then $\mathrm{h} \cong \mathrm{h}_{Gauss-Newton}$; if μ is large then $\mathrm{h} \cong -\frac{1}{\mu}\mathrm{F}'$ performing a shorter step in the descent direction.

This "damped" version of the Gauss-Newton method was the Levenberg's contribution. Here, μ affects both the direction and the size of the step h.

If x is close to the solution, then the faster convergence of the Gauss-Newton method plays an important role; if x is far from x^* then the importance of the robustness of the steepest descent method grows.

The Marquardt's contribution consisted in linking the initial values μ_0 to the size of the elements in $\mathrm{J_f}(x)^T\,\mathrm{J_f}(x)$ and so to its eigenvalues $\{\lambda_j\}$ and eigenvectors $\{v_j\}$. So in the final form of the Levenberg-Marquardt method the initial I, identity matrix, is substituted by the diagonal elements of $(\mathrm{J_f}(x)^T\,\mathrm{J_f}(x))$:

$$\mathrm{h} = -\sum_{j=1}^{n} \frac{v_j^T\,\mathrm{F}'}{\lambda_j + \mu} v_j \tag{150}$$

To update the damping parameter, two classes of procedures may be adopted: the first one is based on a line search and the second one is based on the observation that through the choice of μ both, direction and size, of h may be influenced. So μ itself is decreased when the descending condition,

$F(x_{k+1}) < F(x_k)$, is respected. This second approach results in a reduction of the iteration steps compared with the first one.

The LMA is a very popular curve-fitting algorithm for solving generic curve-fitting problems. However, the LMA finds only local minimum and not global ones and has to be used with care.

6.3.3. Procedure to determine pressure losses and liquid level

A C++ computer program was developed in the framework of this doctoral activity. It is called *Dp_hL_pipe_calc* and its purpose is the calculation of pressure losses and liquid level in the pipe cross section with a 0D computational approach.

This tool may perform runs in series to test the application of the new liquid-wall friction factor correlations, together with the proposed interfacial friction factors, in the prediction of the experimental measurements.

So, for each set of closure laws different input settings are introduced into the *DP_hL_pipe_calc* model, proposed in Figure 67.

The inlet operational conditions are read by the procedure that assumes a guessed value of the liquid level, evaluates the geometrical parameters for each phase, determines phase-wall and interfacial friction factors and calculates pressure drops in both phases. These pressure losses are compared and, if they differ by more than a fixed tolerance, the procedure restarts from the first step with a new guessed liquid level.

This model predicts then pressure losses in the cross section and values of the liquid level that are subsequently compared with experimental measurements in order to validate the accuracy of the tested correlations.

To complete the analysis, a statistical evaluation of the errors between measured and predicted values has been also performed, in order to compare the addressed friction factor correlations and to choose the best set of friction factors.

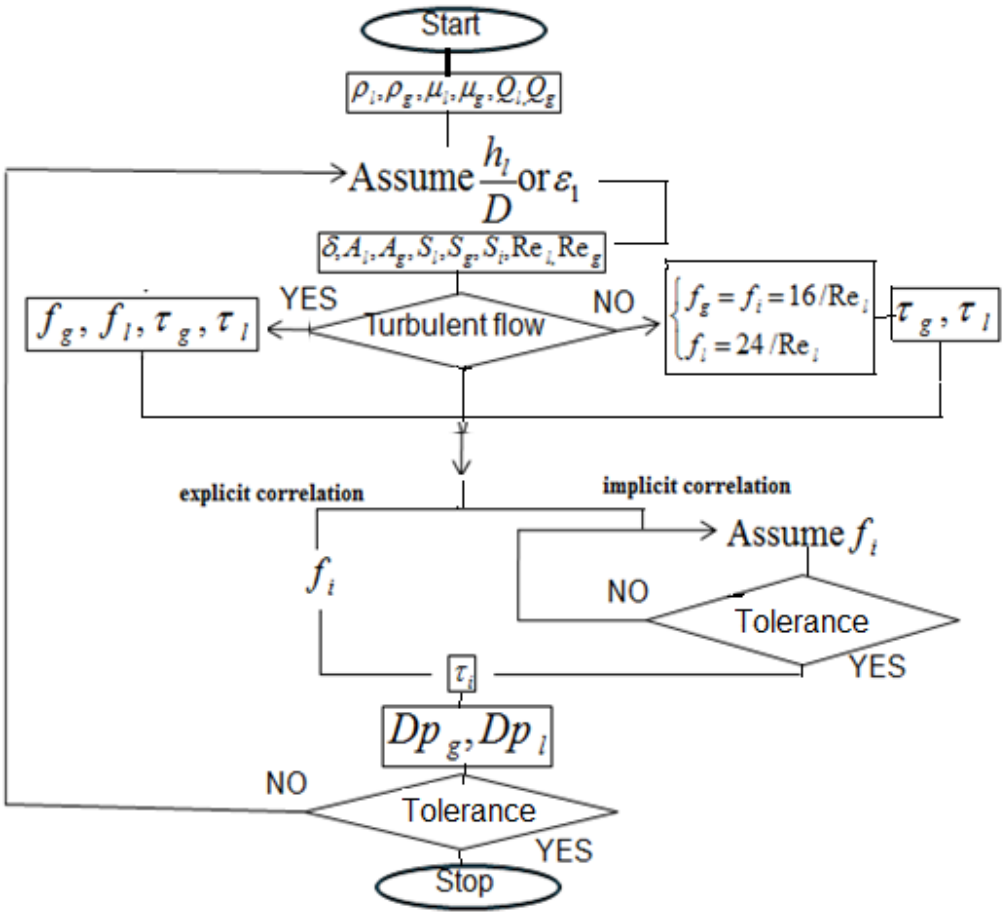

Figure 67: Flow chart of Dp_hL_pipe_calc

In particular, statistical comparisons are based on the assessments of the Root Mean Squared Error (RMSE) and of its relative value, the Root Mean Square Error Percent (RMSEp) as proposed below:

$$RMSE = \sqrt{\frac{\sum_{i=1}^{N}(x_i - \hat{x}_i)^2}{N-1}} \tag{151}$$

$$RMSEp = \sqrt{\frac{1}{N-1}\sum_{i=1}^{N}\left(\frac{x_i - \hat{x}_i}{x_i}\right)^2} \tag{152}$$

where x_i is the measured value and $\hat{x}_i$ is the corresponding predicted one.

More details about the examined measurements and obtained prediction concerning friction factor correlations are presented in the following Chapter 7.

Chapter 7 Proposed friction factor correlations

7.1 Development of correlations for stratified-wavy gas-liquid flow

Stratified gas-liquid flow in a near-horizontal pipeline cannot be completely described without considering the phenomenon of interfacial waves. In fact, although this flow pattern is characterized by a simple geometrical representation of phase perimeters, in its basic configuration with a flat gas-liquid interface at low gas velocity, it undergoes significant changes at increasing gas velocities.

This is caused by the onset of 2-3 D waves on the liquid surface which cause a significant increase of the interfacial drag (Andritsos, 1986).

In particular, when two fluids flow in parallel directions with different velocities, their interface undergoes a Kelvin-Helmholtz instability (IKH) phenomenon.

As already mentioned, this instability is characteristic of two fluids flowing with different velocities and determines the relationship among gas-liquid relative velocity, gravity, surface tension and liquid level on the growth of interfacial waves.

In a 1D configuration, the disturbances can be mathematically described by a linear instability analysis with small amplitude waves as shown by Milne-Thompson since 1968; this theory is briefly summarized below in its classical formulation.

If a small sinusoidal disturbance is induced at the interface in a steady stratified inviscid gas-liquid flow, as represented by $\eta = \bar{h} + \hat{\eta}\exp\left[ik(x - Ct)\right]$, where $\bar{h}$ is the average height of the liquid, $\hat{\eta}$ is the amplitude of the disturbance, $k = 2\pi/\lambda$ is the wave number, and $C = C_R + iC_I$ is the wave velocity, a dispersion relation is produced considering linear momentum balance in the liquid and in the gas phase. Further considerations on neutral stability of a stratified flow, for which the imaginary part of the wave velocity C_I could be set to zero:

$$(\overline{U}_G - \overline{U}_L)^2 = \left[(\frac{g}{k}) \cos\theta \frac{(\rho_L - \rho_G)}{\rho_G} + \frac{\sigma k}{\rho_G} \right] \cdot \left[\tanh(k\overline{h}_G) + \frac{\rho_G}{\rho_L} \tanh(k\overline{h}) \right] \quad (152)$$

$$C_R = \frac{\rho_G \overline{U}_G \tanh(k\overline{h}) + \rho_L \overline{U}_L \tanh(k\overline{h}_G)}{\rho_L \tanh(k\overline{h}_G) + \rho_G \tanh(k\overline{h})} \quad (153)$$

where $\overline{h}_G$ is the average gas height.

The hypothesis of shallow water and much higher liquid than gas density enables the following simplification that could be assumed in most applications, especially in the gas condensate transportation pipeline design:

$$(\overline{U}_G - \overline{U}_L)^2 = \left[(\frac{g}{k}) \cos\theta \frac{(\rho_L - \rho_G)}{\rho_G} + \frac{\sigma k}{\rho_G} \right] \quad (154)$$

where

$$C_R = \overline{U}_L \quad (155)$$

This dispersion equation obtained from the IKH analysis for a two-phase gas-liquid flow has been analyzed by Hanratty and collaborators (Andritsos and Hanratty, 1987; Hurlburt and Hanratty, 2002) in order to find the minimum value of the relative velocity that triggers the interfacial instabilities.

They proposed to define a critical wavenumber k_{crit} that minimizes the (r.h.s.) of the Eq. (154). The corresponding (l.h.s) of Eq. (154) represents the critical velocity that defines the boundary between flat and wavy two-phase flow.

The critical wavenumber and the critical relative velocity are then:

$$k_{crit} = (\frac{\rho_L g \cos\vartheta}{\sigma})^{0.5} \quad (156)$$

$$(\overline{U}_G - \overline{U}_L)^2_{crit} = 2\sqrt{\frac{\sigma g \cos\theta}{\rho_L}} \frac{\rho_L}{\rho_G} \quad (157)$$

Typical values are $(\overline{U}_G - \overline{U}_L)^2_{crit}$ = 6.6 m/s for air-water flow at atmospheric pressure and k_{crit} =3.7 cm^{-1}. For high pressure gas-oil mixture $(\overline{U}_G - \overline{U}_L)^2_{crit}$ and k_{crit} could be 0.5 m/s and 8 cm^{-1} respectively.

These definitions of the critical wavenumber and the critical velocity are retained in the present study.

7.2 A first tentative set of friction factor correlations

At the beginning of the present doctoral research, when only data from open literature were available, a first set of tentative friction factor correlations was developed. A summary of this activity is briefly presented below to show the introductory work that enabled the formulation, in the second part of the work, of another set of friction factor correlations competitive with the best available correlations from literature and developed on the basis of a wide experimental database at low, medium and high operating pressure conditions.

In particular, an attempt was made, in this first part, to improve the critical gas-liquid differential velocity definition in a newly formulated velocity group. Both the concepts of turbulence and instability in a gas-liquid flow have been used, as described below, to formulate a new approach for the calculation of the interfacial friction factor and then of pressure losses and holdup in two-phase gas-liquid flows.

Gas-liquid two-phase flow, in high enough Reynolds numbers conditions, is characterized by turbulent flow phenomena also in the proximity of their interfacial area.

The turbulent structures of flow at the interface could be modeled analyzing the stress tensor with its tangential component together with the friction velocity definition.

When modelling turbulent two phase flow, the Boussinesq approximation, applied to the Reynolds-averaged Navier-Stokes equations, can be taken into account to close the problem. In particular, both the basic eddy viscosity and mixing length relations are be applied in the definition of a flow model representing the turbulent single phase flow in a pipe. The Boussinesq assumption is:

$$\tau_{xy} = \mu^t \frac{du}{dy} \tag{158}$$

in which τ_{xy} is the tangential component of the stress tensor.

The Prandtl hypothesis on mixing length is:

$$\mu^t = \rho l U^* \tag{159}$$

in which l is the mixing length and U^* is a characteristic turbulent velocity scale.

Prandtl assumed that:

$$U^* = l\left|\frac{du}{dy}\right| \tag{160}$$

Combining the last three equations, the friction velocity U^* can be defined as follows, in fact : $\sqrt{\frac{|\tau_{xy}|}{\rho}} = l\left|\frac{du}{dy}\right|$ and

$$U^* = \sqrt{\frac{|\tau_{xy}|}{\rho}} \tag{161}$$

An interfacial friction velocity U_i^* has been similarly defined for the purposes of the present developments in order to represent the turbulent nature of gas-liquid two-phase flows close to their interface with large enough Reynolds numbers; moreover, it enables the description of friction forces exchanged between phases. Any viscous sub-layer that could possibly exist at the interface is disregarded.

7.2.1. Interfacial and liquid-wall shear stress correlations

An attempt is then made to represent the interfacial shear stress between the gas and the liquid phase through the combination of two different highly representative momentum exchanging phenomena: turbulence and instability.

In particular, the correlation described below has been tested on the basis of experimental measurements of holdup and pressure gradient, compared with various relationships and models existing in literature. The proposed dimensionless groups characterizing the friction at the gas-liquid interface are:

$$\frac{f_i}{f_s} \approx f\left[\frac{h_L}{D}, \left(U_i^* \sqrt{\frac{k_{crit}\rho_G}{g\rho_L}}\,\frac{1}{f_s}\right), \frac{\rho_G}{\rho_L}\right] \tag{162}$$

where k_{crit} is the critical wavenumber and $U_i^* = \sqrt{\frac{|\tau_i|}{\rho_G}}$.

The values of all coefficients have been determined on the basis of the nonlinear least square curve fitting method of Levenberg-Marquardt presented in the previous chapter.

A new interfacial friction factor correlation is proposed below and composed by a first correlation for the prediction of friction factor between stratified flow and capillary 2D waves at the interface, Eq. (163); a second correlation defines the transition between capillary waves and 3D roll waves, Eq. (164). A third

correlation predicts the interfacial friction factor in presence of roll waves, Eq. (165):

$$\frac{f_i}{f_G} = 1, \text{for} \left[(\frac{U_i^*}{U_{Crit}^*})^{0.8} < 1.7(\frac{\rho_G}{\rho_L})^{0.2} \right] \tag{163}$$

$$\frac{f_i}{f_G} = 2, \text{for} \left[(\frac{U_i^*}{U_{Crit}^*})^{0.8} < 1.7(\frac{\rho_G}{\rho_L})^{0.2} \right] \tag{164}$$

$$\frac{f_i}{f_s} = 0.6 + 1.8(\frac{h_L}{D})^{0.2} \left[(\frac{U_i^*}{U_{Crit}^*})^{0.83} - 1.7(\frac{\rho_G}{\rho_L})^{0.2} \right], \quad \text{for} \left[(\frac{U_i^*}{U_{Crit}^*})^{0.8} > 1.7(\frac{\rho_G}{\rho L})^{0.2} \right] \tag{165}$$

where $f_s = 2 f_G$.

$$U_i^* = \sqrt{\frac{|\tau_i|}{\rho_G}} = \sqrt{\frac{1}{2}(U_G - U_L)^2 f_i} \tag{166}$$

and

$$U_{crit}^* = \sqrt{\frac{|\tau_{crit}|}{\rho_G}} = \sqrt{\frac{1}{2}(U_{crit})^2 f_G} \tag{167}$$

In order to solve the full set of balance equations for momentum in the gas and in the liquid phase and to enable the prediction of pressure losses and liquid holdup in the cross section, a relation for liquid-wall friction factor is also needed.

The Blasius equation underestimates the observed values of f_L for stratified-wavy flow pattern; in particular, this phenomenon was described in detail by Andritsos and Hanratty, (1987), Kowalski, (1987) and Andreussi and Persen, (1987).

Their correlations do not seem to fit well with high pressure and highly viscous fluids and a more accurate relationship is presented below:

$$f_L = 0.875 \mathrm{Re}_G^{0.6} \mathrm{Re}_L^{-1} (\frac{h_L}{D})^{0.8} (\frac{\mu_w}{\mu_L})^{0.7} \quad (168)$$

where Re_G, Re_L, $\frac{h_L}{D}$, μ_L, μ_w are respectively the Reynolds number of gas and liquid, the dimensionless liquid level, the liquid viscosity and the viscosity of water taken as reference.

In particular, $\mathrm{Re}_k = D_k U_k / \nu_k$ where k=G,L, and $D_G = 4\frac{A_G}{S_G + S_L}$ and $D_L = 4\frac{A_L}{S_L}$ where D_k, ν_k, A_k, S_k are respectively the hydraulic diameter, the kinematic viscosity, the flow area and the wetted perimeter of the phase k. The proposed correlation is formulated on the basis of well-known dimensionless groups, used by several authors in the literature (Kowalski, 1987; Ottens et al., 2001; etc.). The obtained power law was optimized by a least square method on the available data from open literature.

Nevertheless, its form was not obtained from any consideration about phenomena characterizing the instabilities at the gas-liquid interface and, as only semi-empiric approaches were envisaged to be used for the development of new correlations in this doctoral activity, a new liquid-wall friction factor correlation has been developed, as presented in next sections.

7.2.2. Comparison with experimental data from open literature in horizontal and slightly horizontal flow configuration

The data from Ottens et al., (2001), were obtained for air-water and air-glycerol flows (ID=0.052m) in both horizontal and inclined configuration. The data from Badie et al., (2000), were obtained for air-water and gas-oil flows (ID = 0.078m) in horizontal configuration. Data from Andritsos and Hanratty, (1987) were collected for air-liquid with different viscosity (ID= 0.0952m). All the mentioned experimental campaigns were performed under atmospheric pressure condition.

In the routine for the calculation of pressure losses and liquid height for stratified flow in a pipe, a double loop is involved: the principal loop estimates the liquid holdup by the differential gas-liquid momentum balance equation; the nested one calculates the implicit interfacial friction factor f_i anytime a new liquid holdup value is guessed and a new iteration step starts. The main computational steps are described in the previous chapter.

The prediction of pressure losses and liquid film thickness calculated from the procedure described above are compared with data from Ottens, Andritsos and Badie in Figure 68 and in Figure 69 respectively.

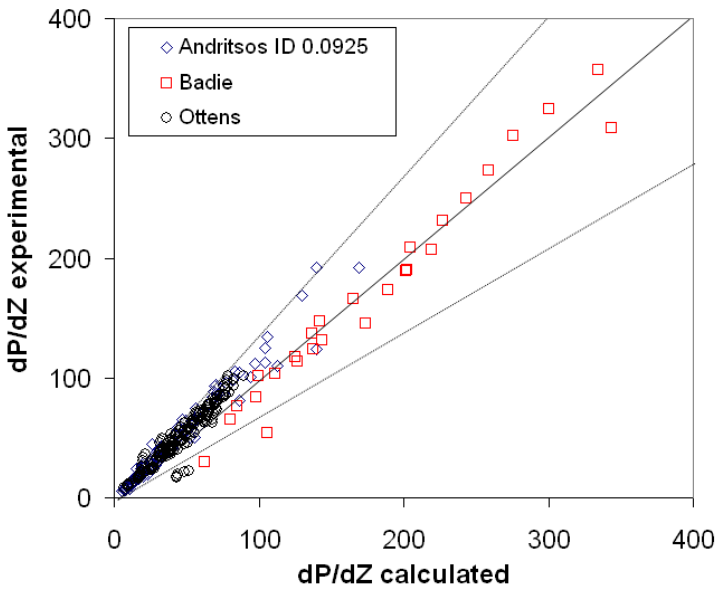

Figure 68: Comparison between measured and calculated pressure gradient

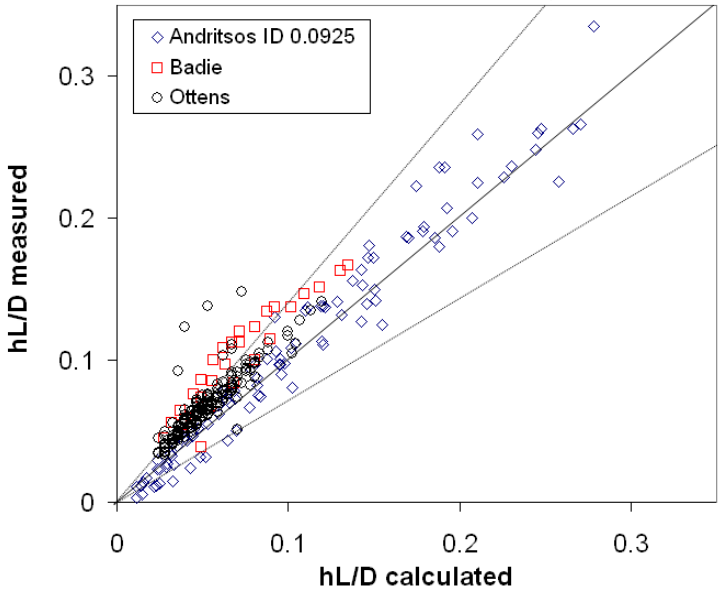

Figure 69: Comparison between measured and calculated liquid film thickness

7.3 New correlations validity domain

The experimental database used in the second part of the work covers a wider range of operational conditions, a domain bounding the validity interval of the new correlations developed during this activity.

The boundaries are 1-100 bar for pressure, 0.025-0.18 cm for internal diameter, 1-40 centipoise for liquid viscosity.

The detailed information about each group of data is presented in Table 10.

Database	Diameter [m]	Liquid Viscosity	Pressure
Andritsos1 (1984)	0.0252 ID	1-40 cp	atmospheric
Andritsos2 (1984)	0.0952 ID	1-16	atmospheric
Ottens (1998)	0.0525 ID	1 cp	atmospheric
Sesame (TEA Sistemi)	0.079 ID	1 cp (water-nitrogen)	3-20 bar
SINTEF	0.189 ID	0.2-20 cp	20-90 bar

Table 10: Reference database for the development of new interfacial and liquid wall friction factor

In this reference database, fluid properties, inlet liquid and gas superficial velocities, corresponding measured pressure losses and liquid levels are listed.

On the basis of the momentum balance equation of gas and liquid phases, the experimental liquid-wall and interfacial friction factors were obtained thanks to the knowledge of measured pressure drop and liquid level, fixing a flat interface between gas and liquid and selecting a correlation for the prediction of gas-wall friction factor.

The obtained friction factors, called “measured” in next sections, are used to optimize the new proposed correlations for liquid-wall and interfacial friction factors, as presented in details below.

7.4 New friction factor correlation for liquid-wall shear stress calculation

Several correlations have been proposed in the open literature for the prediction of the liquid-wall friction factor. In general, these correlations are derived from data taken at atmospheric pressure, in small diameter pipes using water as liquid phase.

This is the reason why they often fail in the prediction of friction factors when the interfacial instability phenomenon takes place between a gas and a liquid.

So, the first goal of the present activity is the improvement of the performance of existing liquid-wall and interfacial friction factors.

The approach chosen for the development of a new liquid-wall friction factor takes its origin from several authors' publications and in particular from the work of Biberg, (1999).

In his work, Biberg stated that the presence of instabilities at the interface disturbs the well-known single phase liquid-wall shear stress, in such a way that a new contribution should be added to the liquid-only formulation in order to take into account the influence of gas flow.

Before Biberg, (1999), other authors suggested this theory of an increased liquid-wall friction factor in presence of interfacial instabilities. Among them, Andreussi and Persen (1987) stated that the increase in the liquid-wall friction factor is triggered by the transition between stratified and stratified-wavy flow pattern. Andritsos (1986) confirmed the strict dependence of the liquid-wall friction from the interfacial friction, continuing the work of Hanratty, (1976) on the effect of instabilities on friction factors to the limit of annular flow.

7.4.1 Contribution of the present activity

In the proposed correlation the two-phase liquid-wall friction contribution was assumed to be given by the expression

$$f_L = f_{L0} * (1 + c\,(\frac{U_G - U_L}{U_L})^a\,(\frac{\rho_G}{\rho_L - \rho_G})^b) \tag{169}$$

where the parameters a, b, c have been obtained through the interpolation of the reference database:

$$\frac{f_L}{f_{L0}} = 1 + (2.5(\frac{U_G - U_L}{U_L})(\frac{\rho_G}{\rho_L - \rho_G})^{0.6}) \tag{170}$$

where $f_{L0} = 0.079\,\mathrm{Re}_L^{-0.25}$

and $\mathrm{Re}_L = D_L U_L / \nu_L$ and $D_L = 4\frac{A_L}{S_L}$ where D_L, ν_L, A_L, S_L are respectively the hydraulic diameter, the liquid kinematic viscosity, the liquid flow area and the liquid wetted perimeter.

This correlation was developed on the basis of the previously presented theories concerning the influence of the presence of the gas phase on the liquid-wall friction factor. Such an influence was hypothesized proportional to the gas phase velocity and density.

So, to the well-known correlation for, f_{L0}, a new term representing the contribution of the gas phase was added in the r.h.s of Eq. (170).The process that has brought to the final form of the correlation has been performed using

the MATLAB^{TM} platform by the least squares method described in previous section.

The correlation has been optimized on the entire reference database (351 measurements) and its behavior can be observed in Figure 70 where the comparison between the measured liquid-wall friction factor and the predicted liquid-wall friction factor is presented.

90% of the measurements are predicted inside error bands of $\pm 20\%$. All points are within the $\pm 30\%$ bands.

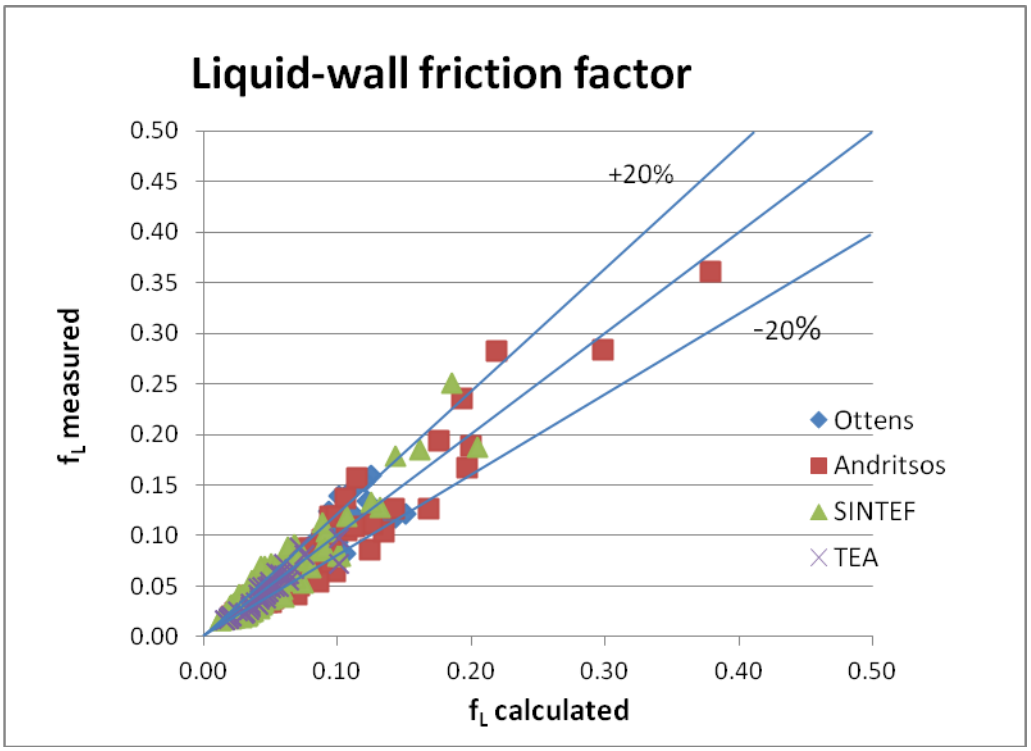

Figure 70: New predicted liquid wall friction factor values versus measured data

Considering the SESAME Project database, constituded by 52 experiments, the results are presented in the Figure 71 below, where measured and calculated Darcy friction factors are compared.

Even if the correlation was not obtained on the basis of this specific group of measurements, this result presents a good agreement between predicted values and experiments.

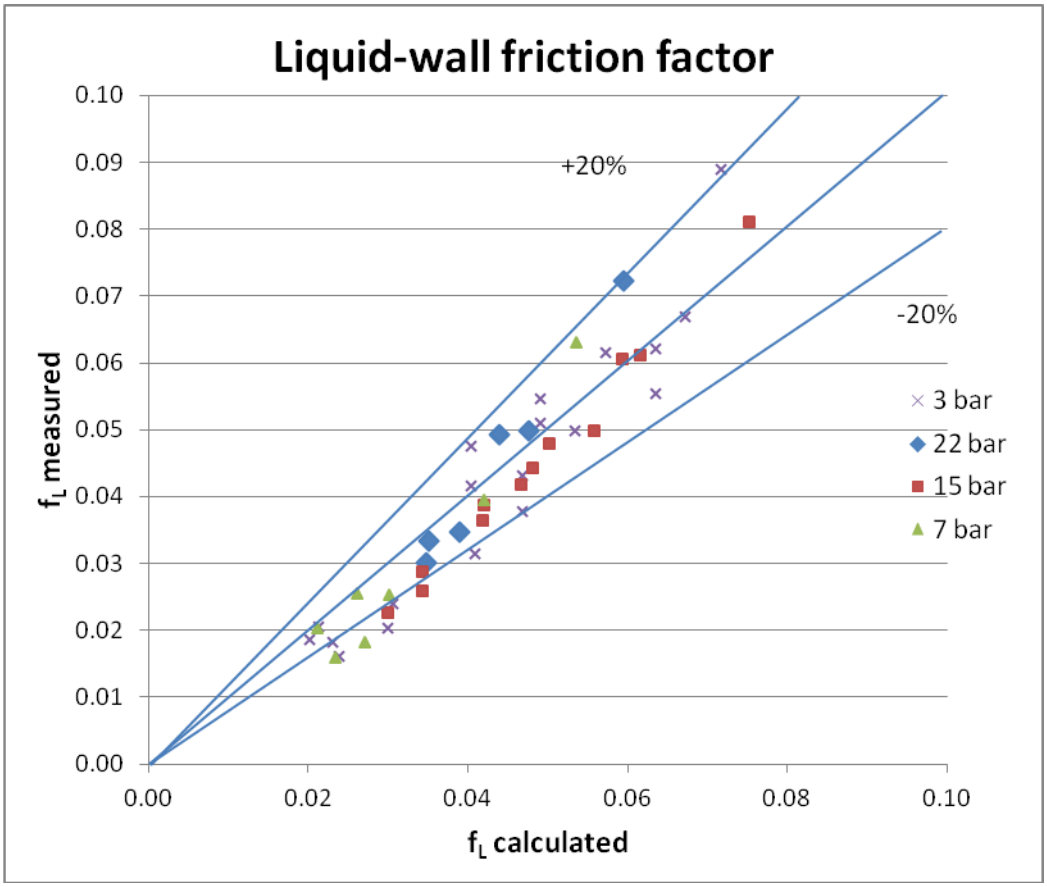

Figure 71: New liquid-wall friction factor values versus measured data (SESAME data only)

The choice of the best friction factor correlation was performed through a quantitative analysis of the RMSE. A summary of the statistical errors for all data is presented in the Table 11.

	Reference database	RMSE
Liquid-wall friction factor	All data	0.028
	SESAME data	0.015

Table 11: Predicted versus measured error estimation for the new liquid-wall friction factor correlation

7.5 Obtained results – Part I

The importance of the application of a two-phase liquid-wall friction factor in the adopted two-phase flow model was proven through the use of this friction correlation together with already existing closure laws for the gas-wall and the interfacial friction, in a 0D numerical model for the calculation of pressure losses and liquid level in pipe cross section.

The analysis procedure, explained below in detail, shows the improvement in the prediction of pressure losses and liquid level if the new two-phase liquid-wall friction factor coefficient TeaL is applied.

In particular, in the 0D computational tool, called DP_hL_pipe_calc, several runs have been performed to test the application of the new liquid-wall friction factor together with the most important interfacial friction factors from literature.

So, for each set of closure laws different input settings are introduced in the DP_hL_pipe_calc model.

The list of simulated test cases and the list of selected correlations are presented in Table 12.

Short name	**Input setting**
AH-AH	Blasius: $f_G = 0.046\ \mathrm{Re}_L^{-0.2}$
	Andritsos-Hanratty,1987: $h^+ = \left\{ (1.082\,\mathrm{Re}_L^{0.5})^5 + \left[0.098\,\mathrm{Re}_L^{0.85} / (1 - \frac{h_L}{D})^{0.5} \right]^5 \right\}^{0.2}$
	Andritsos-Hanratty,1987: $\frac{f_i}{f_G} = 1 + 15 \left(\frac{U_{SG}}{5\sqrt{\frac{\rho_{G0}}{\rho_G}}} - 1 \right) \frac{h_L}{D}^{0.5}$
AP-Mo	Blasius: $f_G = 0.046\ \mathrm{Re}_L^{-0.2}$
	Moody (Hall, 1957): $f_L = 0.01375 \left[1 + \left(\left(\frac{2 \cdot 10^4 \kappa_s}{D_{eL}} \right) + \frac{10^6}{\mathrm{Re}_L} \right)^{0.3334} \right]$

	Andreussi-persen,1985: $\frac{f_i}{f_G} = 1 + 29.7\ (Fr - 0.36)^{0.67} \frac{h_L}{D}^{0.2}$
AH-TeaL	Blasius: $f_G = 0.046\ \mathrm{Re}_L^{-0.2}$
	TEAL: $\frac{f_L}{f_{L0}} = 1 + (2.5(\frac{u_G - u_L}{u_L})(\frac{\rho_G}{\rho_L - \rho_G})^{0.6})$ Con $f_G = 0.079\ \mathrm{Re}_L^{-0.25}$
	Andritsos-Hanratty,1987: $\frac{f_i}{f_G} = 1 + 15\ (\frac{U_{SG}}{5\sqrt{\frac{\rho_{G0}}{\rho_G}}} - 1)\frac{h_L}{D}^{0.5}$
AP-TeaL	Blasius: $f_G = 0.046\ \mathrm{Re}_L^{-0.2}$
	TEAL: $\frac{f_L}{f_{L0}} = 1 + (2.5(\frac{u_G - u_L}{u_L})(\frac{\rho_G}{\rho_L - \rho_G})^{0.6})$ Con $f_G = 0.079\ \mathrm{Re}_L^{-0.25}$
	Andreussi-Persen,1985: $\frac{f_i}{f_G} = 1 + 29.7\ (Fr - 0.36)^{0.67} \frac{h_L}{D}^{0.2}$

Table 12: List of assessed sets of friction factors from literature with and without the newly proposed liquid-wall correlation

The Table 13 summarizes the statistical assessment, through the Root Mean Squared Error percent (RMSEp), of each proposed input settings.

Short name	RMSEp (Dp/Dx)	RMSEp (hL/D)
AP-Mo	22.8	19.8
AH-AH	21.85	18.12
AP-TeaL	20.19	19.93
AH-TeaL	19.77	17.81

Table 13: Performance of friction factors from literature with and without the newly proposed liquid-wall correlation

Further conclusions can be drawn from Figure 72 up to Figure 75, where the results of comparison of predicted versus measured values are respectively shown.

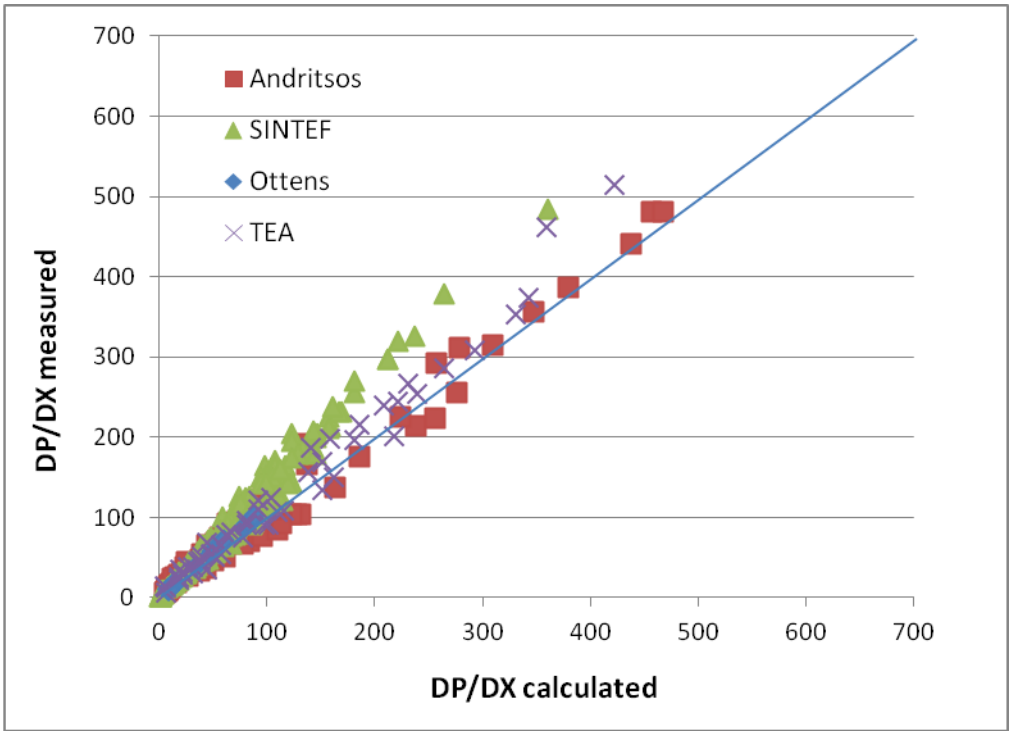

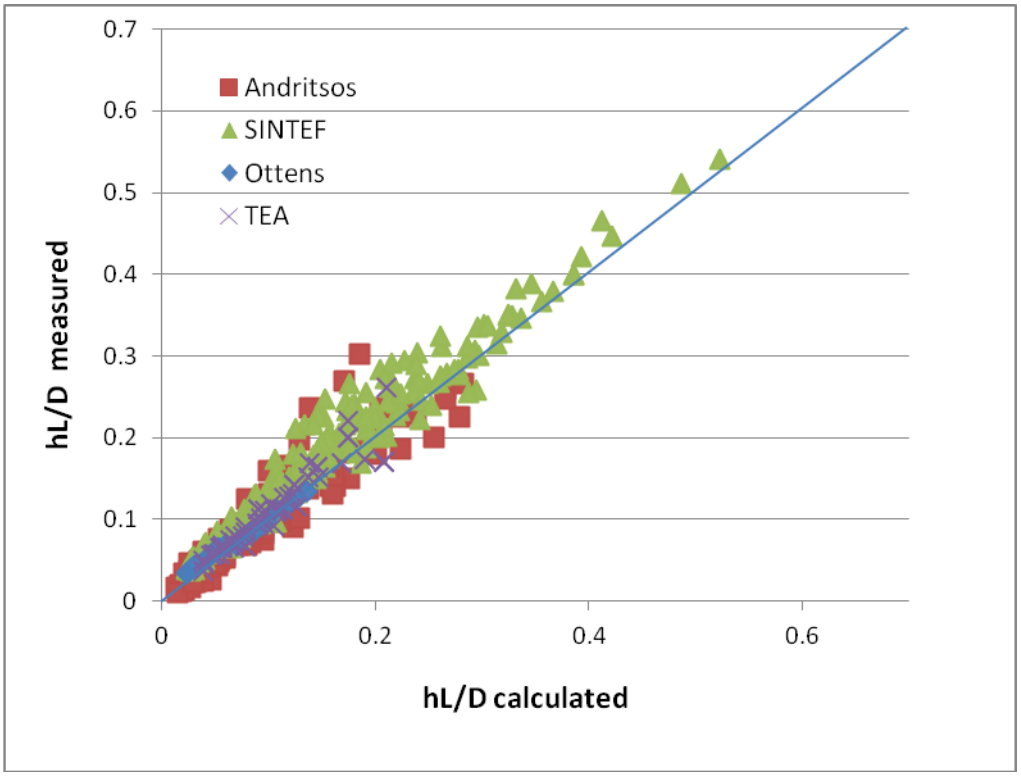

Figure 72: The Andreussi and Persen (1987) interfacial friction factor coupled with the Moody liquid-wall friction factor and the Blasius gas-wall friction correlation

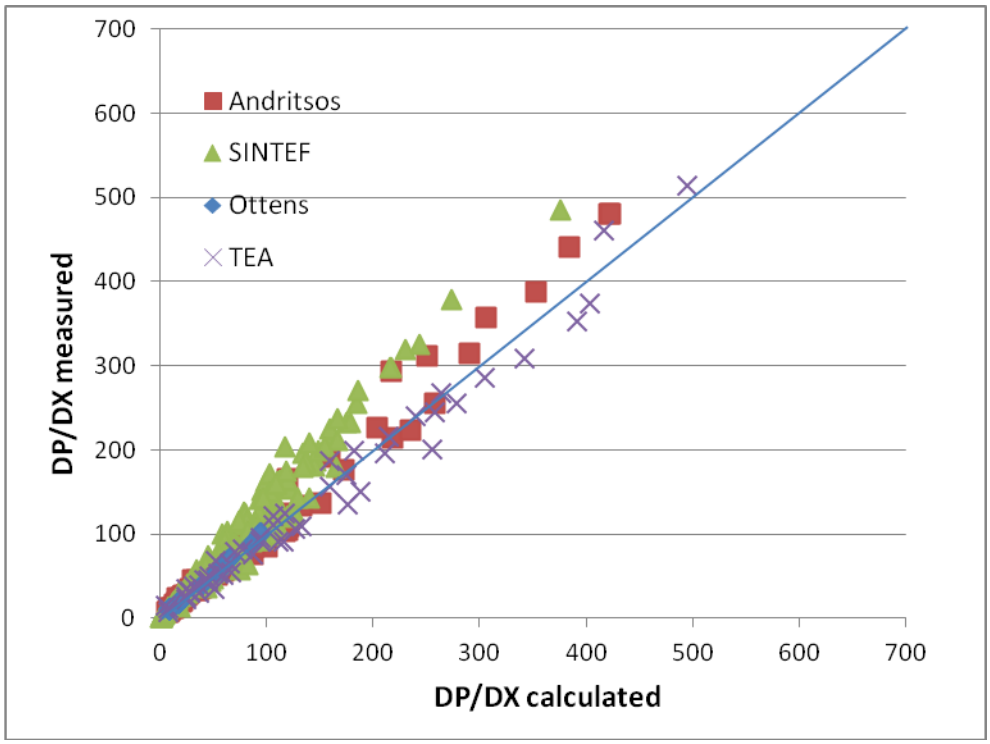

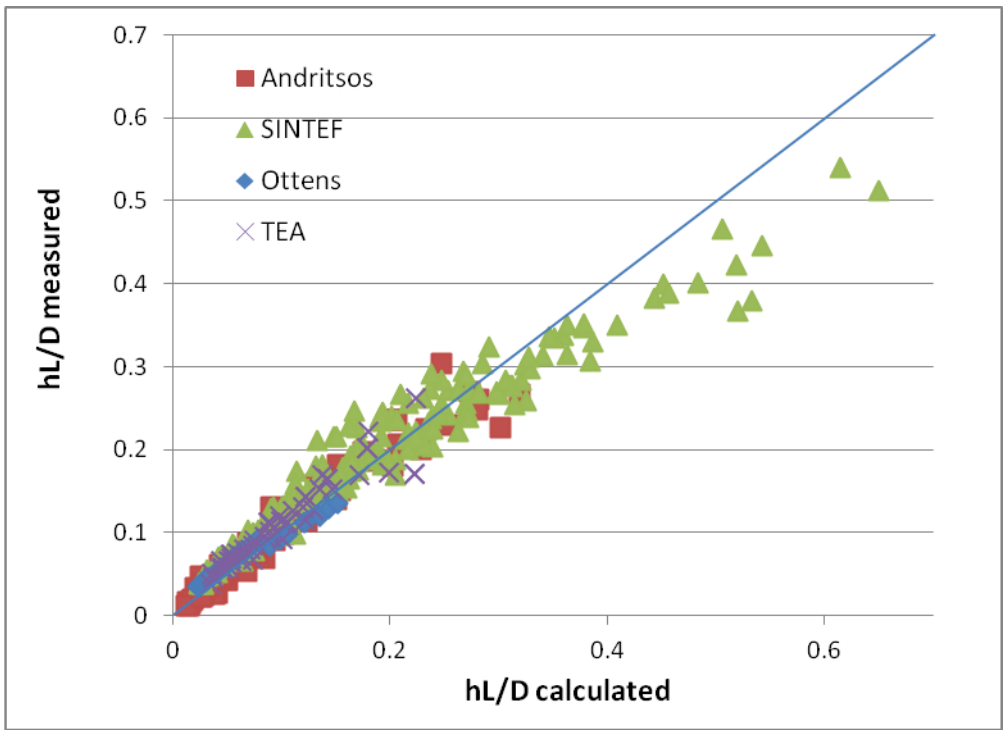

Figure 73: Results obtained by the Andritsos and Hanratty (1987) interfacial friction factor coupled with their liquid-wall friction factor and the Blasius gas-wall friction correlation

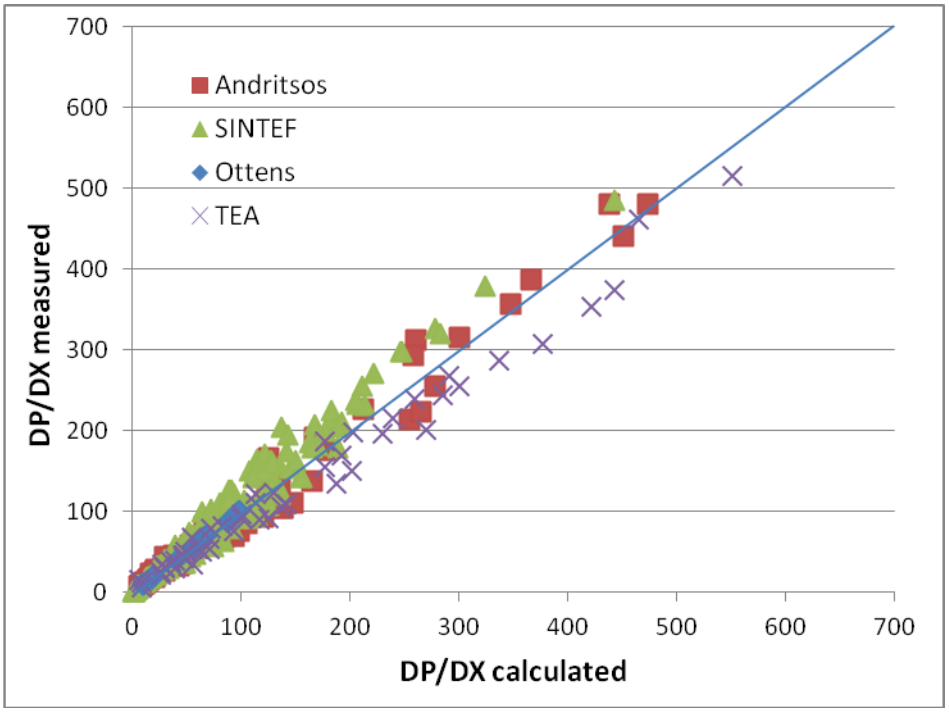

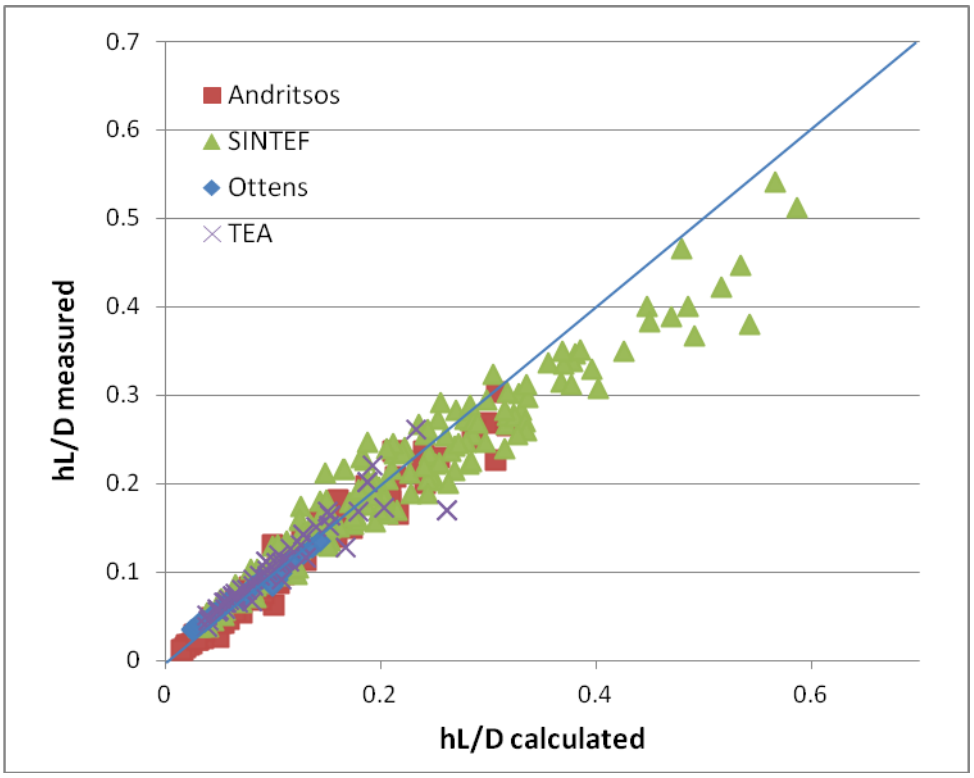

Figure 74: Results obtained by the Andritsos and Hanratty (1987) interfacial friction factor coupled with the TeaL liquid-wall friction factor and the Blasius gas-wall friction correlation

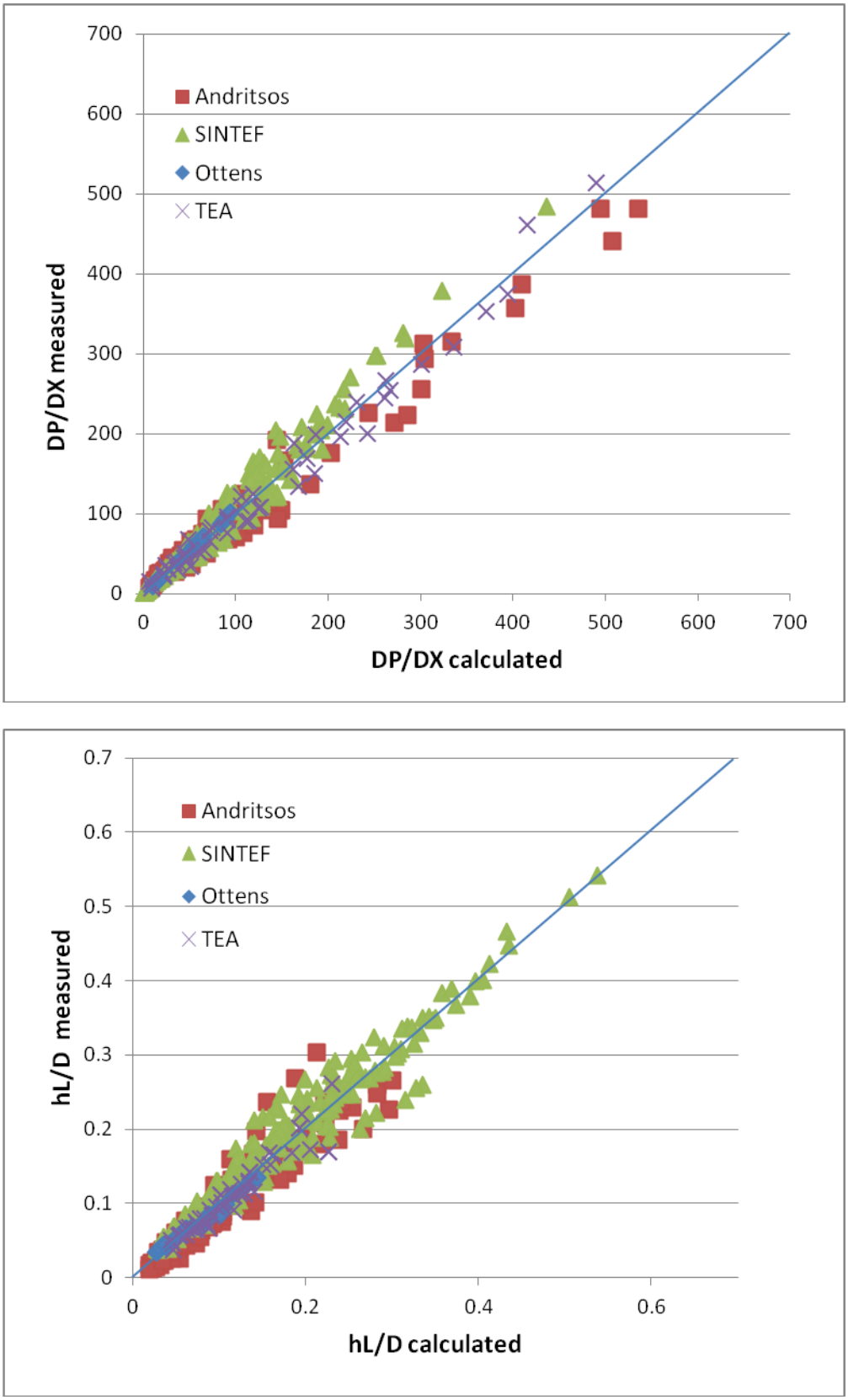

Figure 75: Results of the Andreussi and Persen (1987) interfacial friction factor coupled with the TeaL liquid-wall friction factor and the Blasius gas-wall friction correlation

7.6 New interfacial friction factors

In the present work, new correlations for the gas-liquid interfacial friction factor have been assessed starting from the correlations proposed by Andritsos and Hanratty, (1987) (AH) and Andreussi and Persen, (1987) (AP) in order to investigate the complete panorama of dimensionless groups that play a role in this analysis.

At the basis of the work by AH there is the association of the onset of instabilities to a critical velocity, i.e. the minimum value of the difference between the gas and liquid velocities that causes the onset of interfacial waves. The AP approach differs from the AH one because AP associates the onset of instabilities to a dimensionless Froude number and so the waves are expression of an unbalance between the pressure and the gravity forces.

These two different approaches lead to different dependences of the interfacial friction factor from the pipe diameter and the gas-liquid density ratio.

7.6.1. Definition of a new interfacial friction factor correlation

During the present analysis various combinations of dimensionless groups have been studied (focusing on both Andritsos and Hanratty, (1987) and Andreussi and Persen, (1987) approaches) and the judgment on their performance rises from the minimum root mean square error percent (RMSEp) between the predicted value and the measured one.

The original AH correlation:

$$\left(\frac{f_i}{f_G}\right)_{AH} = 1+15\left(\frac{U_{SG}}{5\sqrt{\frac{\rho_{G0}}{\rho_G}}}-1\right)\frac{h_L}{D}^{0.5}$$

has been set in the form:

$$\left(\frac{f_i}{f_G}\right)_{AHset} = 1+c\left(\frac{U_{SG}}{U_{Gcirt}}-a\sqrt{\frac{\rho_{G0}}{\rho_G}}\right)\frac{h_L}{D}^{b} \qquad (171)$$

The parameters a, b and c have been optimized by a least squares method on the basis of the available database.

This allowed obtaining the following correlation, Andritsos-Hanratty modified (AH_{mod}):

$$\left(\frac{f_i}{f_G}\right)_{AH\,\mathrm{mod}} = \begin{cases} 1, \ for\ U_{SG} \le U_{Gcrit} \\ 1+10\left(\frac{h_L}{D}\right)^{0.2}\left(\frac{U_{SG}}{U_{Gcrit}}-0.5\sqrt{\frac{\rho_{G0}}{\rho_G}}\right), \ for U_{SG} > 0.5\sqrt{\frac{\rho_{G0}}{\rho_G}}U_{crit} \end{cases}$$

where $f_S = f_G = 0.046\ \mathrm{Re}_L^{-0.2}$,

$$U_{Gcrit} = U_L + \sqrt{\left[\left(\frac{k_m \sigma}{\rho_G}\right) + \left(\frac{\rho_L g}{\rho_G k_m}\right) \right]} \text{ and}$$

$$k_m = \left(\frac{\rho_L g \cos\theta}{\sigma}\right)^{0.5}.$$

A similar procedure has been followed with the AP correlation:

$$\left(\frac{f_i}{f_G}\right)_{AP} = 1 + 29.7\ (Fr - 0.36)^{0.67} \left(\frac{h_L}{D}\right)^{0.2},$$

where

$$Fr = U_G \sqrt{\left(\frac{\rho_G}{\rho_L - \rho_G}\right) \frac{\frac{dA_L}{dh_L}}{A_G} \frac{1}{g\cos\theta}} \text{ and}$$

A_G, A_L the gas and liquid flow area respectively,

which has been set in the form

$$\left(\frac{f_i}{f_G}\right)_{APset} = 1 + c\ (Fr - Fr_{crit})^a \left(\frac{h_L}{D}\right)^b \tag{172}$$

In this correlation, the constant 0.36, which represents the critical Froude number at the onset of the disturbance waves in the AP equation, has been replaced by:

$$Fr_{crit} = U_{G\,crit} \sqrt{\left(\frac{\rho_G}{\rho_L - \rho_G}\right) \frac{1}{D \cdot g\cos\theta}} \tag{173}$$

with

$$U_{G\,crit} = U_L + \sqrt{2\left(\frac{\rho_L g}{\rho_G k_m}\right)} \tag{174}$$

The result obtained is the Andreussi-Persen Modified (AP_{mod}) correlation:

$$\left(\frac{f_i}{f_G}\right)_{AP\,\mathrm{mod}} = \begin{cases} 1, \ for F \le F_0 \\ 1 + 29.0(F_r - F_{r\ crit})^{0.7} \left(\frac{h_L}{D}\right)^{0.2}, \ for F > F_0 \end{cases} \tag{175}$$

7.7 Obtained results – Part II

The Root Mean Square Error percent (RMSEp) obtained with the various correlations considered in this work are compared in Table 14 below.

Short name	RMSEp DP/DX	RMSEp h_L/D
AP-Mo	22.8	19.8
AH-AH	21.8	18.12
AH_{mod}-TeaL	17.64	17.33
AP_{mod}-TeaL	15.56	16.90

Table 14: Performance of newly proposed friction factor correlations

This analysis shows the performance of the new sets of friction factor correlations presented above and, in particular, their accuracy in the prediction of pressure losses and liquid holdup in a pipe cross section. In Table 14 TEAL is the new liquid-wall friction factor correlation proposed in Eq. (170).

In the following sections, the set of liquid-wall and interfacial friction factor correlations made up of AH_{mod} and TEAL correlations will be called TEA1. Similarly, the set made up of AP_{mod} and TeaL correlations will be called TEA2.

The coupling of both new liquid-wall and interfacial friction factor correlations, set up during the present activity, improves the prediction of the stratified wavy gas-liquid flow at low, medium and high pressure operating conditions.

This results are presented in Figure 76 and Figure 77 where the predicted versus measured values for pressure losses and liquid level are shown.

In Figure 78 the direct comparison, based on the SESAME data only, between the different friction factor correlations listed in Table 14 is presented as well.

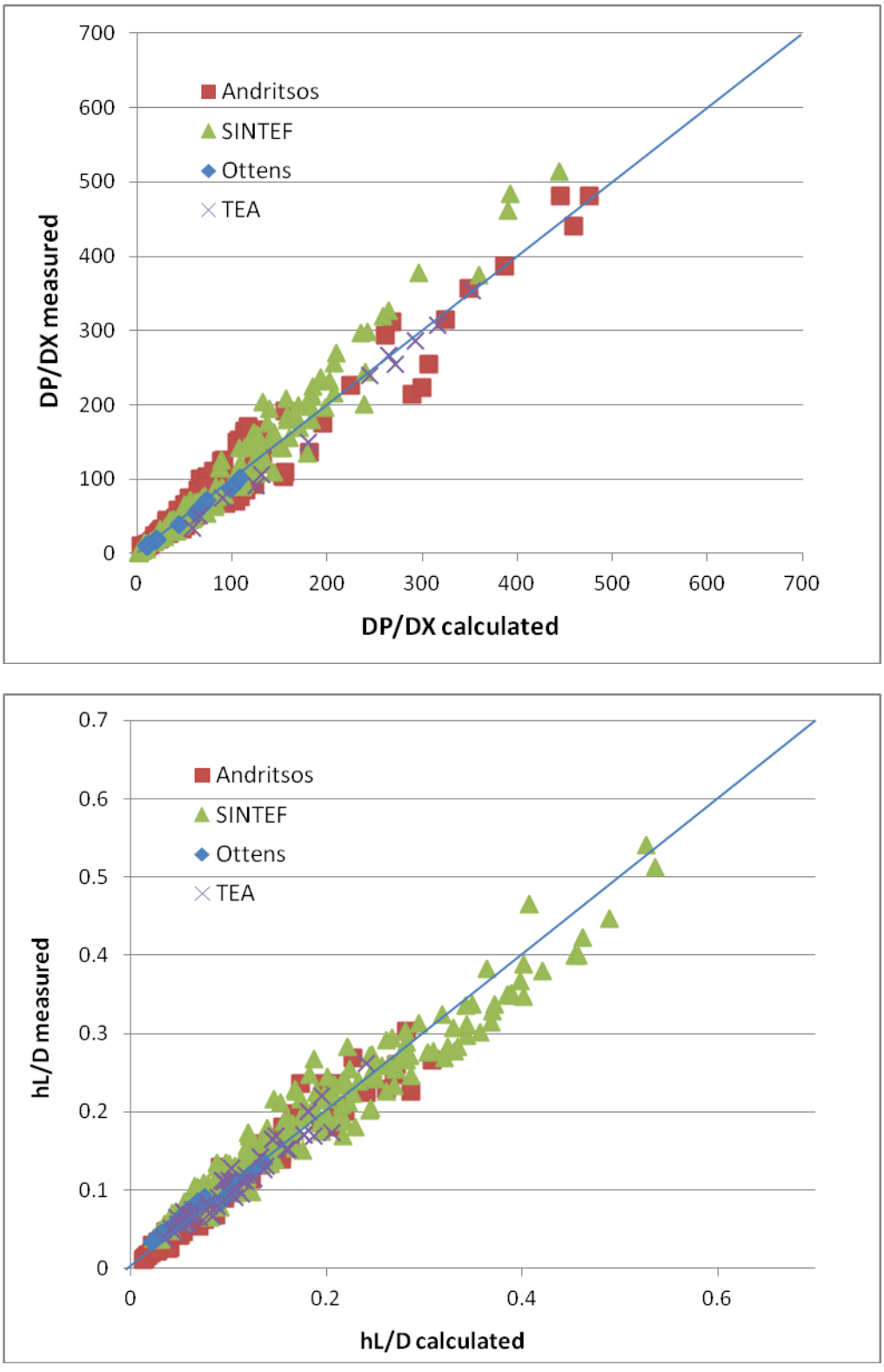

Figure 76: Results obtained by the AHmod interfacial friction factor coupled with the TeaL liquid-wall friction factor and the Blasius gas-wall friction correlation

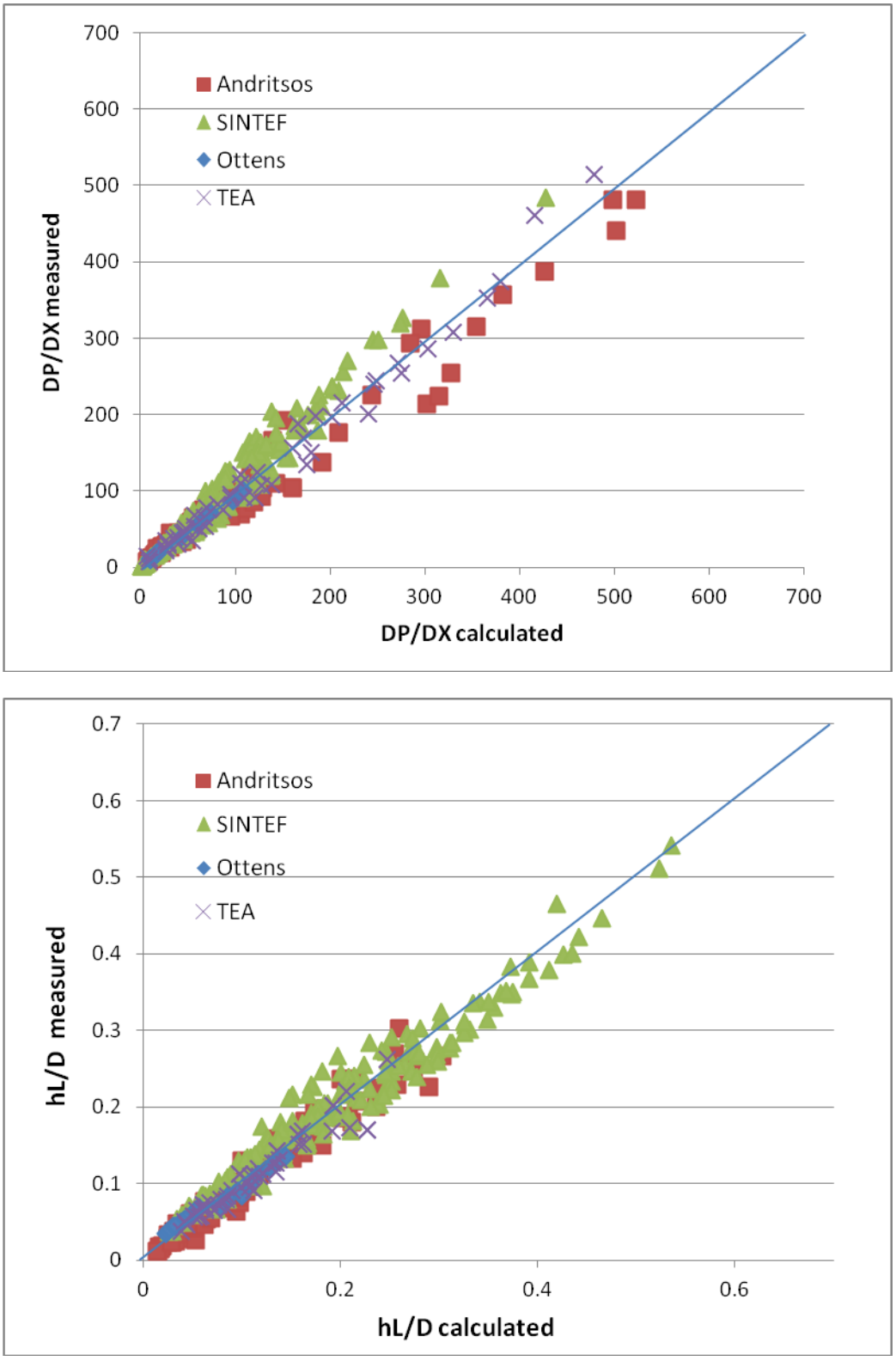

Figure 77: Results of the APmod interfacial friction factor coupled with the TeaL liquid-wall friction factor and the Blasius gas-wall friction correlation

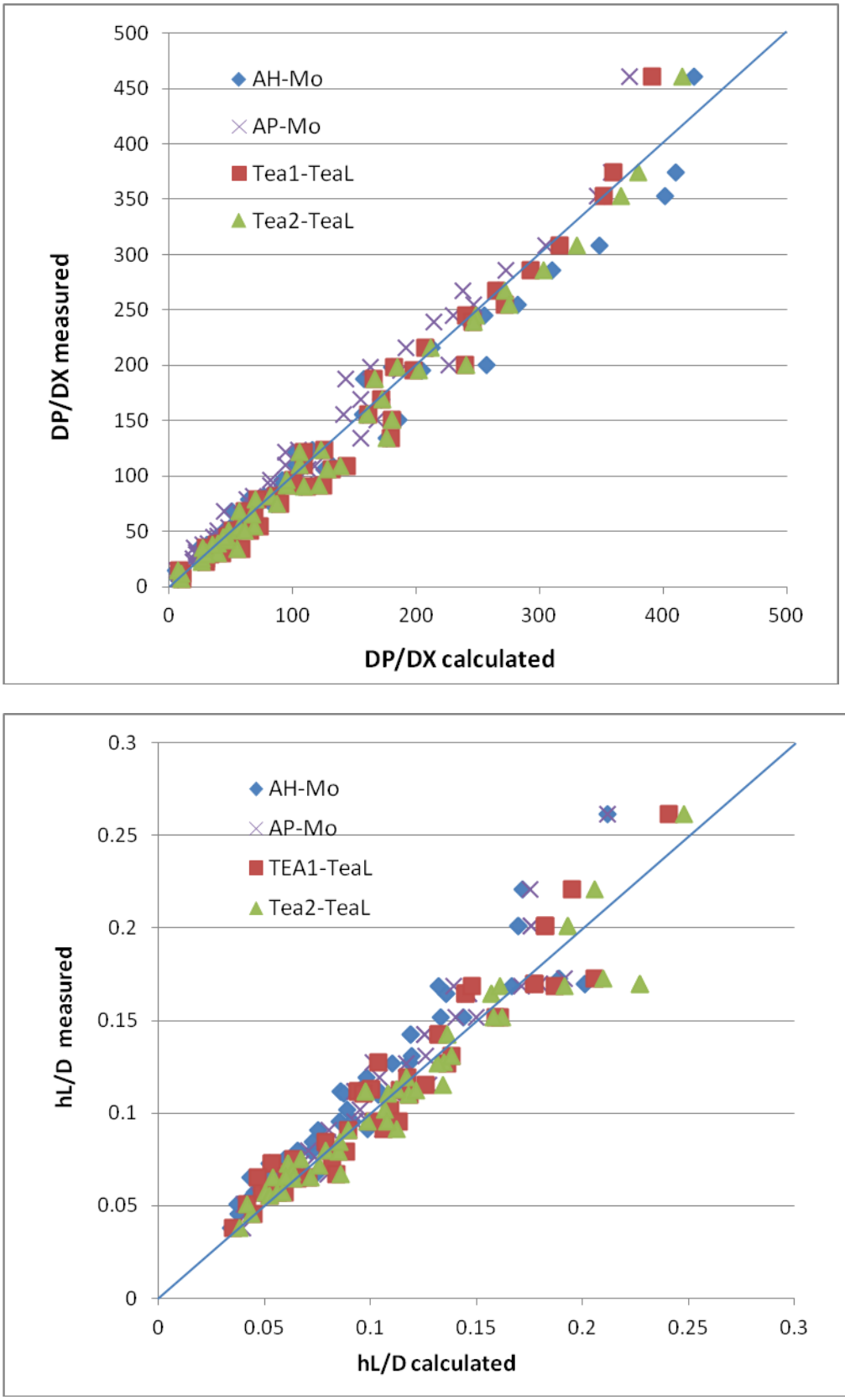

Figure 78: Comparisons for SESAME data only

For validation purposes, the newly presented friction factor correlations were compared with other existing models and the results are proposed in Figure 79 and Figure 80. This comparison against existing commercial codes usually applied in the Oil&Gas field for the design of long transportation pipelines and then abundantly already validated in high pressure, high diameter and liquid viscosity operation conditions, confirming the good performance of the new friction factor correlations, supports even more the adequacy of these new developments.

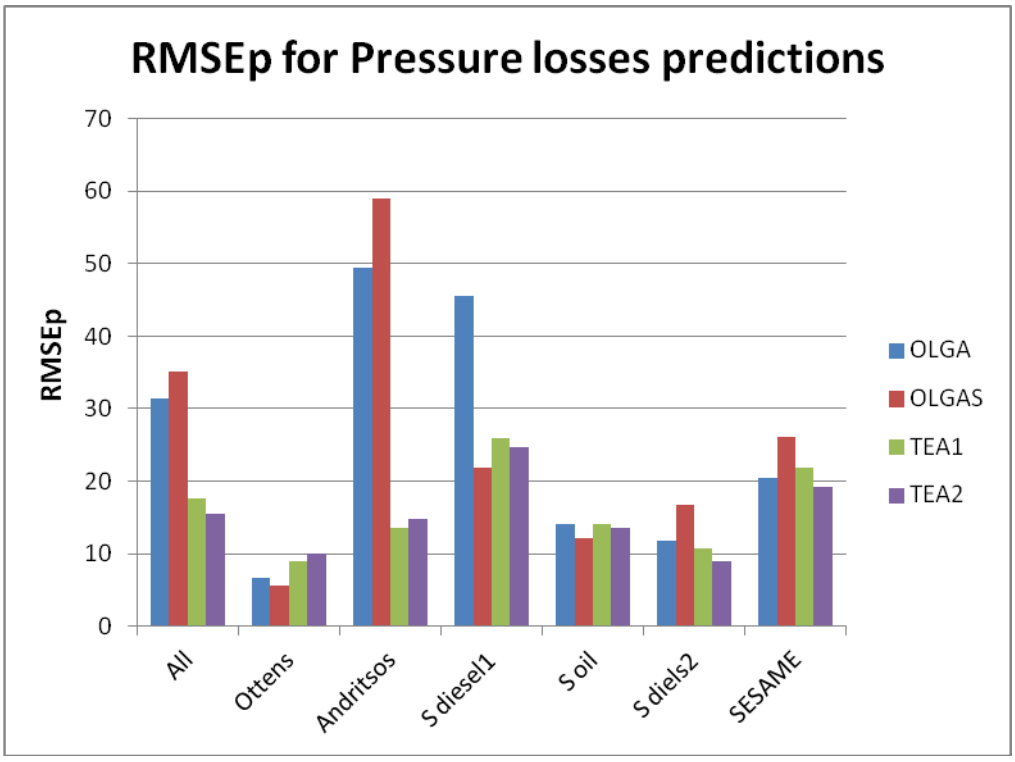

Figure 79: Comparison between predictions obtained by the new friction factor correlations and commercial codes OLGA and OLGAS for the calculation of pressure losses

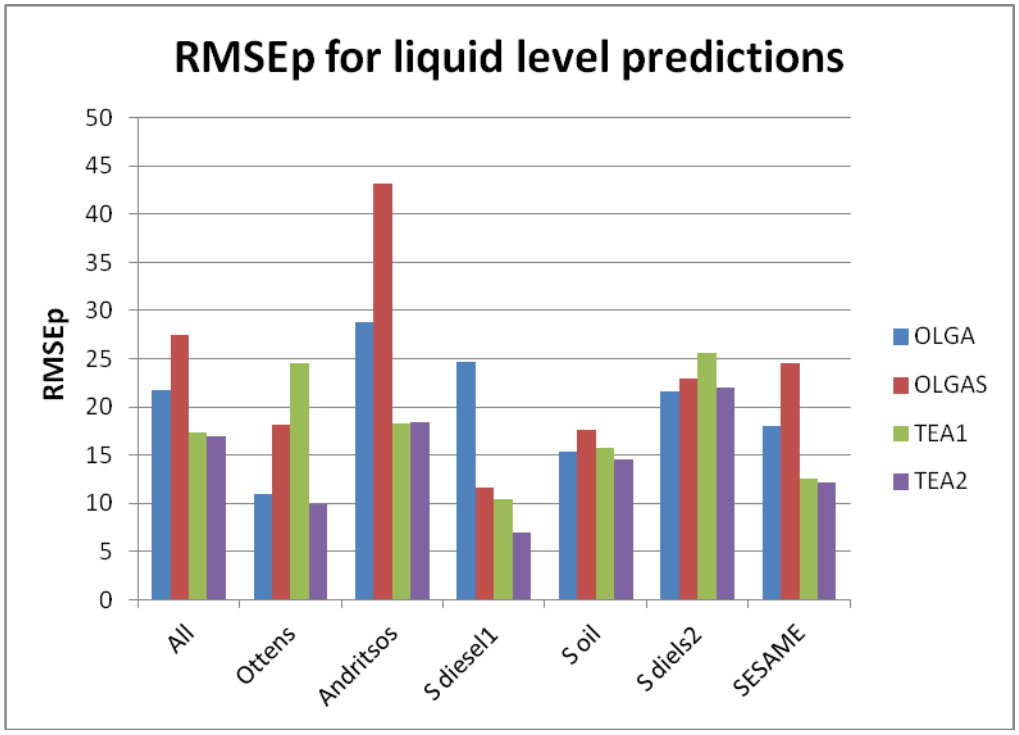

Figure 80: Comparison between predictions obtained by the new friction factor correlations and commercial codes OLGA and OLGAS for the calculation of liquid level

Chapter 8 Conclusions and future enhancements

The analyses performed during the present doctoral work, developed at TEA Sistemi SpA with the contribution of the University of Pisa, are included in the context of R&D activities funded by ENI E&P for the improvement of the understanding of transient multiphase flows in the Oil&Gas field.

The knowledge of time varying flow characteristics, such as the fluid phase fractions, the velocity and the pressure losses, is very important to properly design long hydrocarbon transportation pipelines avoiding major failures and technical constraints in the industrial facilities.

In this chapter, the most important goals of the present work, the results and some suggestions for future developments in this research are summarized.

8.1 Conclusions from the performed work

A review of the most important models existing in literature for two-phase gas-liquid flow has been presented in a first part of the work and a particular attention was devoted to the presentation of these models and of their applications in the Oil&Gas field.

The forms of the different models adopted for two-phase flow were also presented and discussed, together with the classical choices adopted for flow pattern prediction, with a special attention to the transition between stratified and slug flow, that was of major interest here.

In particular, it was seen that the two-phase flow models were designed for describing in greater detail the interactions between the phases and, in the case of long nearly-horizontal pipelines for the transportation of oil and/or gas, the 1D approach was extended to the dispersed fields in each phase, liquid droplets and gas bubbles, with the so-called multi-field model approach.

A new multi-field model, recently developed in TEA Sistemi SpA with the support of ENI E&P and addressing the Oil&Gas field, was presented in detail during this activity and validated against experimental measurements for the investigation of the long slug flow sub-regime. This model is called MAST, Multiphase Analysis and Simulation of Transition; it is a four-field model and solves the full set of balance equations for each of the continuous and dispersed fields.

This model, to be considered complete, needed well assessed closure laws, to be carefully validated against experimental data. In this context, the present work was performed with the purpose of improving the prediction of friction factors, having an important effect in the prediction of pressure drops and

liquid hold-up, through a better formulation, extended to real hydrocarbon transportation pipeline operational conditions.

Most of this doctoral study was then devoted to the investigation of the best available friction factor correlations from the open literature and to the formulation of a new set of liquid-wall and gas-liquid interfacial friction factor correlations. In particular, the attention was focused on the improvement of existing correlation performances when applied to the design of long transportation pipelines.

In this aim, a new set of data related to nitrogen-water flow in a 80 mm pipe operating at pressures in the range 5-25 bar has been used along with data published in the open literature, (mainly concerning air-water flows at atmospheric pressure). These data were used to develop the new correlations for friction factors in horizontal stratified gas-liquid flow conditions.

The new data were collected in the framework of the SESAME project, carried out at TEA Sistemi laboratories, and in this work support was provided to the validation of the obtained measurements.

It was shown that the new two-phase liquid wall friction factor correlation, presented and described in the last part of this thesis, already contributed to the improvement of the predictions of available correlations for interfacial shear in terms of pressure drop and observed hold up.

Then, two new correlations for the interfacial friction factor, AH_{mod} and AP_{mod}, were developed. They represent improvements of respectively the academic works published by Andritsos and Hanratty (1987) and Andreussi and Persen (1987).

Both these correlations, together with the new liquid-wall friction factor correlation, obtained the best performances in comparison with existing correlations in terms of pressure drops and liquid hold-up. In particular, the best fit to the dataset is provided by the modified version of the Andreussi and Persen correlation, AP_{mod}.

For validation purposes, this new set of correlations was tested against the predictions of other commercial models that were also optimized for typical hydrocarbon transportation operational conditions and the comparisons confirmed the quality of the new correlations and the results of this research.

8.2 Future developments

In general, it is believed that improving mathematical models and numerical methods for two-phase flows will remain an active research area for many years to come in several areas, not only in the application domain of 1D tools for prediction of flow behavior in the Oil&Gas field.

Moreover, even if considerable fundamental work has been undertaken in the literature in measuring stratified flow waves, frequency, amplitude, transitions, and propagation velocity, crucial effects for the prediction of the onset of slugging should be better defined in order to enable physical models to correctly predict stratified-wavy and slug flow patterns.

The presented friction factor correlations still need further validations against a new experimental measurement database for stratified-wavy horizontal gas-liquid flow. In fact, if the derivation of new modified expressions of the Andritsos and Hanratty and Andreussi and Persen correlations is very promising and will be a good basis for further investigations, their coefficients could be better assessed through the availability of a more extended experimental database.

Nomenclature

Roman:

A	Flow area	$[m^2]$
D	Pipe diameter	$[m]$
dP/dx	Pressure gradient	$[Pa/m]$
Fr	Froude number	[-]
h_L	Liquid height	$[m]$
g	Gravitational acceleration constant	$[m/s^2]$
J	Jacobian term	
S	Source term	
S_k	Wetted perimeter of the phase k	$[m]$
U_{SG}	Superficial gas velocity	$[m/s]$
U_{LG}	Superficial liquid velocity	$[m/s]$
U_k	Velocity of phase k	$[m/s]$
V_k	Volume of phase k	$[m^3]$
X^2	Martinelli parameter	

Greek:

θ	Pipe inclination	$[rad]$
φ_k	General property of phase k	
v_L	Kinematic liquid viscosity	$[m^2/s]$
ρ_k	Density of the k-phase	$[kg/m^3]$
ρ_G	Density of the gas phase	$[kg/m^3]$
ρ_L	Density of the liquid phase	$[kg/m^3]$

References

Alipchenkov, V., Nigmatulin, R., Soloviev, S. S., & Zaichik, L. Z. (2004). A three-fluid model of two-phase dispersed annular flow. *Int.J.Heat Mass Transfer , 47*, 5323-5338.

Andreussi, P., & Persen, L. (1987). Stratified gas-liquid flow in downwardly inclined pipes. *Int.J.Multiphase flow , 13*, 565-575.

Andreussi, P., Bendiksen, K., & Nydal, O. (1993a). Void distribution in a slug flow. *Int.J.of Multiphase Flow , 19*, 817-828.

Andreussi, P., Bonizzi, M., DiLullo, A., Scotti, A., & Taddei, S. (2008). Advanced simulation of gas-liquid pipelines. *6° North American Conference on Multiphase Technology.* Banff.

Andreussi, P., Minervini, A., & Paglianti, A. (1993b). A mechanistic model of slug flow in near horizontal pipes. *AIChE. J. , 39*, 1281-1291.

Andreussi, P., Paglianti, A., & Sanchez, F. (1999). Dispersed bubble flow in horizontal pepes. *Chem.Eng.Sci. , 54*, 1101-1107.

Andritsos, N. (1986). *Effect of pipe diameter and liquid viscosity on horizontal stratified flow.* Urbana-Champaign: PhD Thesis, University of Illinois.

Andritsos, N., & Hanratty, T. (1987). Influence of interfacial waves in stratified gas-liquid flows. *J.AICh E , 33*, 444-454.

Badie, S., Hale, C., Lawrence, C., & Hewitt, G. (2000). Pressure gradient and holdup in horizontal two-phase gas-liquid flows with low liquid loading. *Int.J.Multiphase Flow , 26*, 1525-1543.

Banerjee, S., & Chan, A. (1980). Separated flow models 1. Analysis of the averaged and local instantaneous formulations. *Int.J.Multiphase Flow , 6*, 1-24.

Banerjee, S., & Mulpuru, F. (1979). *AIAA Journal , 17*, 537-540.

Banerjee, S., & Weaver, K. (1978). Transient two-phase flow. . *Proc.of FirstOECD/NEA Specialist Meeting on Transient Two-Phase Flow.* Hemisphere Press.

Barnea, D. (1987). A unified model for prediction flow pattern transitions in the whole range of pipe inclination. *Int.J.Multiphase Flow* , 1-12.

Barnea, D., & Taitel, Y. (1993). A model for slug length distribution in gas-liquid slug flow. *Int. J. Multiphase Flow* , 829-838.

Barnea, D., & Taitel, Y. (1994). Interfacial and structural stability of separated flow. *Int.J.Multiphase Flow , 20*, 387-414.

Barnea, D., & Taitel, Y. (1993). Kelvin-Helmhotz stability criteria for stratified flow: viscous versus non-viscous (inviscid) approaches. *Int.J.Multiphase Flow , 19*, 639-649.

Barnea, D., & Taitel, Y. (1996). Stratified three-phase flow in pipes- Stability and transition. *Chemical Engineering Communication , 141-142*, 443-460.

Bendiksen, K. (1984). An experimental investigation of the motion of the long bubbles in inclined tubes. *Int.J.Multiphase Flow , 10*, 467-483.

Bendiksen, K. (1984). Experimental investigation of the motion of long bubbles in inclined pipes. *Int.J.Multiphase Flow , 10*, 467-483.

Bendiksen, K., Malnes, D., Moe, R., & Nuland, S. (1991). The dynamic two-fluid model OLGA: Theory and Application. *SPE Paper , 19451*, 171-180.

Bendiksen, K., Malnes, D., Moe, R., & Nuland, S. (1991). The dynamic two-fluid model OLGA: Theory and Application. *SPE* , 171-180.

Bendiksen, K., Malnes, D., Straume, T., & Hedne, P. (1990). A non-diffure numerical model for transient simulation of oil-gas transportation systems., (pp. 508-515). Nuremberg, France.

Biberg, D. (2005). A mathematical model for two-phase stratified turbulent duct flow. *Multiphase Science and Technology* .

Biberg, D. (1999). Two-phase stratified pipe flow modelling. A new expression for the interfacial shear stress. *Two-Phase Flow Modelling and Experimentation.* Pisa, Italy: G.P. Celata, P. Di Marco and R.K. Shah (Editors), 1999 Edizioni ETS.

Black, P. S., Daniel, L. C., Hoyle, N. C., & Jepson, W. P. (1990). Studying transient multiphase flow using the Pipeline Analysis Code (PLAC). *J. Energy Resources Tech.* , 25-29.

Bonizzi, M. (2003). *Transient one-dimensional modelling of multiphase slug flows.* Department of Mechanical Engineering. London: Imperial College London.

Bonizzi, M., Andreussi, P., & Banerjee, S. (2009). Flow regime indipendent, High resolution multifield modelling of near-horizontal gas-liquid flows in pipelines. *Int. J. of Multiphase Flow* , 34-46.

Bonizzi, M., Issa, R., & Kempf, M. (2001). Modelling of gas entrainment in horizontal slug flow. *Proceedings of the ICMF 2001 Conference*, (p. Paper 402). New Orleans, USA.

Brauner, N., & Maron, D. (1992). Stability analysis of stratified liquid-liquid flow. *Int.J.Multiphase Flow , 18*, 103-121.

Caretto, L., Gosman, A., Patankar, S., & Spalding, D. (1972). wo calculation procedures for steady, three-dimensional flows with recirculation. *Proc.hird Int. Conf.Numer.Methods Fluid Dyn.* Paris.

Chen, X., Cai, X., & Brill, J. (1997). Gas-liquid stratified wavy flow in horizontal pipelines. *J. of Energy Resources Technology , 119*.

Cheng, M., Chang, K., & Lee, S. (2002). Numerical solution of hyperbolic two-phase flow model with non-reflecting boundary conditions. *International Journal of Engineering Science , 40*, 787-803.

Cohen, L., & Hanratty, T. (1968). Effects of waves at a gas-liquid interface on a turbulent air-flow. *J.Fluids Mech. , 31*, 467.

Crank, J., & Nicolson, P. (1947). A practical method for numerical evaluation of solutions of partial differential equations of the heat conduction type. *Proc.Camb.Phyl.Soc.*, *43*, pp. 50-67.

Daniels, L., Guardino, C., & Thompson, C. (2003). An implicit two-phase compressible flow solver for pipelines. *Multiphase Science and Technology , 21(3)*, 335-349.

Demirdzic, Lilek, Z., & Peric, M. (1993). A collocated finite volume method for predicting flows at all speeds. *Int.J.for Numerical methods in Fluids , 16*, 1029-1050.

Dinh, T., Nourgaliev, R., & Theofanous, T. (2003). Understanding the ill-posed two-fluid model. *The 10th International Topical Meeting on Nuclear Reactor Thermal Hydraulics (NURETH-10).* Seoul.

Dinh, T., Nourgaliev, R., & Theofanous, T. (2003). Understanding the ill-posedness two-fluid model. *The 10th Internation Topic Meeting on Nuclear Reactor Thermal Hydraulics (NURETH-10).* Seoul, Korea, October 5-9, 2003.

Dobran. (1987). Nonequilibrium modeling of two-phase critical flows in tubes. *J.Heat Transf.*

Drew, D. (1983). Mathematical modeling of two-phase flows. *Annual review of Fluid Mechanics , 15*, 261-291.

Drew, D., & Passman, S. (1999). *Theory of Multicomponents Fluids.* Springer.

Drew, D., Cheng, L., & Lahey, J. (1979). The analysis of the virtual mass effects in two-phase flow. *Int.J.Multiphase Flow , 5*, 233-242.

Dukler, A. E., & Hubbard, M. (1975). A model for gas-liquid slug flow in horizontal. *Ind. Eng. Chemistry Fundamentals , 14*, 337–347.

Espedal, M. (1998). *An experimental investigation of stratified two-phase pipe flow at small inclinations, PhD Thesis.* Trondheim, Norway, 1998: Department of applied Mechanics NTNU.

Fernandez, R., Jutte, B., & Rodriguez, M. (2004). Drag reduction in horizontal annular two-phase flow. *Int.J.Multiphase Flow , 30*, 1051-1069.

Ferziger, J., & Peric, M. (1999). *Computational methods for fluid dynamics.* Germany: Springer.

Fletcher, R. (1976). Conjugate gradient methods for indefinite systems. *Notes in Mathematics , 506*, 773-789.

Gidaspow, D. (1974). Modeling of two phase flow. *Proceedings of the 5th International Heat Transfer Conference VII* .

Glimm, J., Saltz, D., & Sharp, D. (1999). Two-phase modeling of a fluid mixing layer. *Journal of fluid mechanics , 378*, 119-143.

Gregory, G., Nicholson, M., & Aziz, K. (1978). Correlation of the liquid volume fraction in the slug for horizontal gas-liquid slug flow. *Int.J-Multiphase Flow , 4*, 33-39.

Grolman, E., & Fortuin, J. (1997). Gas-liquid flow in slightly inclined pipes. *Chemical Engineering Science , 52*, 4461-4471.

Hageman, L., & Young, D. (1981). *Applied iterative methods.* New York: Wiley.

Haland, S. (1983). Simple explicit formulas for the friction factor in turbulent pipe flow. *J.Fluids Eng. , 98*, 89-90.

Hale, C., & Hewitt, G. (2001). *Two-phase, gas-liquid transient experiments performed in a 1.5° downwardly inclined testline. Report MPS/125 TMF/7 TMF(P)/187(01).* Imperial College, London, UK: Chem.Eng.Dept.

Hall, N. (1957). *Thermodynamics of fluid flow.* Longmans, Green and Co.

Hand, N. (1991). *Gas-liquid co-current flow in a horizontal pipe.* Belfast, UK: Dept. Chem. Eng. Queen's University.

Harlow, F., & Amsden, A. (1971). *J.Comp.Physics , 8*, 197.

Harlow, F., & Welsh, J. (1965). Numerical calculation of time dependent viscous incompressible flow with free surface. *Phys.Fluids , 15*, 2182-2189.

Hart, J., Hamersma, P., & Fortuin, J. (1989). Correlation predicting frictional pressure drop and liquid holdup during horizontal gas-liquid pipe flow with a small liquid holdup. *Int.J.Multiphase Flow , 15*, 947-964.

Hewitt, G. (2005). Three-phase gas-liquid-liquid flows in the steady and transient states. *Nuclear Engineering and Design , 235*, 1303-1316.

Holmas, H., Biberg, D., Schulkes, R., Johnson, G., & Sira, T. (2008). Stability analysis of the Biberg pre-integrated stratified two-phase flow model including profile factors., (pp. 127-141). Banff, Canada.

Hurlburt, E., & Hanratty, T. (2001). Prediction of the transition from stratified to slug and plug flow for long pipes. *Int.J.Muliphase Flow , 2002*, 707-729.

Ishii, M. (1977). *Argonne National Laboratory Report.*

Ishii, M. (1975). *Thermo-fluid dynamic theory of Two-phase flows.* Paris: Eyrolles.

Ishii, M., & Mishima, K. (1984). Two-Fluid Model and Hydrodynamic Constitutive. *Nuclear Engineering and Design , 82*, 107-126.

Ishii, M., & Zuber, N. (1979). Relative Motion and Interfacial Drag Coefficient in Dispersed Two-Phase Flow of Bubbles, Drops and Particles. *AIChE Journal , 25*, 843-855.

Issa, R. I., & Kempf, M. H. (2003). Simulation of slug Flow in Horizontal and Nearly Horizontal Pipes with the Two-Fluid Model. *Int. J. Multiphase Flow* .

Issa, R. I., & Woodburn, P. J. (1998). Numerical prediction of instabilities and slug formation in horizontal two-phase flows. *3rd Int. Conf. Multiphse Flow ICMF98.* Lion, France.

Issa, R. (1986). Solution of implicitly discretized fluid flow equations by operator-splitting. *J.Comput.Phys. , 62*, 40-65.

Issa, R., & Abrishami, Y. (1986). *Computer modelling of slugging flow.* London, UK: Mech.Eng.Dept.Imperial College.

Issa, R., Bonizzi, M., & Barbeau, S. (2006). Improved closure models for gas entrainment and interfacial shear for slug flow modeling in horizontal pipes. *International Journal of Multiphase Flow , 32*, 1287-1293.

Jones, A., & Prosperetti, A. (1985). On the stability of first-order differential models for two-phase flow prediction. *Int.J.Multiphase Flow , 11*, 133-148.

Kadri, U. (2009). *Long liquid slugs in stratified gas/liquid flow in horizontal and slighly inclined pipes, PhD Thesis.* Saba: Israel Institute of Technology.

Kadri, U., Mudde, R., & Oliemans, R. (2010). Influence of the operation pressure on slug length in near horizontal gas-liquid pipe flow. *Int.J.Multiphase Flow* .

Kadri, U., Zoeteweij, M., Mudde, R., & Oliemans, R. (2009a). A growth model for dynamic slugs in gas-liquid horizontal pipes. *Int.J.Multiphase Flow , 35*, 439-449.

Kawaji, M., & Banerjee, S. (1987). Application of a two-field model to reflooding of a hot vertical tube-i.model structure and interfacial phenomena. *J.Heat Trasnsfer , 109*, 204-211.

Kempf, M. (1999). *Simulation of the slug flow in a V-section.* Imperial College, London, UK: Interim.Report, Mech.Eng.Dept.

Kolev, N. I. (2004). 25-Years three-fluid modeling-experience:successes and limits. *European congress on Computational methods in applied sciences and engineering-ECCOMAS 2004.* Jyvaskyla, 24-28 July 2004.

Kowalski, J. (1987). Wall and interfacial shear stress in stratified flow in a horizontal pipe. *J. AIChE , 33*, 274-281.

Kristiansen, O. (2004). *Experiments on the transition from stratified to slug flow in multiphase pipe flow.* Norvegian University of Science and Technology, PhD Thesis. Trondheim: NTNU.

Lahey, R., & Drew, D. (1988). Three dimensional time and volume averaged conservation equations of two-phase flow. *Advances in Nuclear Science Technology , 20*, 1-69.

Lamb, H. (1932). *Hydrodynamics.* Dover: 6th Edn, pp. 77 & 124. (reprinted 1997).

Levenberg, K. (1944). A method for the solution of certain problems in least squares. *Quart. Appl.Math , 2*, 164-168.

Liao, J., Mei, R., & Klausner, J. (2008). A study on the numerical stability of the two-fluid model near ill-posedness. *Int.J. of Multiphase flow , 34*, 1067-1087.

Liao, J., Renwei, M., & Klausner, J. F. (2008). A study on the numerical stability of the two-fluid model near ill-posedness. *Int.J.Multiphase Flow , 34*, 1067-1087.

Liles, D., & Reed, W. (1978). A semi-implicit method for two-phase fluid dynamics. *J.Comput.Phys. , 26*, 390-407.

Lin, P., & Hanratty, T. (1986). Prediction of the initiation of slugs with the linear stability theory. *Int.J.Multiphase Flow , 12*, 79-98.

Mahaffy, J. (1982). A stability enhancing two-step method for fluid flow calculation. *J.Comput.Phys , 46*, 329-341.

Mahaffy, J. (1979). *NUREG/CR-0971.*

Mandhane, J. M., Gregory, G. A., & Aziz, K. (1974). A flow pattern map for gas-liquid flow in horizontal pipes. *Int.J.Multiphase Flow* , 537-553.

Manolis, I. (1995). *High pressure gas-liquid slug flow.* Imperial college, London, UK: PhD Thesis, Chem.Eng.Dept.

Marquardt, D. (1963). An algorithm for least squares estimation on nonlinear parameters. *SIAM J.Apll.Math. , 11*, 431-441.

Meng. (1999). Experimental study of low liquid loading gas-liquid flow in near-horizontal pines. *SPE annual technical conference and exhibition.* , Houston TX.

Milne-Thomson, L. (1968). *Theoratical hydrodynamics (5th. edition).* London: Macmillan.

Nerinckx,K., Vierendeels,J., Dick,E., (2004). A pressure-correction algorithm with mach-uniform efficiency and accuracy. *ECCOMAS 2004 European*

Congress on Computational Methods in Applied Science and Engineering. , Jyvaskyla, 24-28 July 2004.

Nielsen, H. B. (1999). *Damping parameter in Marquardt's method.* Lyngby, Denmark: IMM Depertment of Mathematical modelling.

Nikuradse. (1933). Stromungsgesetze in rauhen Rohren. *NACA Technical Memorandum 1292.* Forschung auf dem Gebiete des Ingenieurwesens.

Nydal, O. J., & Banerjee, S. (1996). Dynamic slug tracking simulations for gas-liquid flow in pipelines. *Chem.Eng.Comm* , 141-142.

Nydal, O., & Andreussi, P. (1991). Gas entrainment ina long liquid slug advancing in a near horizontal pipe. *Int.J.Multiphase Flow , 17*, 179-189.

Nydal, O., Pintus, S., & Andreussi, P. (1992). Statistical characterization of slug flow in horizontal pipes. *Int.J.Multiphase Flow , 17*, 179-189.

Odozi, U. (2000). *Three-phase gas/liquid/liquid slug flow.* Imperial College, London, UK: PhD Thesis, Chem.Eng.Dept.

Omgba-Essama, C. (2004). *Numerical modelling of stratifed gas-liquid flows (Application toStratified & Slug flow regimes).* School of Engineering: Cranfield University-PhD Thesis.

Ottens, M., Hoefsloot, H., & Hamersma, P. (2001). Correlations predicting liquid hold-up and pressure gradient in steady-state (nearly) horizontal co-current gas-liquid pipe flow. *Trans IChemE , 79*, 581-592.

Paillèr, H., C.Corre & Garcìa, J.R. (2003). On the extension of the AUSM+ scheme to compressible two-fluid models. *Computers&Fluids , 32*, 891-916.

Pan, L., & Hanratty, T. (2002). Correlation of entrainment for annular flow in horizontal pipes. *Int.J.Multiphase Flow , 28*, 385-408.

Patankar, S. (1980). *Numerical heat transfer and fluid flow.* New York: McGraw-Hill.

Patankar, S., & Spalding, D. (1972). *Int.J.Heat Mass Transfer , 15*, 1787.

Pauchon, C., Dhulesia, H., Bini-Cirlot, G., & Fabre, J. (1994). TACITE: A transient tool for manltiphase pipeline and well simulation. *SPE Annu. Tech. Conf. and Exhibition* .

Petalas, N., & Aziz, K. (1998). A mechanistic model for multiphase flow in pipes. *49th Annual Technical Meeting of the Petroleum Society of the Canadian Institute of Minim, Metallurgy and Petroleum*, (pp. 98-39). Calgary, Canada.

Ramshaw, J., & Trapp, J. (1978). Characteristics, stability, and short-wavelength phenomena in two-phase flow equation systems. *Nucl.Sci.Ang. , 66*, 93-102.

Ransom, V. (1984). *RELAP5/MOD2 Code manual Vol.I, Code structure, System models and solution methods.* EGG-SAAM-6377.

Ransom, V., & Hicks, D. (1984). Hyperbolic two-pressure models for two-phase flow. *Journal of Computational Physics , 53*, 124-151.

RELAP5. (1984). *NESC N°917.3033, RELAP5/MOD1/008 Tape and implementation information.* National Energy Software Center Note.

Renault, F. (2007). *A lagrangian slug capturing scheme for gas-liquid flows in pipes.* Trondheim, June 2007: PhD Thesis of Norwegian University of Science and Technology.

Rippiner, J. (1998). *Transient slug flow modelling in horizontal and near horizontal pipelines.* Imperial College, London, UK: Technical Report, Mech.Eng.Dept.

Saad, Y., & Schultz, M. (1986). GMRES: a generalized residual algorithm for solving non-symmetric linear systems. *J.Sci.Stat.Comput , 7*, 856-869.

Saha, J. (1999). *Phase interactions in transient stratified flow.* London, UK: PhD Thesis, Department of Chemical Engineering, Imperial College.

Sarkhi, A., & T.J., H. (2002). Effect of pipe diameter on the drop size in a horizontal annular gas-liquid flow. *Int.J.Multiphase Flow , 28*, 1617-1629.

Saurel, R., & Abgrall, R. (1999). A multiphase Gudunov method for compressible multifluid and multiphase flows. *Journal of Computational Physics , 150*, 425-467.

Song, J., & Ishii, M. (2000). The well-posedness of incompressible one-dimensional two-fluid model. *Int.J.Heat Mass Trasfer , 43*, 2221-2231.

Sonneveld. (1989). CGS, a fast Lanczos type solver for non-symmetric linear systems. *J.Sci.Stat.Comput. , 10*, 36-52.

Spalding, D. (1972). A novel finite difference formulation for differential expressions involving both first and second derivatives. *Int.J.Numer.Methods.Engrg. , 4*, 551-559.

Spalding, D. (1979). *Two Phase momentum, heat and mass trasfer in Chemicl proces and Energy Engineering Systems.* Washington: F.Durst, Hemisphere Press.

Spedding, P., & Hand, N. (1997). Prediction in stratified gas-liquid co-current flow in horizontal pipelines. *Int.J.Heat Mass Transfer , 40*, 1923-1935.

Stewart, H., & Wendroff, B. (1984). Two-phase flow: models and methods. *J.Comput.Phys. , 56*, 363-409.

Stone, H. (1968). Iterative solution of implicit approximation of multidimensional partial differential equations. *J.Numer.Anal , 5*, 530-558.

Straume, T., Nordsveen, M., & Bendiksen, K. (1992). Numerical simulation of slugging in pipelines. *Multiphase flow in wells and pipelines* , 144.

Taitel, Y., & Barnea, D. (1990a). A consistent approach for calculating pressure drop in inclined slug flow. *Advanced in heat transfer , 45*, 2089-2097.

Taitel, Y., & Barnea, D. (1990b). Two-phase slug flow. *Advanced in Heat Transfer , 20*, 83-132.

Taitel, Y., & Dukler, A. E. (1976). A model for predicting flow regime transition in horizontal and nearly horizontal gas-liquid flow. *J.AIChE* , 47-55.

Taitel, Y., Barnea, D., & Dukler, A. E. (1980). Flow Pattern Characterization for Two Phase Flow by Electrical Conductance Probe. *Int. J. Multiphase Flow* , 387-397.

Thurgood, M., Cuta, J., Koontz, A., & Kelly, J. (1983). *COBRA/TRAC - A thermalHydraulics code for transient analysis of nuclear reactor vessels and primary coolant systems - Users Manual.* NUREG/CR-3046.

Tomiyama, A., Kataoka, I., Fukuda, T., & Sakaguchi, T. (1995). Drag coefficient of bubbles. *Trans.Japan Soc.Mech.Eng. , B*, 46-53.

TRAC-PD2. (1981). *An advanced best estimate computer program for PWR loss of coolant accident analysis.* Los Alamos National La.Report.

Trasport, E. C.-G. (2008). *EUROPEAN ENERGY AND TRANSPORT TRENDS TO 2030.* Brussels: Office for Official Publications of the European Communities.

Ullmann, A., & Brauner, N. (2006). Closure relations for two-fluid models for two-phase stratified smooth and stratified wavy flows. *Int.J.Multiphase Flow , 32*, 82-105.

Van Doormal, J., & Raithby, G. (1984). Enhancement of the SIMPLE method for predicting incompressible fluid flows. *Numer.Heat Transfer , 7*, 147-163.

Vorst, V. d., & Sonneveld. (1990). *CGSTAB, a more smoothly converging variant of CGS. Tech Report 90-50.* Delft: Delft University of Technology.

Wallis, G. (1968). *One-dimensional two-phase flow.* McGraq-Hill.

Whalley, P., & Hewitt, G. (1987). The correlation of liquid entrainment fraction and entrainment rate in annular two-phase flow. *Tech.Rep.AERE-R 9187, UKAEA, Harwell, Oxon* .

Woodburn, P. (1998). *Slug growth and collapse in gas-liquid mixtures in horizontal pipelines.* Imperial College, London, UK: Mech.Eng.Dept.

Woods, B., & Hanratty, T. (1999). Influence of Froude number on physical processes determining frequency of slugging in horizontal gas-liquid flows. *Int.J.of Multiphase Flow , 25*, 1195-1223.

Woods, B., & Hanratty, T. (1996). Relation of slug stability to shedding rate. *Int.J.Multiphase Flow , 22*, 809-828.

Woods, B., Fan, Z., & Hanratty, T. (2006). Frequency and development of slugs in horizontal pipe at large liquid flows. *Int.J.Multiphase Flow , 32*, 902-925.

Yadigaroglou, G., & Lahey, R. (1976). On the various forms of the conservation equations in two-phase flow. *Int.J.Multiphase Flow , 2*, 477-494.

Zoeteweij, M. (2007). Long liquid slug in horizontal tubes. *PhD thesis.* Delft : University of Technology.

Zuber, N. (1964). On the dispersed two-phase flow in laminar flow regime. *Chemical Engineering Science , 19*, 897-917.

Zuber, N., & Findlay, J. A. (1965). Average volumetric concentration in two phase flow system. *J.Heat Trasfer* , 453-468.